1971

Jet deflection, noise and pressure distribution in proportional amplifiers.

Türken, Ercan.

Monterey, California ; Naval Postgraduate School

JET DEFLECTION, NOISE AND PRESSURE DISTRIBUTION IN PROPORTIONAL AMPLIFIERS

Ercan Türken

United States
Naval Postgraduate School

THESIS

JET DEFLECTION, NOISE AND PRESSURE
DISTRIBUTION IN PROPORTIONAL AMPLIFIERS

by

Ercan Türken

September 1971

Approved for public release; distribution unlimited.

Jet Deflection, Noise and Pressure Distribution in Proportional Amplifiers

by

Ercan Türken
Lieutenant (junior grade), Turkish Navy
B.S., Turkish Naval Academy, 1965

Submitted in partial fulfillment of the
requirements for the degree of

MECHANICAL ENGINEER

from the

NAVAL POSTGRADUATE SCHOOL
September 1971

ABSTRACT

The present study presents the experimental work done on the determination of angle, noise, and pressure distribution for proportional amplifiers. The deflection angles were measured by means of a small, lightstring attached to a needle. The turbulence components in the three directions were obtained through the use of the hot-wire anemometer. The "momentum balance" principal was employed to predict the deflection angles, by taking into account the effects of the momentum, static pressure, and centrifugal forces. The results so obtained were found to be in agreement with those obtained experimentally. The static wall pressures were obtained with a pressure transducer. The "two dimensional-inviscid" flow model was used throughout the work.

TABLE OF CONTENTS

LIST OF ILLUSTRATIONS

LIST OF SYMBOLS

$CF(P)$	Pressure correction factor for rotameter
ΣF_w	Pressure force exerted by the walls on the fluid
M_e	Exit mass flow rate
M_L	Left control jet mass flow rate
M_R	Right control jet mass flow rate
M_P	Power jet mass flow rate
P_L	Left control jet static pressure
P_R	Right control jet static pressure
P_P	Power jet static pressure
$\overline{P}_t$	Mean total pressure at any receiver station
P'_t	Fluctuating component of total pressure
$\overline{P}_s$	Static pressure at any receiver station
P'_s	Fluctuating component of static pressure
Re	Reynolds number
Pat	Atmospheric pressure
$\overline{U}$	Local mean velocity
u', v', w'	Fluctuating components of velocities
$\overline{U}_{max}$	Maximum mean velocity of each profile
$\sqrt{\overline{u'^2}}$, $\sqrt{\overline{v'^2}}$, $\sqrt{\overline{w'^2}}$	R.M.S. values of the fluctuating components
$\overline{U}_e$	Control volume exit mean velocity
V_1, V_2	Entrained flow velocities
V_L	Left control jet velocity
V_R	Right control jet velocity
V_p	Power jet velocity

NOMV — Noise, $NOMV = \frac{\overline{u}'^2 + \overline{v}'^2 + \overline{w}'^2}{\overline{U}^2} \times 10$

UVWS — Noise, $UVWS = \frac{\overline{u}'^2 + \overline{v}'^2 + \overline{w}'^2}{\overline{U}^2_{max}} \times 300$

UATR — Turbulence intensity, $UATR = \frac{\sqrt{\overline{U}'^2}}{\overline{U}} \times 10$

VBTR — Turbulence intensity, $VBTR = \frac{\sqrt{\overline{V}'^2}}{\overline{U}} \times 10$

WCTR — Turbulence intensity, $WCTR = \frac{\sqrt{\overline{W}'^2}}{\overline{U}} \times 10$

VLMN — Normalized mean velocity, $VLMN = \frac{\overline{U}}{\overline{U}_{max}} \times 10$

w_c — Control nozzle width

w_p — Power nozzle width

γ — Deflection angle

γ_1 — Deflection angle calculated without centrifugal forces

γ_2 — Deflection angle obtained only using entering fluid momenta

I. INTRODUCTION

The early works on the proportional amplifiers have started at least twenty years ago and along with the development of these devices new and fairly complex fluid flow problems such as the interaction of incompressible or compressible jets have emerged. To date, most of the theoretical works done were restricted to an inviscid flow and effects of viscosity have been largely ignored.

The proportional amplifiers were designed and operated either through the use of the "pressure control" concept or "momentum control" concept. In either case, both the single-sided and double-sided devices were considered. The pressure controlled device operates on the basis of the differential pressure between the two cavities placed on the two sides of the resultant jet. The vents are not open to the atmosphere. The momentum controlled proportional amplifier operates on the momentum balance of combining jets. We shall confine our attention here to a thorough study of the momentum controlled devices for which basic phenomena is the interaction of small control streams with a larger power stream to deflect the combined jet.

The prediction of the flow deflation and the incoming flow rates in terms of channel geometry and pressures are of interest for design. To accomplish that, one must know the exact mode of the interaction of the jets. There are, obviously, many possible geometric and kinematic variables for the interaction process and it is not economically feasible to experimentally investigate the characteristics of the mode of operation of each and every possible combination.

Various analyses and experiments have been reported. Owczarek, Rockwell, and Cha [Ref. 1] noted the effect of the nozzle geometry to the uniformity of flow at the exit and showed that the planar convergent nozzle having a concave-convex inner wall profile, used without a flow straightener in it, produced a very nonuniform total pressure distribution at the exit. Wuerer [Ref. 2] studied the behavior of interacting jets and concluded that the deflection of a two-dimensional jet by a laterally impinging jet or jets not only determined by the momenta of the interacting jet system but also the pressure forces resulting from the fluid reacting with nearby solid boundaries. Douglas and Neve [Ref. 3] presented the results of preliminary experiments to determine the mode of interaction of the jets using flow visualization on a water table and with a large scale pneumatic model. McCabe and Hughes [Ref. 4] employed "Submerged water operated proportional amplifier" model and showed that the control jets retain their identity and do not actually penetrate the power stream in the mixing region. Reilly and Moynihan [Ref. 5] employed "Two dimensional-inviscid" model in which each jet is assumed to have retained its identity during interaction and is not subject to any viscous effects as it proceeds downstream. Moynihan [Ref. 6] employed "self-preservation" model and showed that the various shear layers formed by the velocity discontinuities of the power and control streams can be a significant noise source. To represent the noise, Moynihan used only one component of turbulence. The experiments have proven that the contributions of the other turbulence components to the noise level are very significant. Sarpkaya [Ref. 7] used the free-stream line theory for beam deflection type fluidic elements with both single and symmetric control jets and

obtained experimental results with a hot-wire anemometer for two typical elements.

The present work presents the experimental work done on the determination of the deflection angle, noise, and pressure distribution for proportional amplifiers. The turbulence components in the three directions are obtained through the use of the hot-wire anemometer. The "momentum balance" principal was employed to predict the deflection angles, by taking into account the effects of the momentum, static pressure and centrifugal forces. The static wall pressures were obtained with a pressure transducer. The "two dimensional-inviscid" flow model was used throughout the work.

II. ANALYSIS OF THE JET DEFLECTION

A control volume type of analysis, similar to that used by Reilly and Moynihan [Ref. 5], was employed in predicting the jet deflection. Momentum, static pressure and centrifugal forces are taken to be essential in the calculation of the deflection angles, and in defining the limits of the control volume. The suggestion made by Reilly and Moynihan [Ref. 5] as "approximately one channel width upstream, the flow is uniform" is used. The following assumptions are made in order to apply the simple momentum balance into the control volume, shown in Fig. 2

(1) B-C is sufficiently far downstream and thus the pressure is uniform and equal to ambient;

(2) The entrained flows, V_1 and V_2 are opposite and equal in magnitude;

(3) The static pressures along A-B and C-D are equal to the ambient.

(4) The flow direction through B-C is uniform.

Using these assumptions and applying the momentum balance into the control volume one obtains

In the x direction

$$M_e \bar{U}_e \sin\gamma - (M_L V_L - M_R V_R) = W_C P_L - W_C P_R + \Sigma F_{Wx} \qquad (1)$$

In the r direction

$$M_e \bar{U}_e \cos\gamma - M_P V_P = W_P P_P + \Sigma F_{Wr} \qquad (2)$$

where F_W is the pressure force exerted by the walls on the fluid (equal and opposite to the fluid pressure forces on the wall). All pressures are referenced to Pat.

Combining equations (1) and (2), one has

$$\tan \gamma = \frac{\Sigma F_{Wx} + W_C (P_L - P_R) + M_L V_L - M_R V_R}{\Sigma F_{Wr} + W_P P_P + M_P V_P}$$

or

$$\tan \gamma = \frac{\Sigma F_{WK} + W_C (P_L - P_R) + \rho W_C (V_L^2 - V_R^2)}{\Sigma F_{Wr} + W_P P_P + \rho W_P V_P^2} = \frac{\Sigma F_x}{\Sigma F_r} \qquad (3)$$

If one neglects the centrifugal forces, the net deflection due just to the entering fluid momenta and the static pressure forces would be

$$\tan \gamma_1 = \frac{W_C (P_L - P_R) + \rho W_C (V_L^2 - V_R^2)}{W_P P_P + \rho W_P V_P^2} \qquad (4)$$

If we consider only the entering fluid momenta, we have

$$\tan \gamma_2 = \frac{W_C (V_L^2 - V_R^2)}{W_P V_P^2} \qquad (5)$$

The results obtained with these equations and the data presented in Figures 3, 4, 5 for different Reynolds numbers are listed in Table I. One can compare these results with the measured deflection angles as a check of the assumptions made in the application of the momentum balance.

III. EXPERIMENTAL EQUIPMENT

The experimental apparatus used in these experiments consisted of a jet assembly, hot-wire anemometer system, a velocity calibrator, and a pressure transducer system.

A. JET ASSEMBLY

The jet assembly consisted of a power jet and two control jets as shown in Fig. 1. The power jet nozzle was 1/4 inch wide and the control-jet nozzle was 5/8 inch wide. Each nozzle was 1/2 inch high. This gave an aspect ratio of two for power jet nozzle and 10/8 for control jet nozzles. The setback was maintained at a value of 1/4 inch.

Planner convergent type of nozzles having a concave-convex inner wall profile were used. The contraction ratios were 1/10 for the power jet and 5/22.8 for the control jet nozzles. A one inch long honey-comb section was used at the uncontracted part of each nozzle for the purpose of straightening the flow. The air was supplied into the inlets via a 1-1/4 inch diameter Tygon tubing.

The pressure taps were placed at the contracted section of each nozzle as shown in Fig. 3. The distances between taps were kept constant as 1/4 inch. A special type of arrangement was made to connect each tap into the pressure transducer while others were kept closed. The holes for these pressure taps were placed at the centerline of the top and bottom plexiglass plates.

A polar-coordinate graph paper which was centered at the pivoting point of the jets, was placed under the bottom plate. This graph was used to read deflection angles measured by means of a small, light string attached to a needle.

The top and bottom plates had two slots cut out to enable the hot-wire anemometer mechanism to traverse along lines parallel to the power nozzle axis.

A 50 H.P. compressor was used to supply air to the system. Air first passed through a micro-filter to remove oil and dust and then through the primary pressure regulator. The three jets were independently supplied from this regulator. A series of pressure regulators on each supply line provided independently regulated flows into three rotameters. Two sizes of rotameters were used. One size was for control jet nozzles with a maximum capacity of 4.5 scfm at 14.7 psia and 70°F. For this size rotameters, the actual flow rates were obtained from

$$Q = (\text{Rotameter reading, \% of full flow}) \times (4.6) \times CF(P)$$

where CF(P) represents the pressure correction factor given by manufacturer chart. A larger size meter was used for the power jet nozzle with a maximum capacity of 17.5 scfm at 14.7 psia and 70°F. The actual flow was obtained from

$$Q = (\text{Rotameter reading, \% of full flow}) \times (17.5) \times CF(P)$$

B. HOT-WIRE ANEMOMETER SYSTEM

A model 1050, constant temperature hot-wire anemometer, manufactured by the Thermo-Systems Inc., was used to measure the mean velocity and turbulence intensities. A double-cross wire with an angle of 45 degrees between the wires was used. The readings were taken by means of D-C voltmeters and RMS voltmeters which were accurate to 0.001 volts.

A specially constructed probe holder which was fitted into the slots in the jet assembly, enabled the probe to move along lines parallel to the power-nozzle axis in any plane. Two different type micrometer mechanisms on the holder provided transverse and vertical movements of the hot-wire across the jet with an accuracy of 0.001 inch.

The calibration curves were obtained by use of Thermo-Systems Calibrator, Model 1125. The stagnation pressures in the calibration of the wire were measured with an inclined manometer.

C. PRESSURE MEASUREMENT SYSTEM

The pressure taps on the jet assembly were connected into the multiple inlet, one output valve system. A pressure transducer, Model KP15, manufactured by Whittaker Corp. Inst. Sys. Div. with a carrier amplifier, Model 8805B and a recorder, Model 7702B manufactured by the Hewlett-Packard Inc., were used to measure the static pressures at different sections.

IV. EXPERIMENTAL PROCEDURE

The experiments were carried out for three different Reynolds numbers (based on the mean velocity and W_p) at a deflection angle of six degrees. For each Reynolds number, distributions of mean velocity and turbulence components in three directions were measured at various distances from the pivoting point, and the results were reduced to actual data through the use of the computerized calibration curve.

The deflection angles were measured at selected normalized average control-jet velocities for different normalized differential control-jet velocities by the use of the floating string and the chart paper combination. The measurements were repeated for each Reynolds number.

The static pressures were measured by means of a pressure transducer for three different Reynolds numbers and for the same deflection-angle combinations.

Most of the experiments were repeated for the purpose of checking the reproducibility of the data. The Reynolds numbers were selected such that the highest one was four times and the medium one was twice the lowest Reynolds number.

V. DISCUSSION OF RESULTS

A. NOISE LEVELS

The noise in proportional amplifiers shows itself in the form of total pressure fluctuations and can be formulated as

$$\bar{P}_t+P'_t = \bar{P}_s+P'_s+1/2\rho((\bar{U}+U')^2 + V'^2 + W'^2) \tag{6}$$

$$\bar{P}_t+P'_t = \bar{P}_s+P'_s+1/2\rho(\bar{U}^2+2UU'+U'^2+V'^2+W'^2) \tag{7}$$

After averaging, one has

$$\bar{P}_t = \bar{P}_s + 1/2\rho\bar{U}^2 + 1/2\rho(\bar{U}'^2 + \bar{V}'^2 + \bar{W}'^2) \tag{8}$$

where the last term represents the fluctuations in the total pressure. If the static pressure is assumed constant across the profile and used as reference, the ratio $(\bar{U}'^2 + \bar{V}'^2 + \bar{W}'^2)/\bar{U}^2_{max}$ can provide a qualitative measure of the noise level to be captured by the receivers located at some r/W_p station.

This type of analysis has been performed by Moynihan [Ref. 6], using only the single component of the turbulence. The experiments have shown that contribution of the other two turbulence components to the noise level could not be overlooked.

The sources of the noise are shear layers which are formed by the velocity discontinuities of the power and control streams. These velocity discontinuities are due to the fact that each jet retains its identity in the mixing zone as noted by McCabe [Ref. 4], Moynihan [Ref. 6], and Sarpkaya [Ref. 7]. In the mixing region, which extends up to a distance of $2\ W_p$ from the pivoting point, the inner and outer shear layers produce two peaks on the noise distribution. Beyond the mixing zone, the

inner shear layers disappear, only two peaks of the noise can be seen and the mean velocity distribution is almost of the Gaussian form.

Figures 6 through 75 show the mean velocity profiles (normalized with respect to the maximum velocity in each profile) and the sum of the squares of RMS velocity fluctuations, normalized by the square of the maximum velocity of the profile, i.e., $(\overline{U}'^2 + \overline{V}'^2 + \overline{W}'^2)/U^2_{max}$. The use of the maximum velocity of the profile as the reference velocity is arbitrary since the noise captured by the receivers depend on the magnitude and distribution of velocity at the entrance of the receivers. Since the mean velocity at the receivers is lower, the actual noise in the signals captured by the receivers will be larger. This can be seen from Figures 76 through 82.

The general characteristics of the noise distributions for the three Reynolds numbers considered can be summarized as follows: They are all similar in shape of distribution, magnitudes of noise levels increase in the downstream direction, and the width of the relatively silent core decreases with distance from the pivoting point. The turbulence intensities at three directions for sections near the pivoting point are higher at the side of the control port with lower velocity. This is due to the larger velocity discontinuity which yields a stronger shear layer between the high velocity power jet and the very low velocity control jet. At sections away from the pivoting point the turbulence intensities on both sides of the jet become nearly identical. The relative magnitudes of turbulence intensities are such that $\sqrt{\overline{U}'^2}/U$ is always highest and $\sqrt{\overline{W}'^2}/U$ is lowest. The maximums in the noise profiles occur at points where there is an inflection in the mean velocity profile. The noise levels remain fairly constant in the jet establishment region (approximately

within a distance of $2W_p$ from the pivoting point) and increases almost linearly with distance in the fully established jet and the noise level reaches approximately 4% at a distance of 8 W_p.

Figures 83, 84 and 85 show the magnitude of the peak values of the noise and the width of the silent core normalized with respect to the power jet nozzle width, W_p. One immediately recognizes that the magnitude of the noise increases with decreasing Reynolds number for all receiver positions. The width of the silent core is larger for higher Reynolds numbers. This is due to the larger penetration of the control jets into the main jet at lower Reynolds-number flows. For the same Reynolds number, the noise levels are lower and the width of the silent core is larger when both control jets are active than that for the case of single active control jet.

Figures 48 through 75 show that the noise levels, mean velocity and turbulence distributions at top and middle planes are almost identical. This result is a good confirmation of the use of a two dimensional flow model.

B. DEFLECTION ANGLES

The measured jet deflection angles are shown in Figures 86 through 91 in terms of the average and differential control-port velocities normalized with respect the power-jet velocity for three different Reynolds numbers. These two parameters have only been used by Sarpkaya [Ref. 7] in the investigation of the proportional amplifiers. The parameters used by the other investigators, such as flow rates, pressures or momenta are not capable of showing the range of linearity or the nonlinearity of the operation of the amplifier.

From the figures presented herein, it is seen that the deflection angle is, in general, a linear function of the normalized differential control-jet velocities. This linearity is distorted at very small and large values of the normalized differential velocity. The nonlinearity at small jet-deflection angles increases with increasing normalized average control-port velocity. At larger angles of deflection, it increases with decreasing average control-port velocity. For all the Reynolds numbers considered, a proportional amplifier becomes less sensitive to the normalized differential-velocity signals (i.e., smaller increase in the deflection angle with a higher change in the differential velocity) for the higher values of the normalized average control-port velocity.

Figures 92 through 94 show the deflection angles plotted for three different Reynolds numbers in terms of the parameters stated above. One can immediately see that the effect of the Reynolds number on the deflection angle distribution is almost negligible when normalized average control-port velocity is kept constant.

The deflection angles obtained from the analysis based on momentum balance are given in Table I. It is seen that one cannot use only the entering fluid momenta to predict the defelction angle. The effect of the static pressure forces both across the nozzles and along the walls contribute to the deflection of the jet. One can use only the entering fluid momenta and static pressure forces to predict the deflection angle within some degree of accuracy with the assumptions stated in the analysis for this geometry. It is also seen that the effect of different Reynolds numbers on the results obtained are very small. One can suggest that the effect of the geometric dimensions such as set back, nozzle width, and offset are more pronounced than the flow conditions.

The theoretical jet-deflection angle distributions obtained by use of the analysis carried out by Hiriart [Ref. 8] using the free-stream line theory with the measured deflection angles are plotted in Figures 95 and 96. For each normalized average control-port velocity, there is a slight variation of the parameter which relates the effective jet width to that used in the analysis. If one determines this parameter experimentally for the amplifier considered, this theory is capable of predicting the jet deflections in proportional amplifiers.

C. STATIC PRESSURE DISTRIBUTIONS

The static wall pressures for the three Reynolds numbers are shown in Figures 3, 4 and 5. The general characteristics of these figures are such that the pressures are higher at higher flow sections. For the lower Reynolds numbers the static wall pressures at lower control-port flow side become less than the atmospheric pressure. The higher Reynolds numbers produce higher static wall pressures at all sections.

VI. CONCLUSIONS

The study of the velocity and turbulence profiles, deflection angle and static pressure distributions in the interaction and flow development region of three interacting jets of unequal velocities have shown that:

(a) The jets preserve their identity in a region of approximately $2W_p$ from the pivoting point;

(b) The mean velocity profiles become Gaussian beyond the mixing region;

(c) Only one component of the turbulence cannot be used to represent the total pressure fluctuations;

(d) The effects of Reynolds numbers on deflection angle distributions are very small as long as normalized average control-port flow is kept constant;

(e) The higher normalized average control flow results in non-linearity and lower sensitivity in terms of jet deflection;

(f) The noise levels are higher for lower Reynolds number at any receiver location;

(g) The mean velocity and noise distributions are almost identical for middle and top planes;

(h) The minimum noise level is on the order of 4% due to the contributions of jet interaction and flow entrainment and could be considerably higher under normal operating conditions due to receiver interference and other oscillations;

(i) The noise levels remain relatively low and constant in the jet-establishment region and increase almost linearly with distance from the pivot point;

(j) The "momentum balance" analysis applied to an appropriately defined control volume can be used to predict the deflection angles;

(k) When one control flow used to obtain the same deflection angle of the two control flow, the same type of mean velocity and turbulence profiles with higher level of noise are obtained.

APPENDIX

DERIVATION OF CALIBRATION EQUATIONS FOR CROSS-WIRE

The heat transfer equilibrium equation on the wire is given by

$$\frac{I^2 Rw}{Rw-Rg} = A + C\sqrt{U} \tag{9}$$

where

I = Current through the wire

Rw = Operating resistance of the wire

Rg = Cold resistance of the wire

A and C = Constants

U = Instantaneous velocity of the fluid

At $U = 0$, $I = I_o$ so,

$$\frac{I^2 Rw}{Rw-Rg} = \frac{I_o^2 Rw}{Rw-Rg} + C\sqrt{U} \tag{10}$$

from $E = IR$, equation becomes

$$E^2 = E_o^2 + C\,(Rw-Rg)\,Rw\,\sqrt{U} \tag{11}$$

or

$$E^2 = E_o^2 + B\sqrt{U}$$

Assuming velocity fluctuations are small, cooling of wire is determined mainly by velocity component vertical to the wire (V_L). Then,

$$E^2 = E_o^2 + B\sqrt{V_L}$$

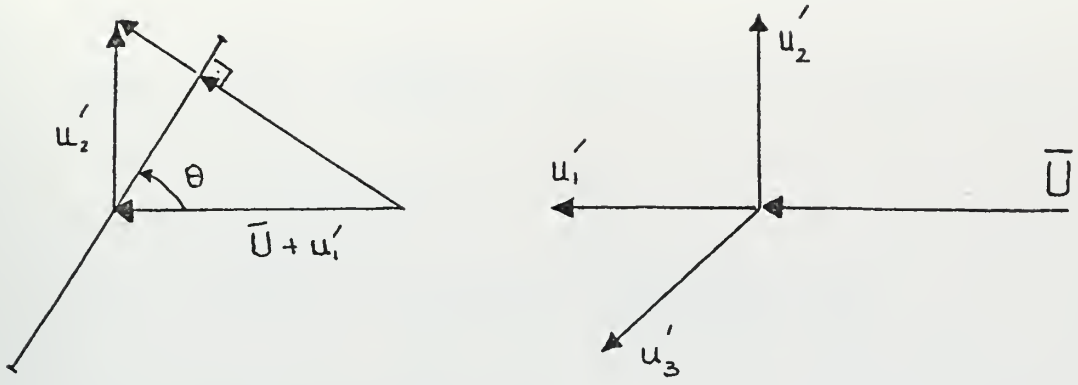

From figure above, one can write

$$V_L = [\{(\bar{u}+u_1')\sin\theta + u_2'\cos\theta\}^2 + u'^2_3]^{1/2} \tag{14}$$

$$V_L = [(\bar{u}+u_1')^2 \sin^2\theta + 2(\bar{u}+u_1')u_2'\sin\theta\cos\theta + U'^2_2\cos\theta + u'^2_3] \tag{15}$$

Neglecting the second order terms

$$V_L = [\bar{U}^2 \sin^2\theta + 2\bar{U}^2 (u_1'/\bar{U}) \sin^2\theta + 2\bar{U}^2 (u_2'/\bar{U}) \sin^2\theta \cot\theta]^{1/2} \tag{16}$$

$$V_L = \bar{U}\sin\theta\,[1+2(u_1'/\bar{U}) + (u_2'/\bar{U})\cot\theta]^{1/2} \tag{17}$$

By using the binomial theorem,

$$V_L = \bar{U}\sin\theta\,\{1 + (u_1'/\bar{U}) + (u_2'/\bar{U})\cot\theta\} \tag{18}$$

From $V_L = \bar{V}_L + v_L'$

$$\bar{V}_L = \bar{U}\sin\theta \tag{19}$$

$$v_L' = U\sin\theta\,\{u_1'/\bar{U} + (u_2'/\bar{U})\cot\theta\} \tag{20}$$

From equation (13) and $E = \bar{E} + e'_w$

$$(\bar{E} + e'_w)^2 = \bar{E}_o^2 + B\sqrt{\bar{V} + v'} \tag{21}$$

$$\bar{E}^2 + 2\bar{E}\, e_w = \bar{E}_o^2 + B\sqrt{\bar{U}\sin\theta}\,[1 + 1/2\,(u'_1/\bar{U}) + 1/2\,(u'_2/\bar{U})\cot\theta] \tag{22}$$

So,

$$\bar{E}^2 = \bar{E}_o^2 + B\sqrt{\bar{U}\sin\theta} \tag{23}$$

$$2\bar{E}\, e'_w = B\sqrt{\bar{U}\sin\theta}\,[1/2\,Ou'_1/\bar{U}) + 1/2\,(u'_2/\bar{U})\cot\theta] \tag{24}$$

$$e'_w = S_w\,[(u'_1/\bar{U}) + (u'_2/\bar{u})\cot\theta] \tag{25}$$

$$S_w = \frac{\bar{E}^2 - \bar{E}_o^2}{4\bar{E}} \tag{26}$$

For cross wire

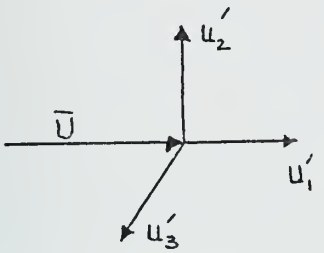

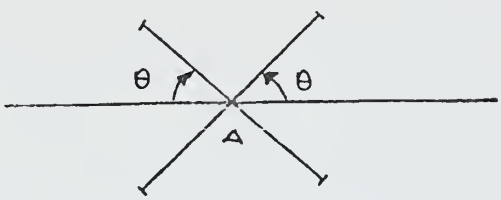

when $\theta = 45^o$

$$e'_I = S_I \left(\frac{u'_1}{\bar{U}}\right)_A + S_I\, u'_2/\bar{U})_A \tag{27}$$

$$e'_{II} = S_{II} \left(\frac{u'_1}{\bar{U}}\right)_A - S_{II} \left(\frac{u'_2}{\bar{U}}\right)_A \tag{28}$$

If $S_I = S_{II}$, one can easily obtain

$$\sqrt{(e'_I + e'_{II})^2} = 2\, S_w \left(\frac{\sqrt{\bar{u}'^2_1}}{\bar{U}}\right)_A \tag{29}$$

$$\sqrt{(e'_I - e'_{II})^2} = 2\, S_w \frac{\sqrt{\overline{u'^2}}}{\overline{U}} \Big)_A \tag{30}$$

$$\overline{e'^2_I} - \overline{e'^2_{II}} = 4\, S_w^2 \frac{\overline{u_1 u_2}}{\overline{U}^2} \tag{31}$$

One can measure $\frac{\sqrt{\overline{u'^2_1}}}{\overline{U}}$, $\frac{\sqrt{\overline{u'^2_3}}}{\overline{U}}$ and $\frac{\overline{u_1 u_3}}{\overline{U}^2}$ in the same way by proper positioning of the cross wire.

TABLE I

	REYNOLDS NUMBER		
	31550	15775	7887
x Direction Forces ($lb_{f/ft}$)			
$S\ W_c\ (V_L^2 - V_R^2)$	0.06689	0.0192	0.004618
$W_c\ (P_L - P_R)$	0.25377	0.07213	0.017376
$\Sigma\ Fw_x$	0.041	0.01209	0.002708
ΣF_x	0.36166	0.10342	0.024702
r Direction Forces ($lb_{f/ft}$)			
$S\ W_p\ V_p^2$	2.9	0.725	0.18126
$W_p\ P_p$	0.1443	0.03554	0.00966
$\Sigma\ Fw_r$	0.11564	0.021	0.004884
$\Sigma\ F_r$	3.15994	0.78154	0.1958
Deflection Angles			
γ Measured	6^o	6^o	6^o
γ (Eq. 3)	6.5^o	7.45^o	7.15^o
γ_1 (Eq. 4)	6.0^o	6.86^o	6.35^o
γ_2 (Eq. 5)	1.34^o	1.52^o	1.47^o

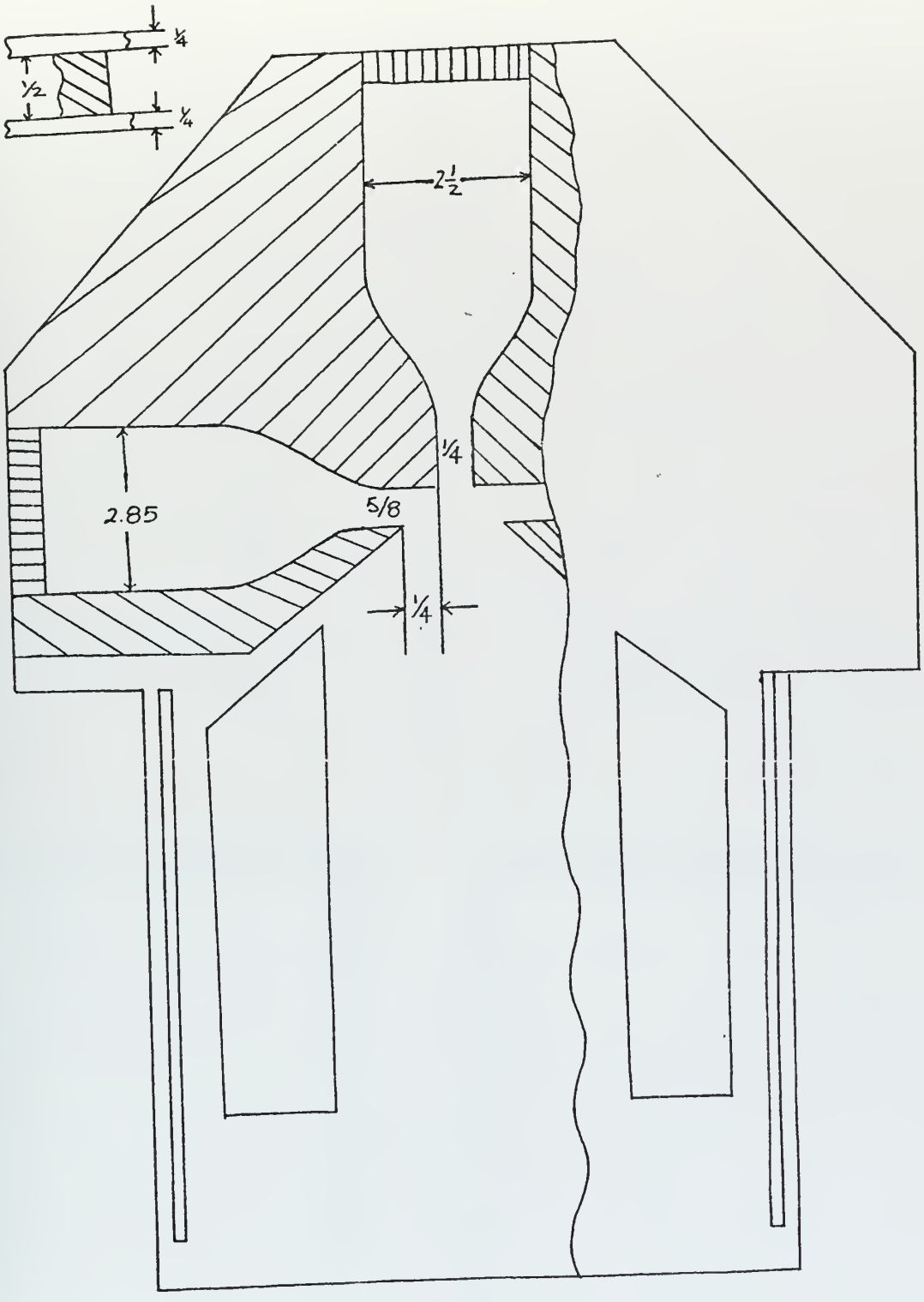

Figure 1. Jet Assembly

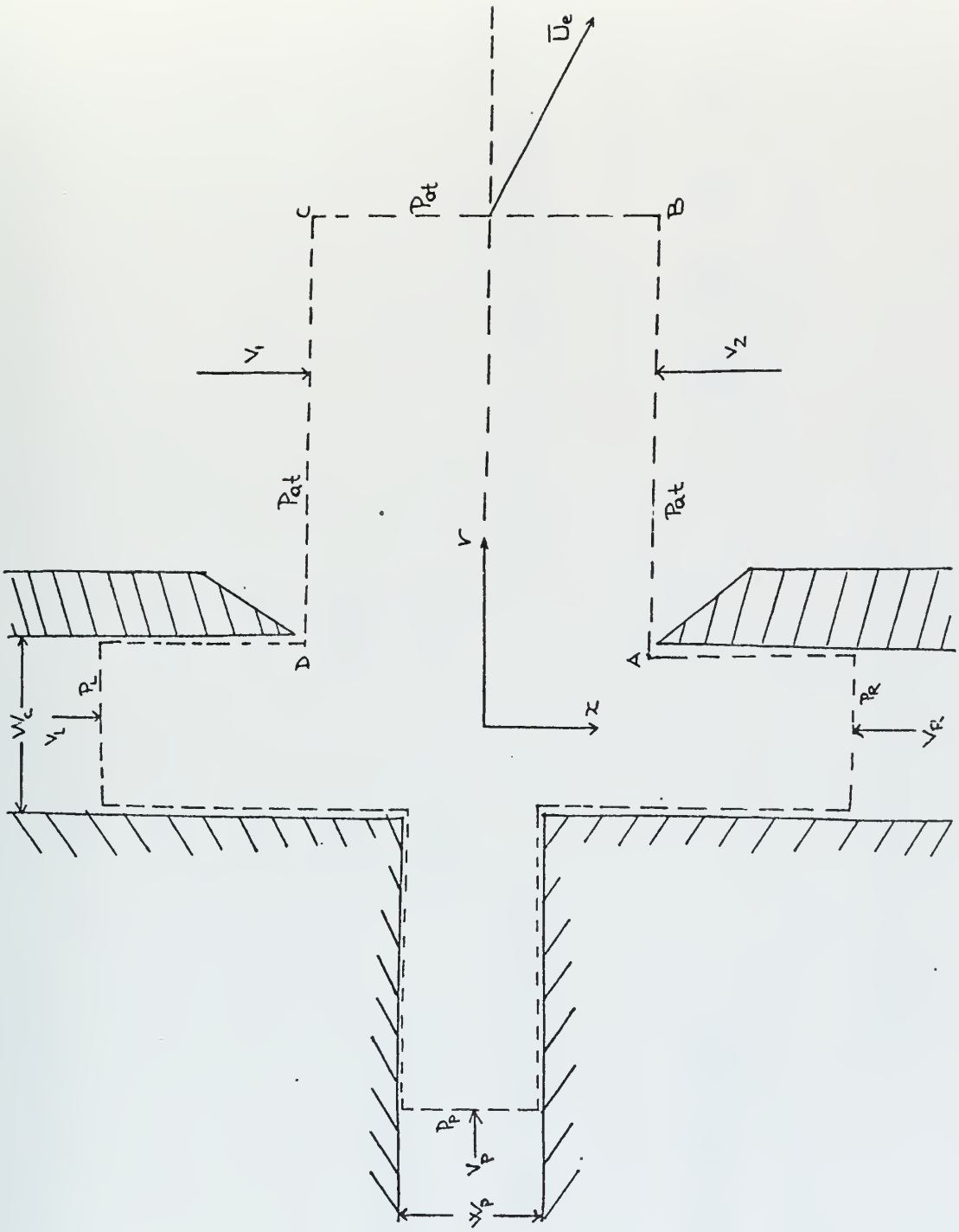

Figure 2. Control Volume

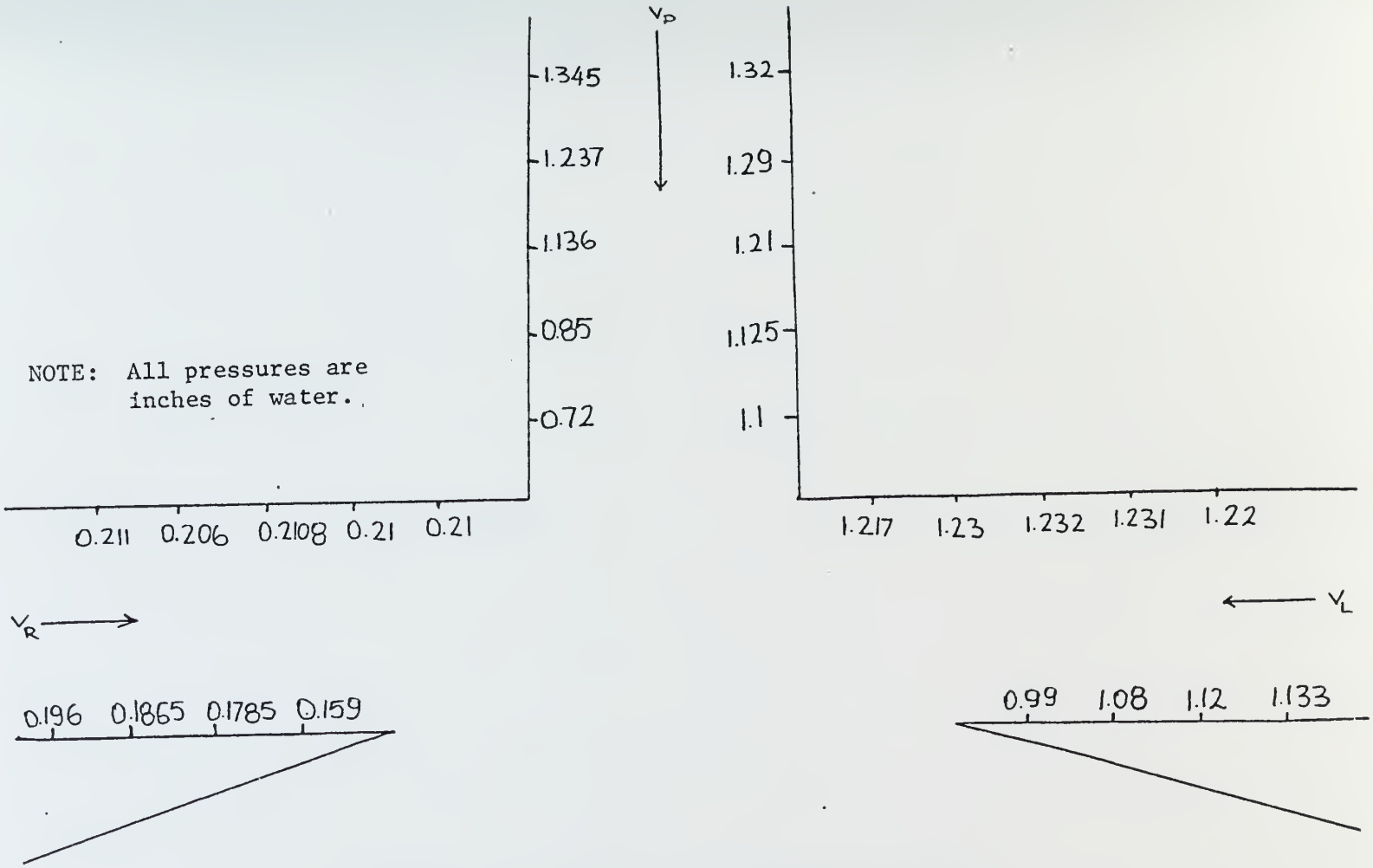

Figure 3. Static Wall Pressures, Re = 31550

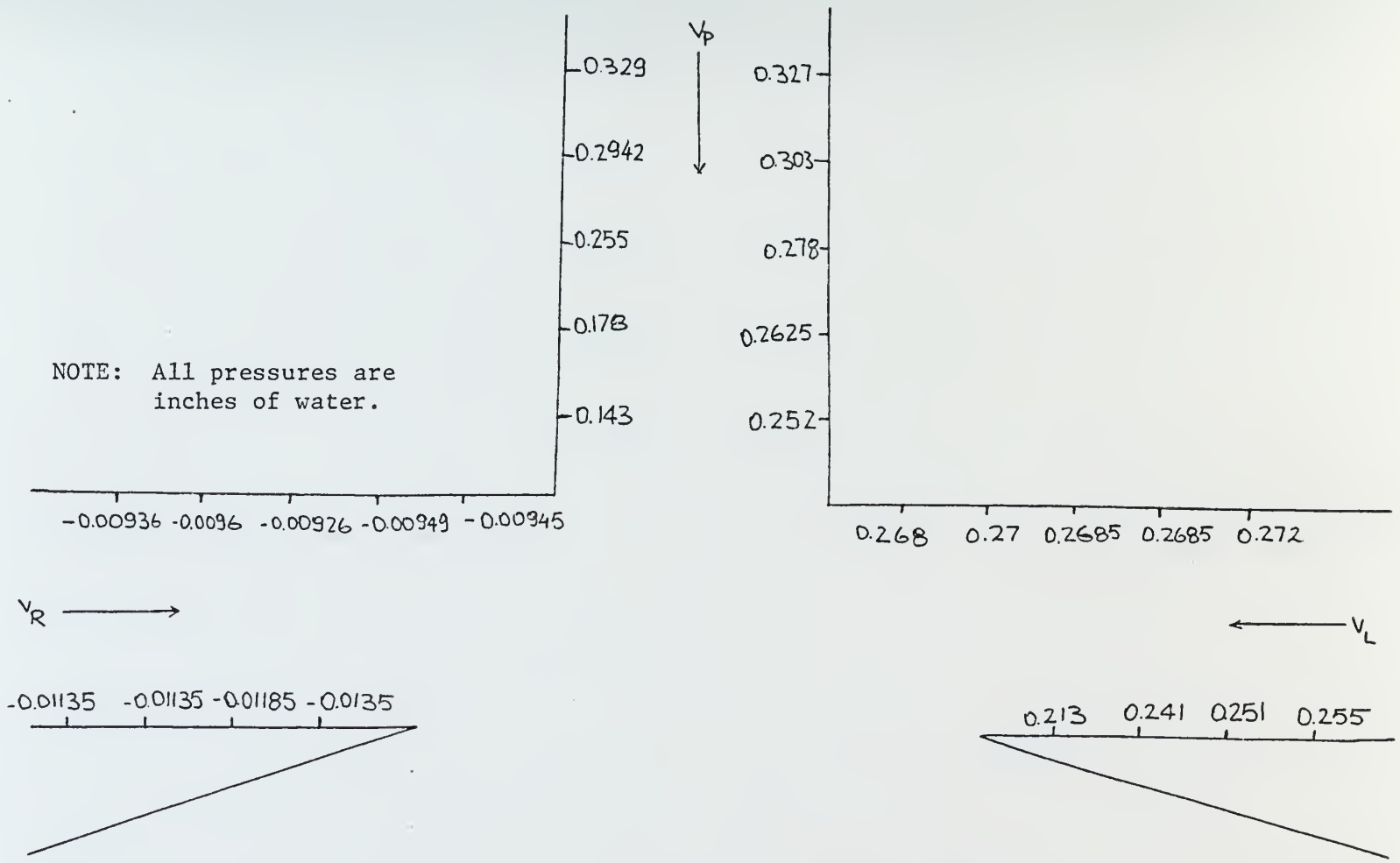

Figure 4. Static Wall Pressures, Re = 15775

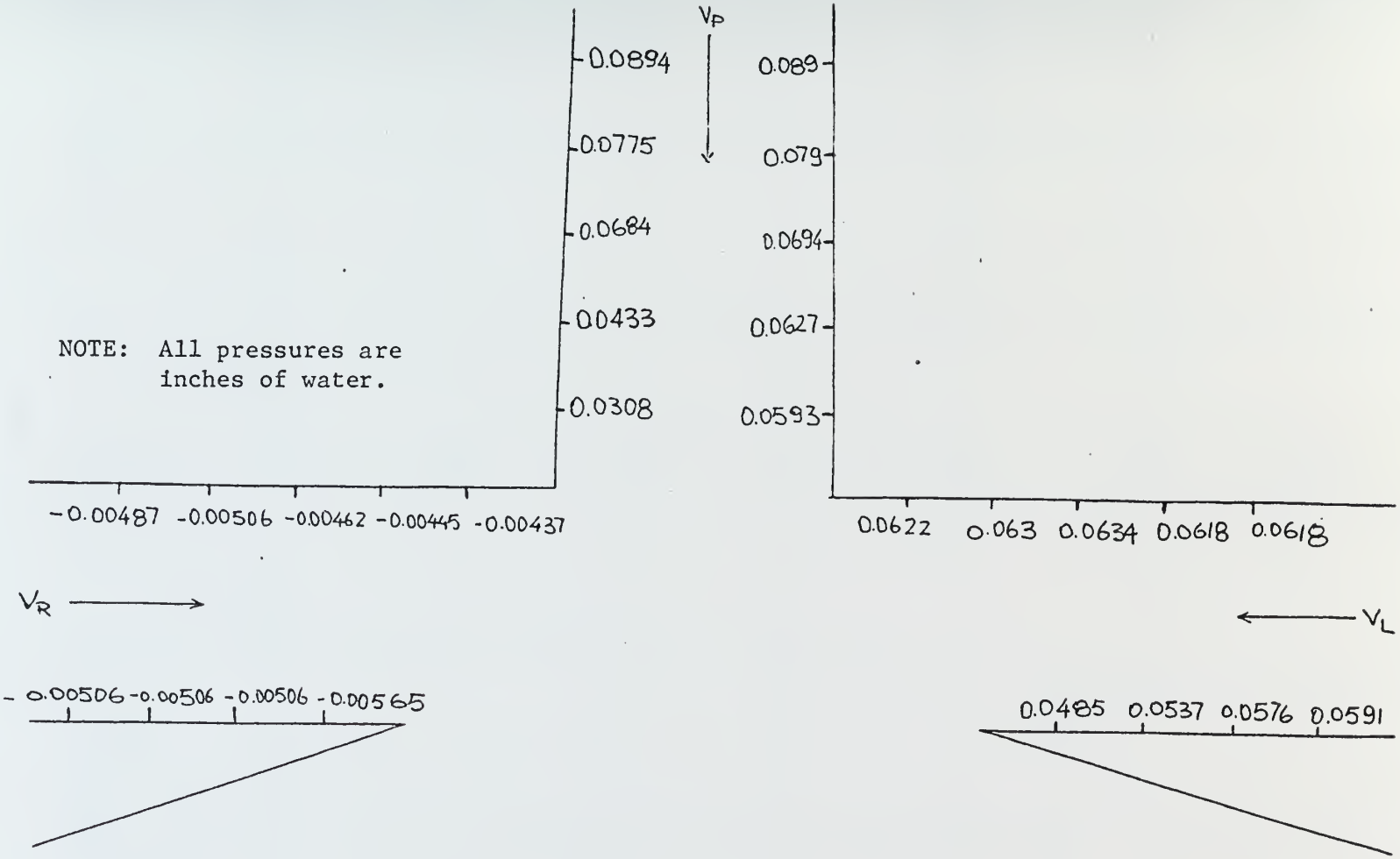

Figure 5. Static Wall Pressures, Re = 7887

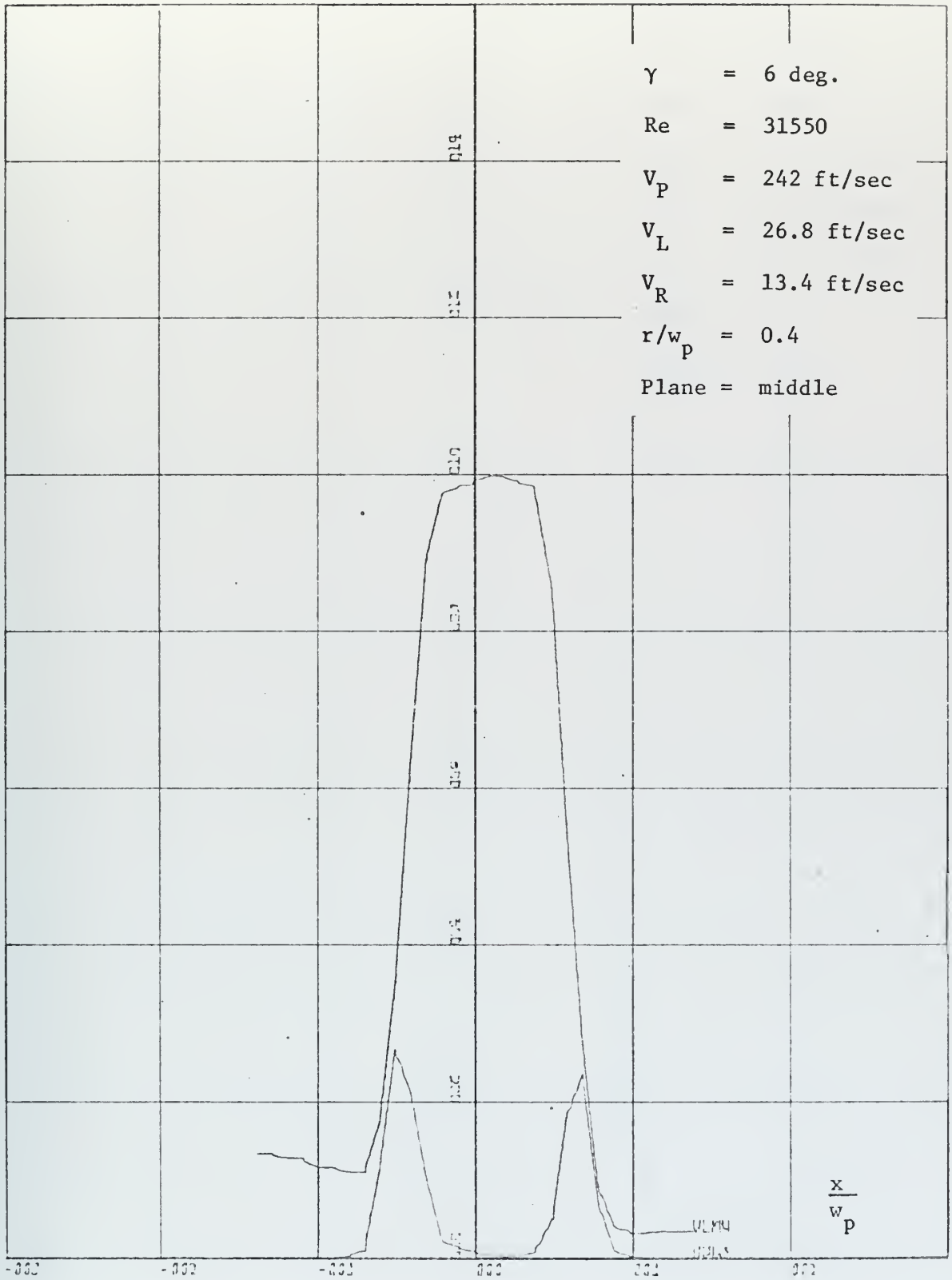

Figure 6. Mean Velocity and Noise

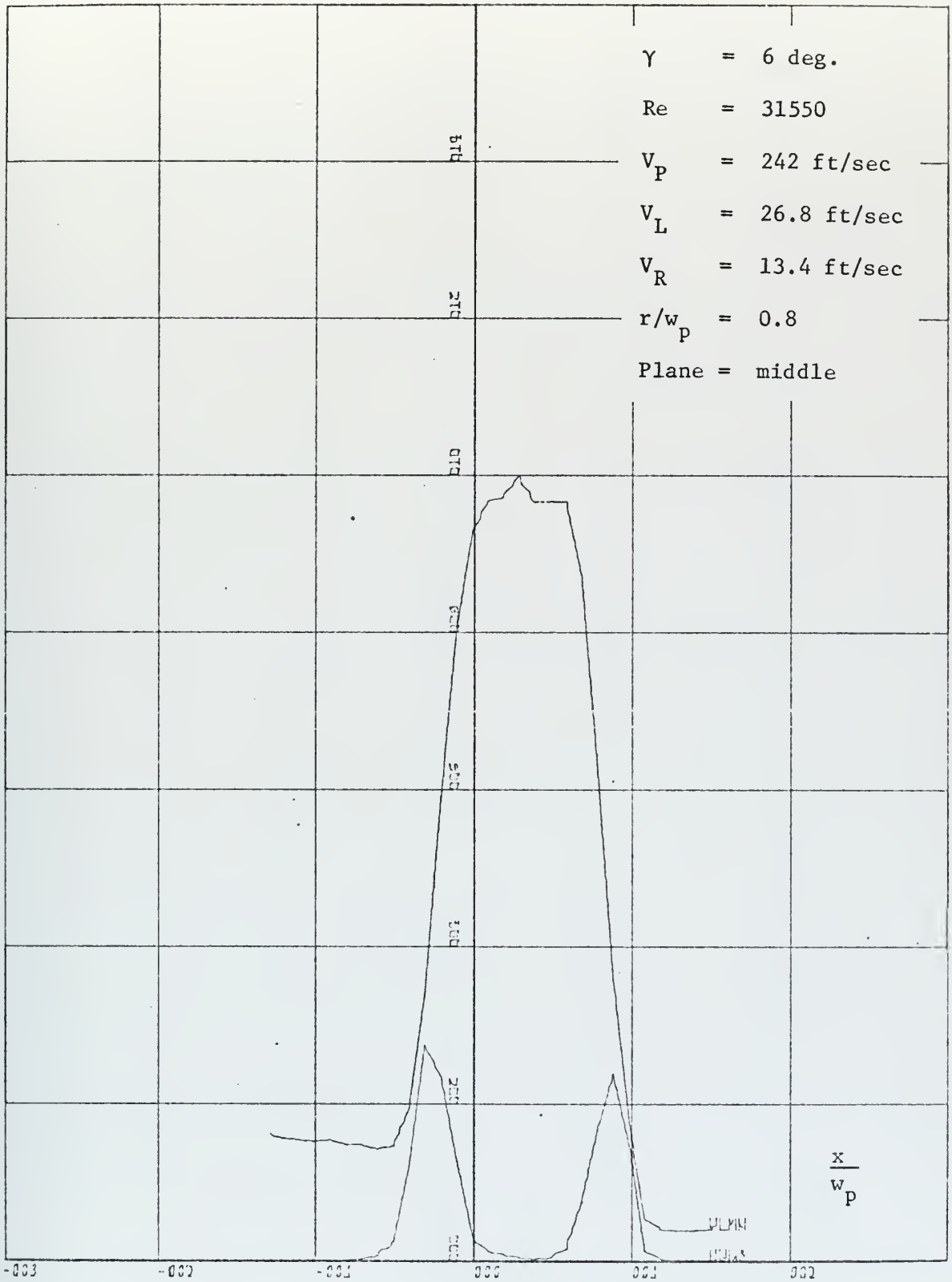

Figure 7. Mean Velocity and Noise

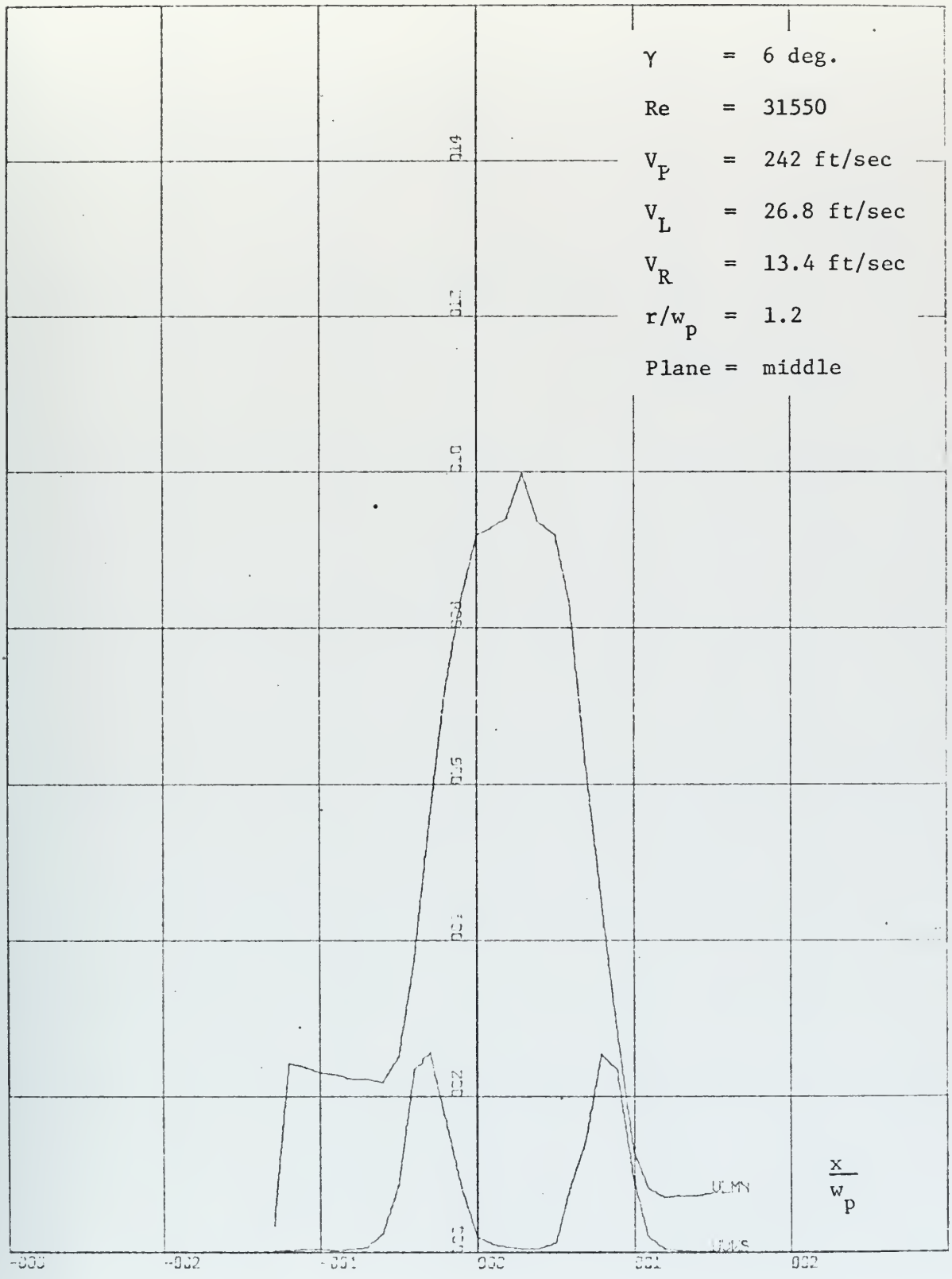

Figure 8. Mean Velocity and Noise

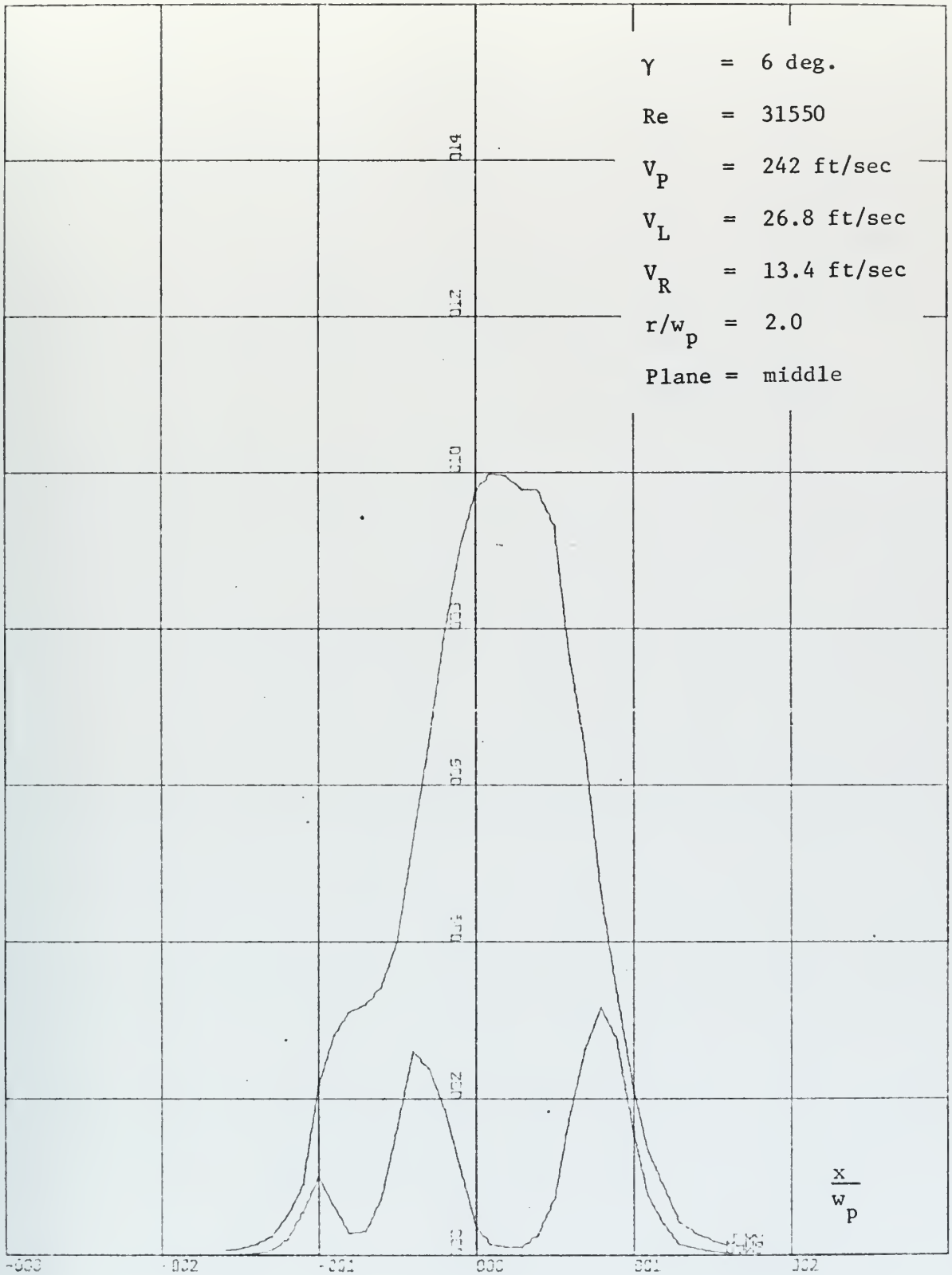

Figure 9. Mean Velocity and Noise

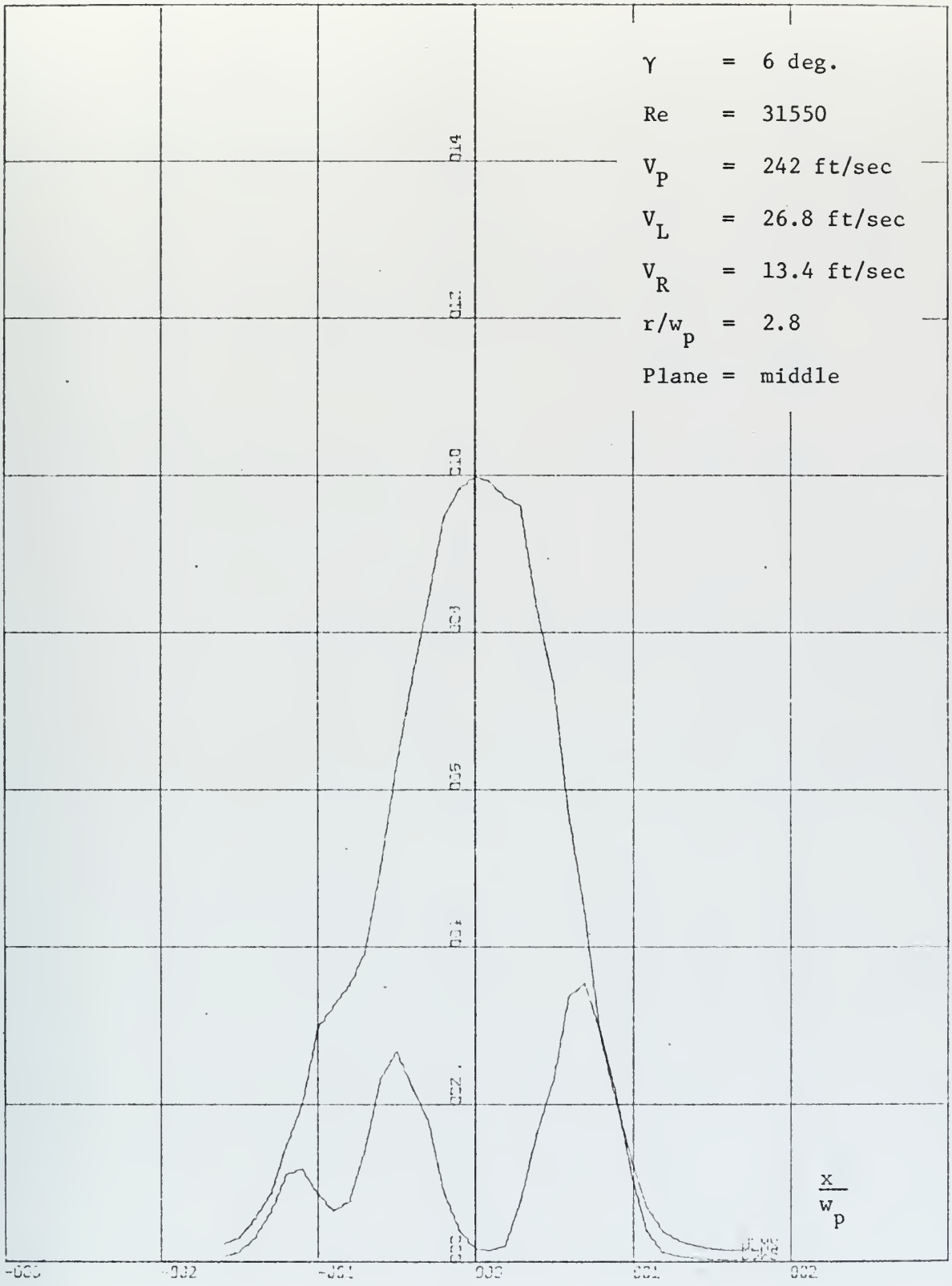

Figure 10. Mean Velocity and Noise

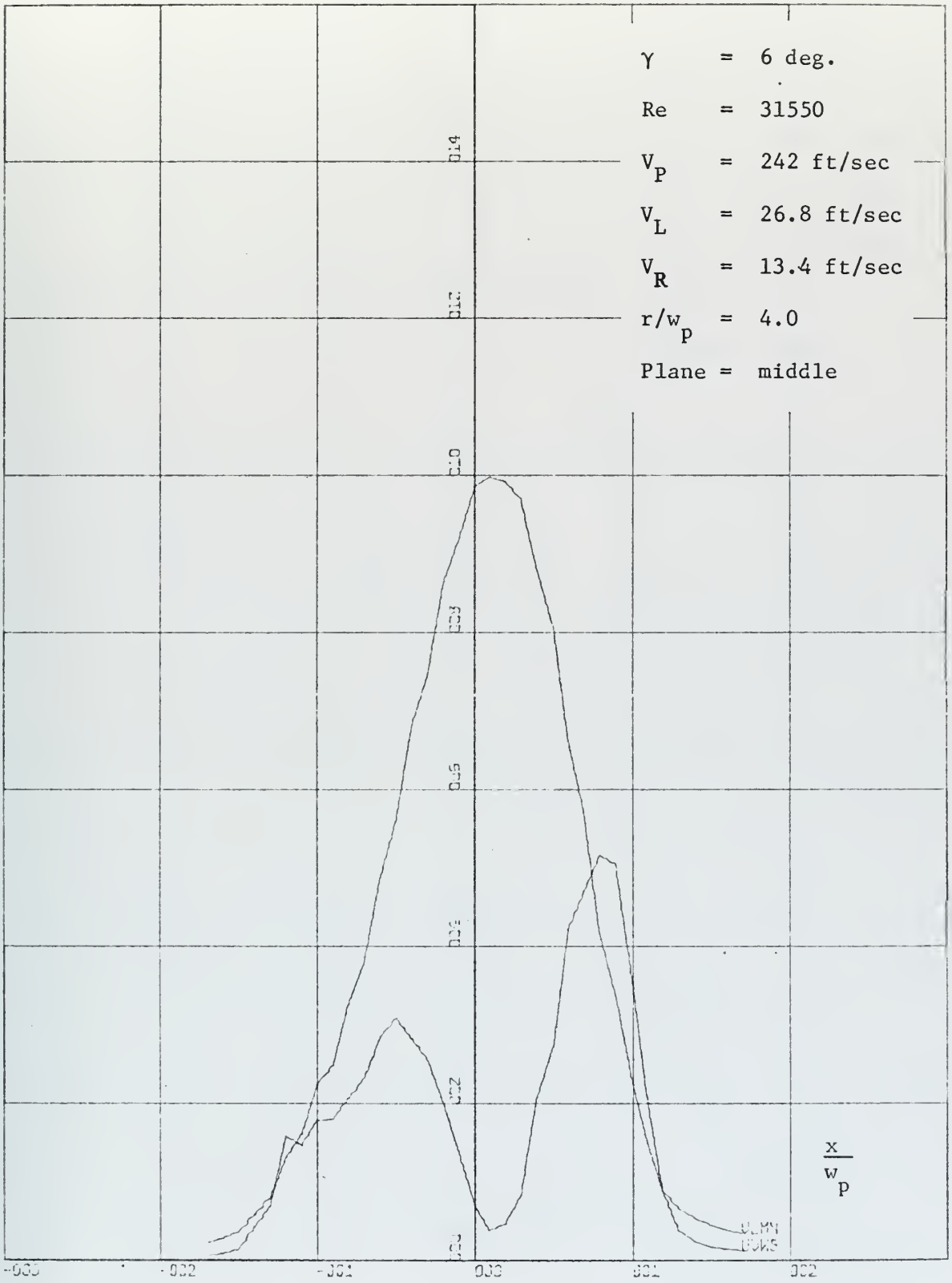

Figure 11. Mean Velocity and Noise

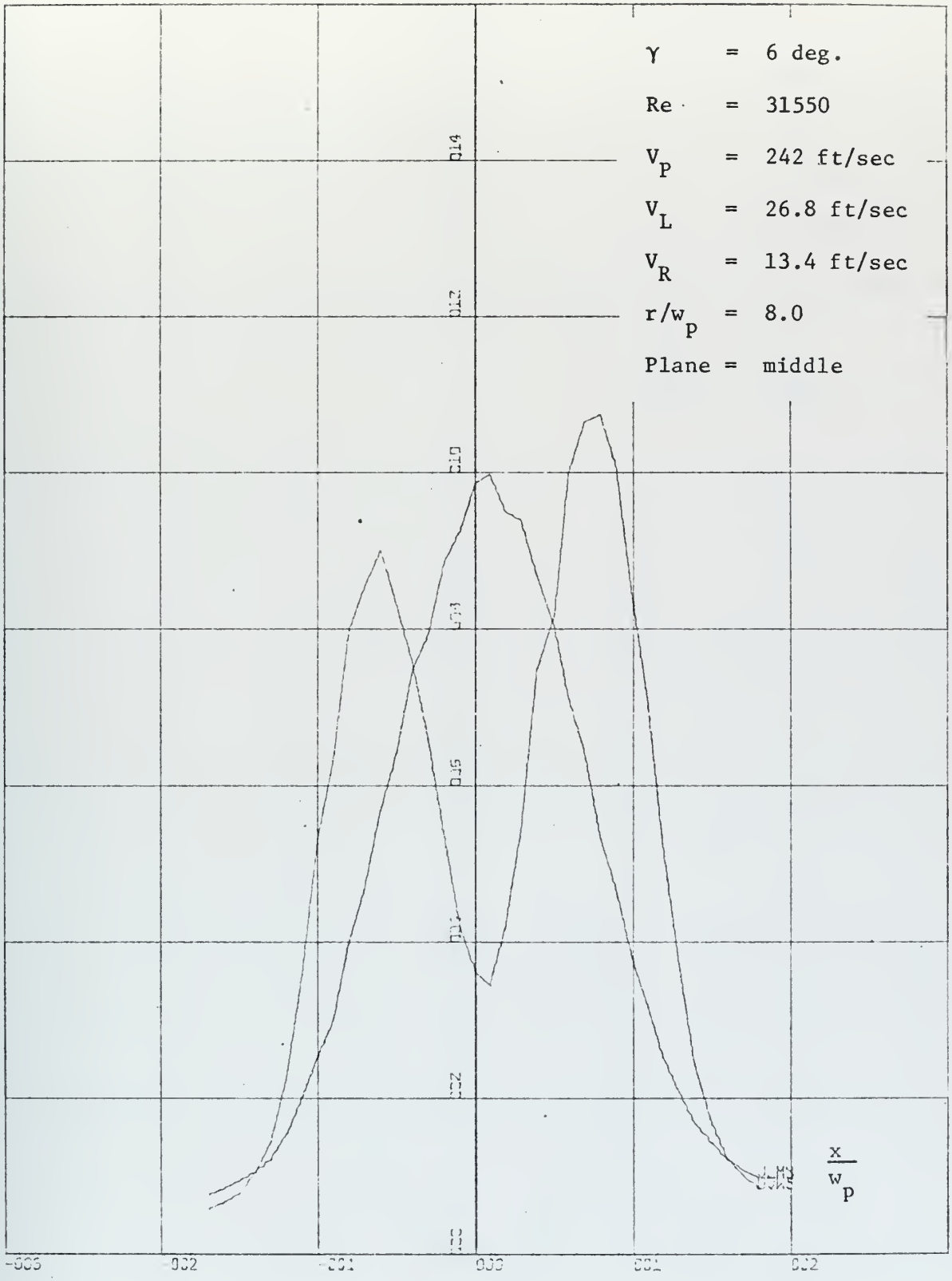

Figure 12. Mean Velocity and Noise

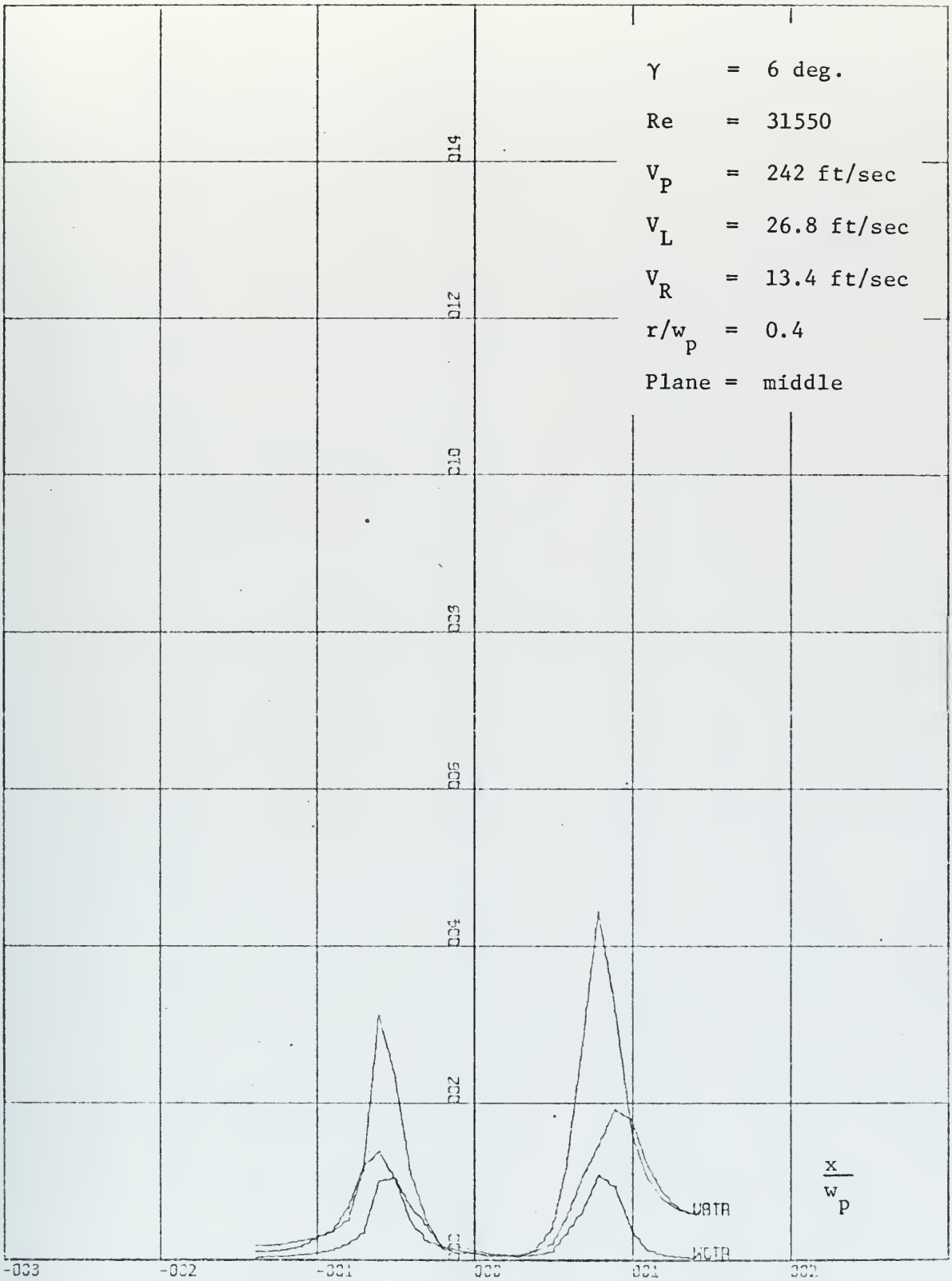

Figure 13. Turbulence Components

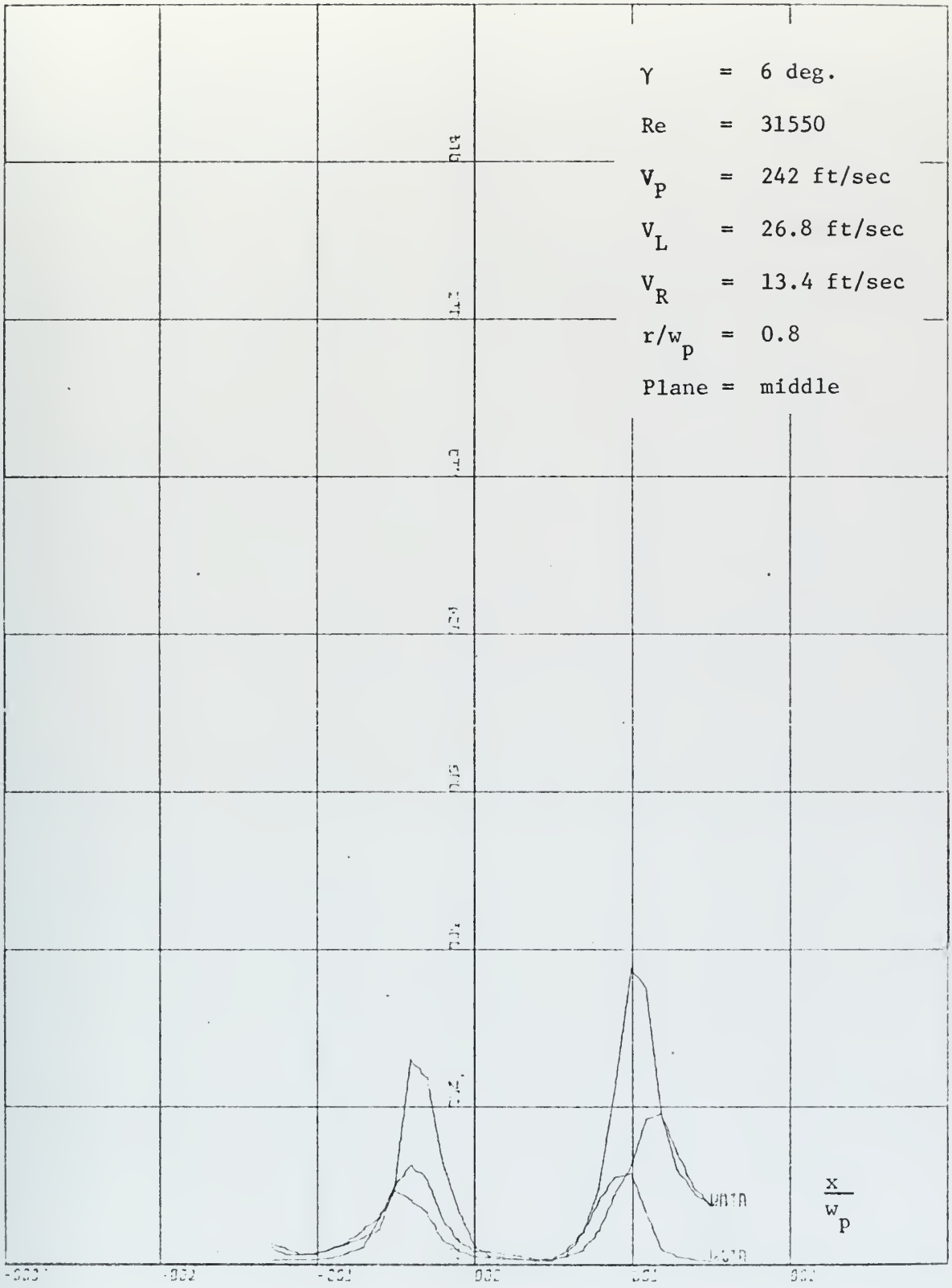

Figure 14. Turbulence Components

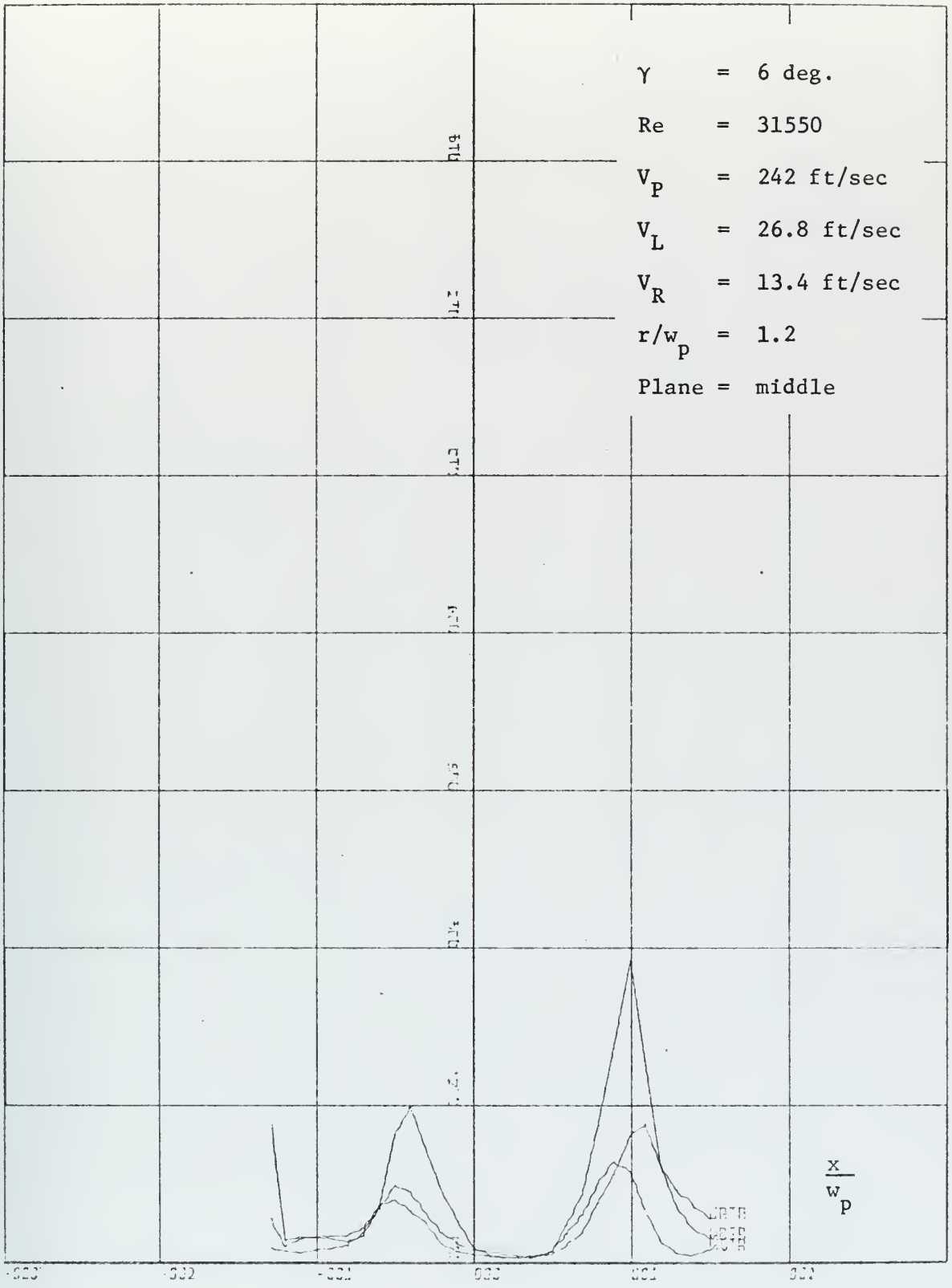

Figure 15. Turbulence Components

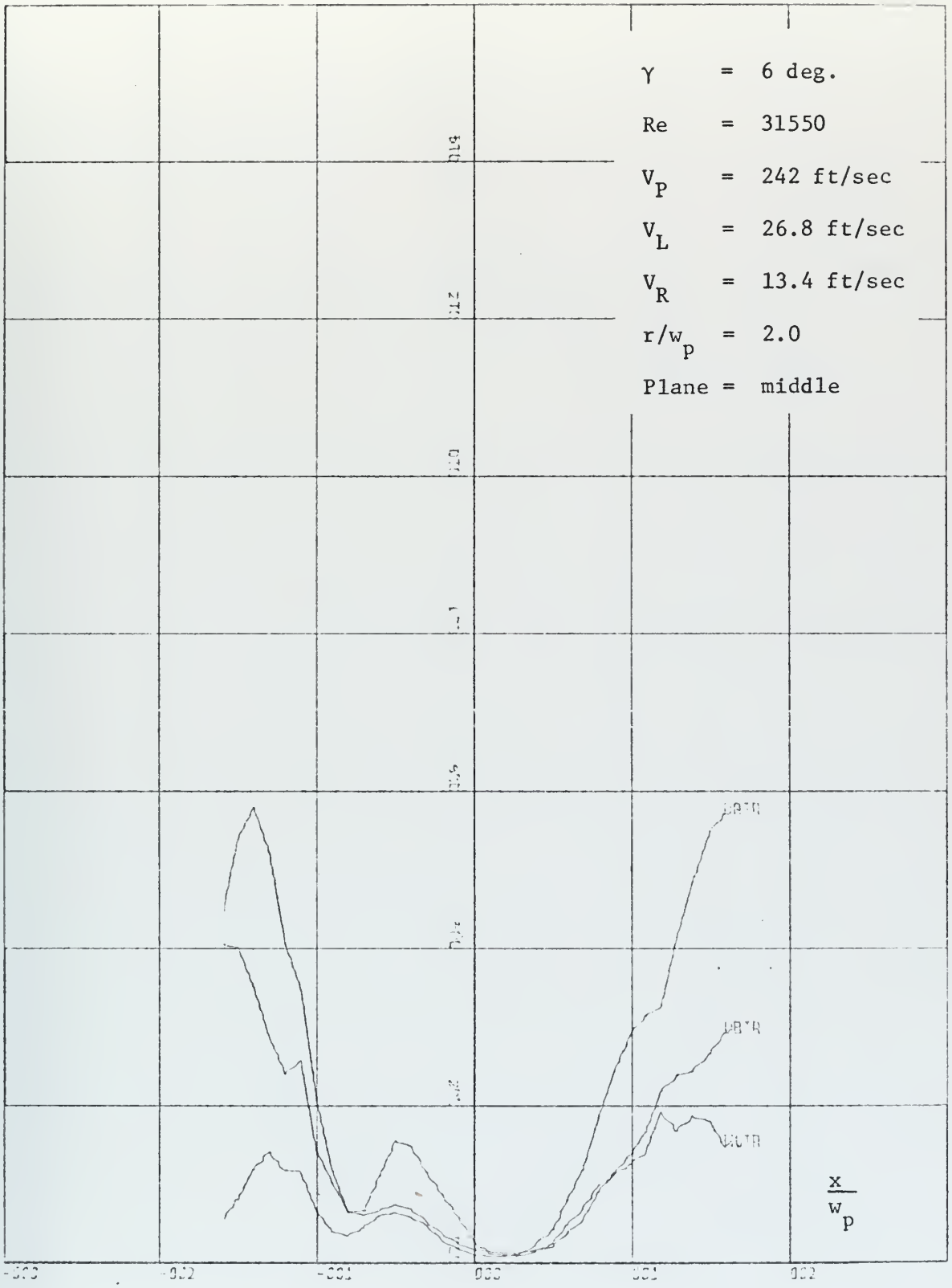

Figure 16. Turbulence Components

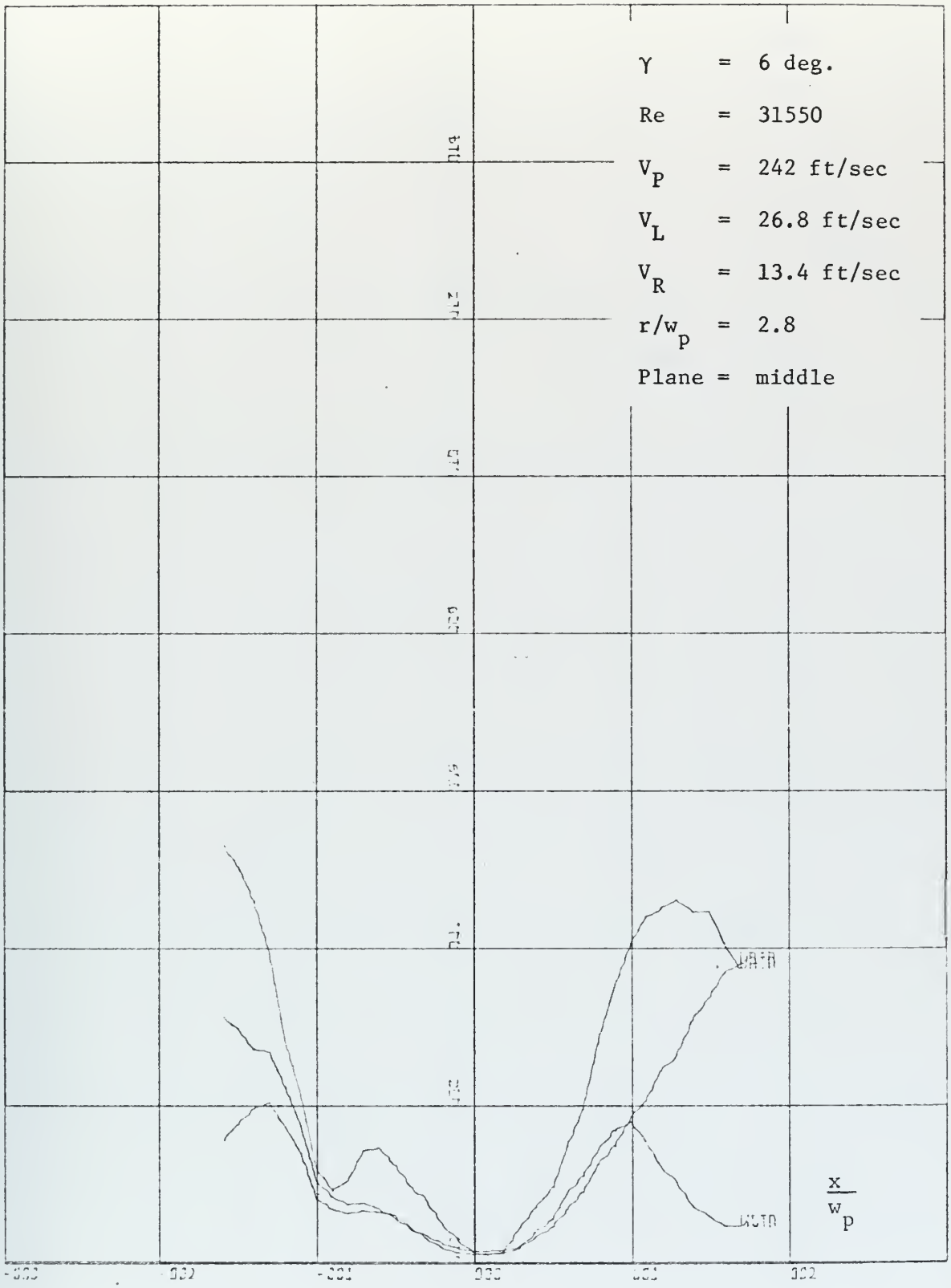

Figure 17. Turbulence Components

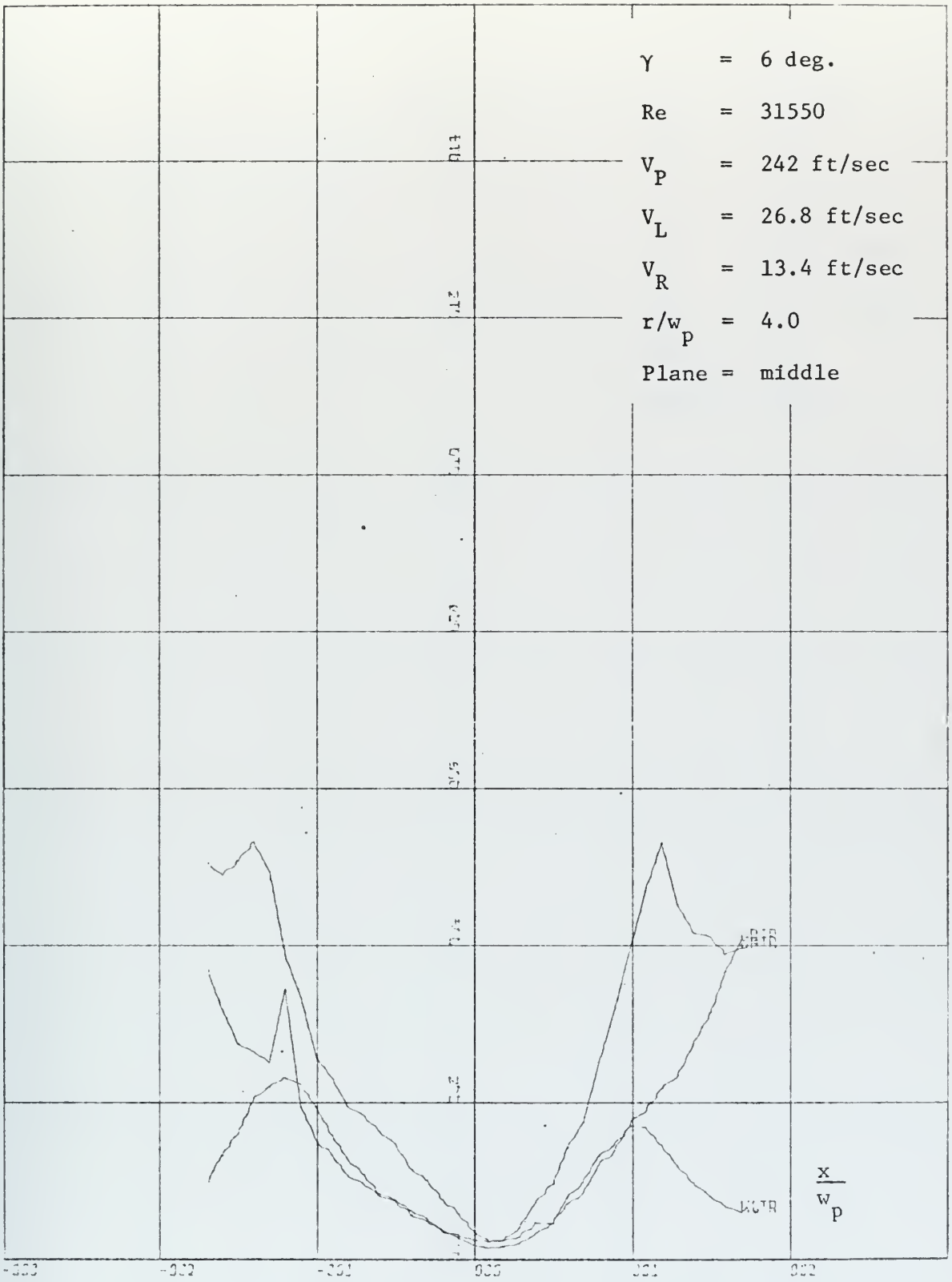

Figure 18. Turbulence Components

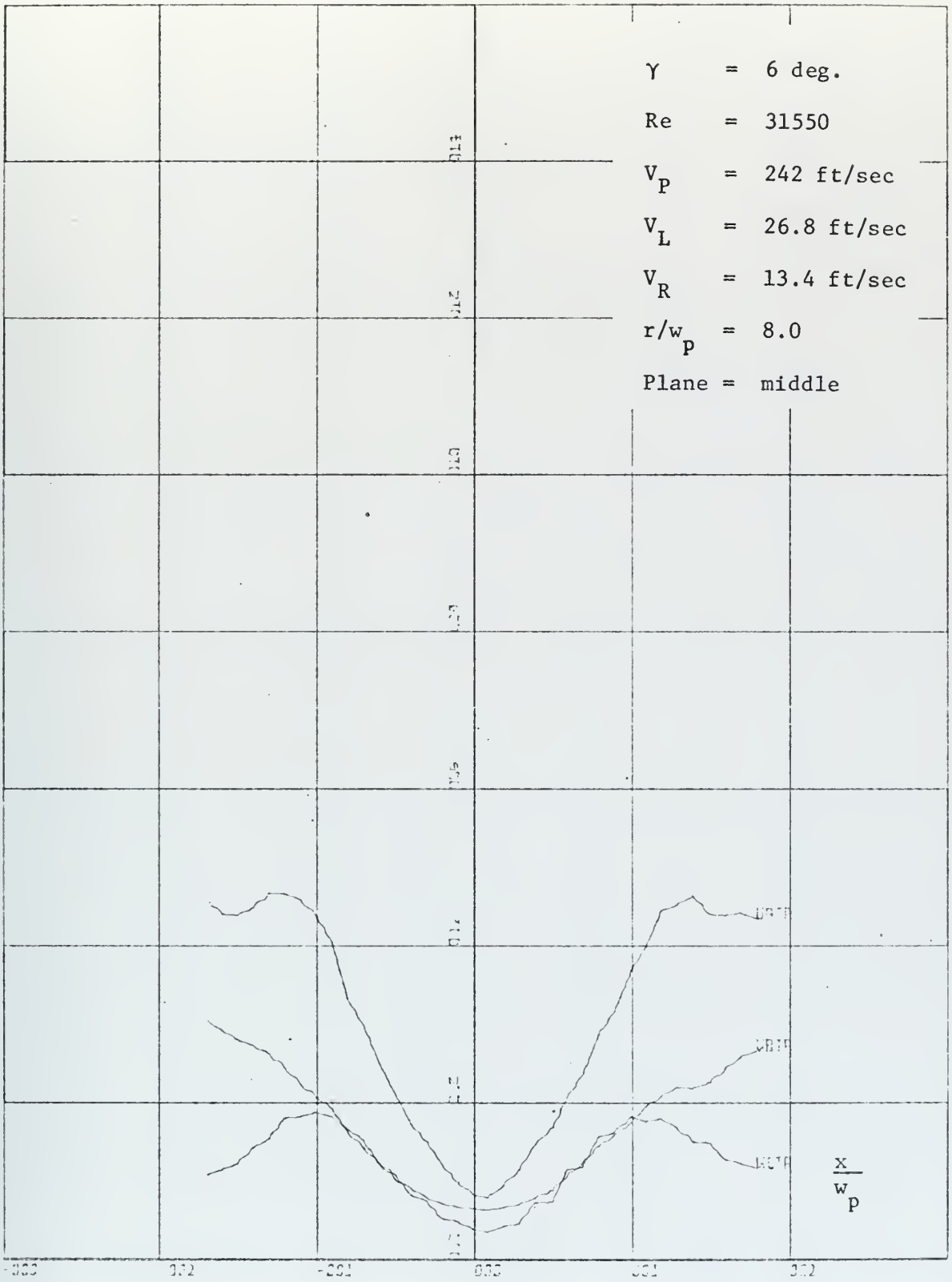

Figure 19. Turbulence Components

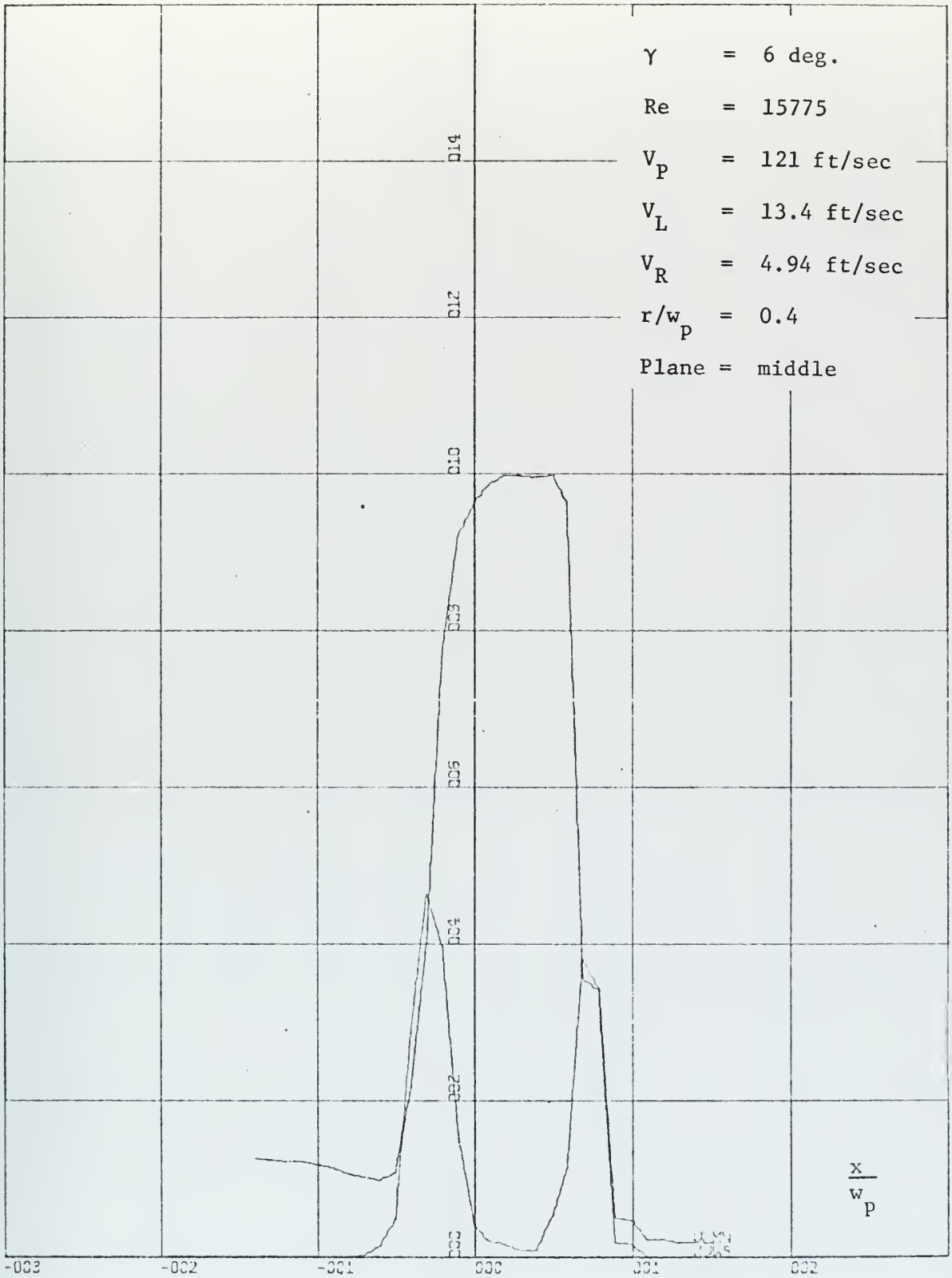

Figure 20. Mean Velocity and Noise

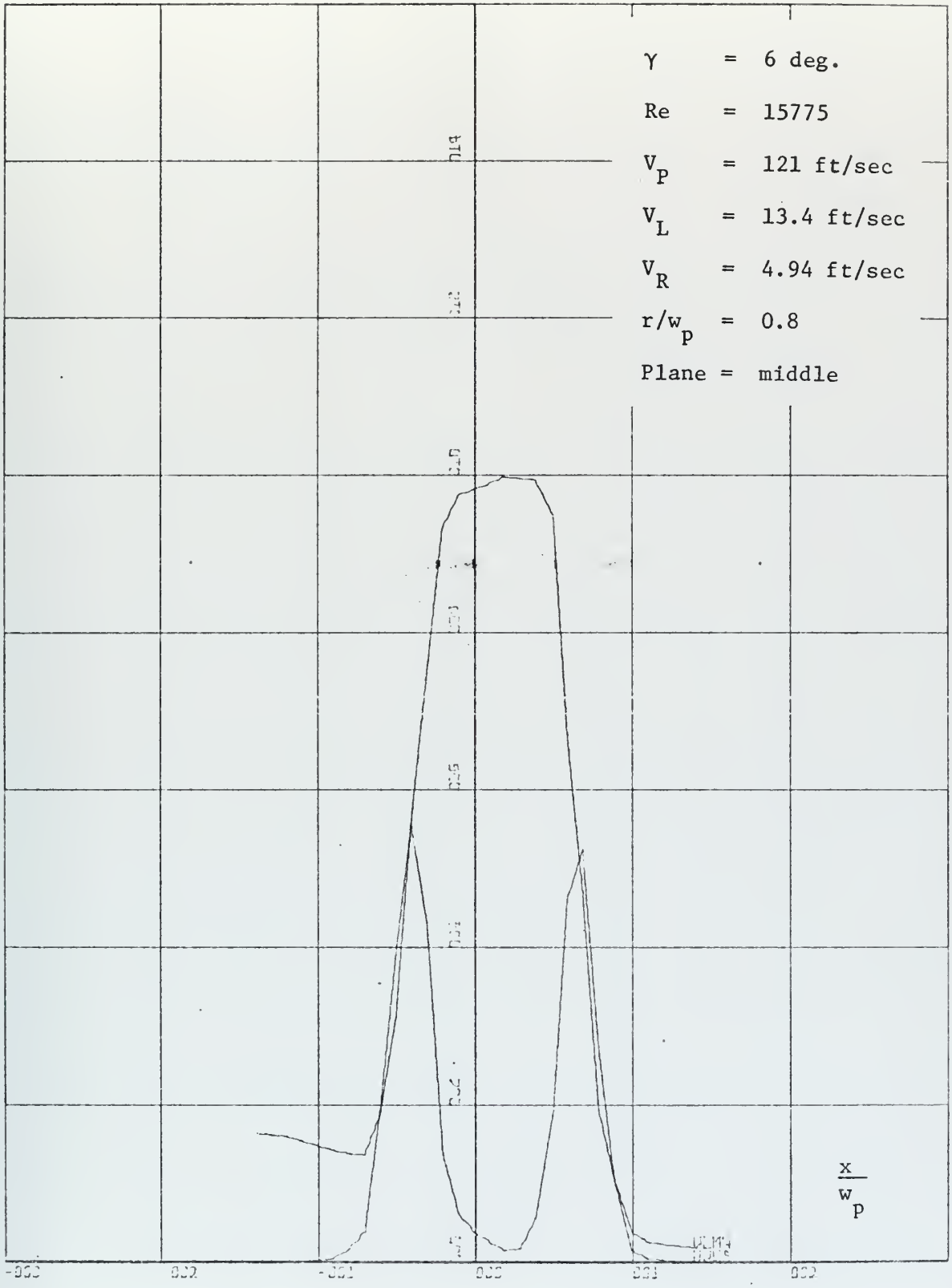

Figure 21. Mean Velocity and Noise

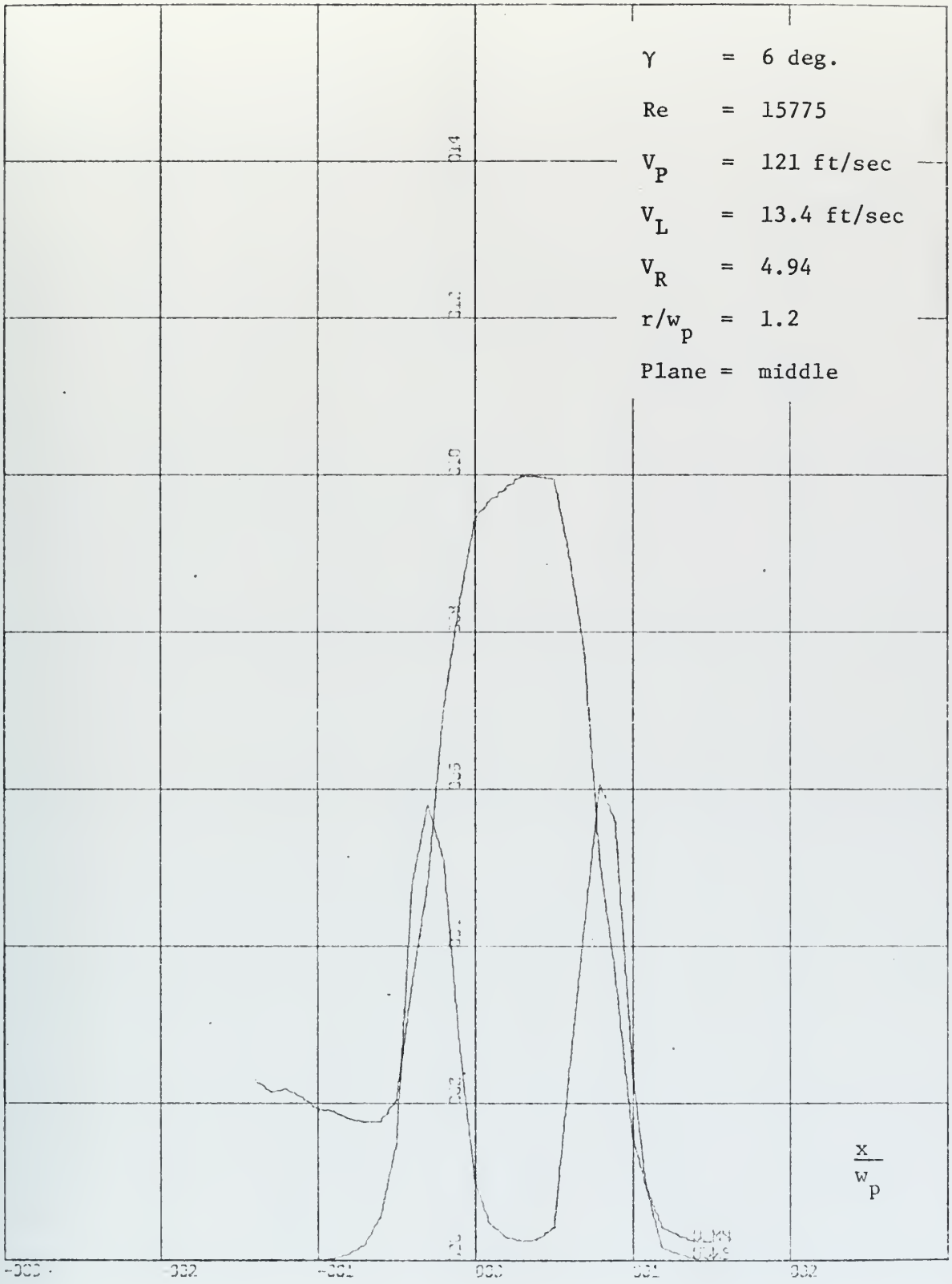

Figure 22. Mean Velocity and Noise

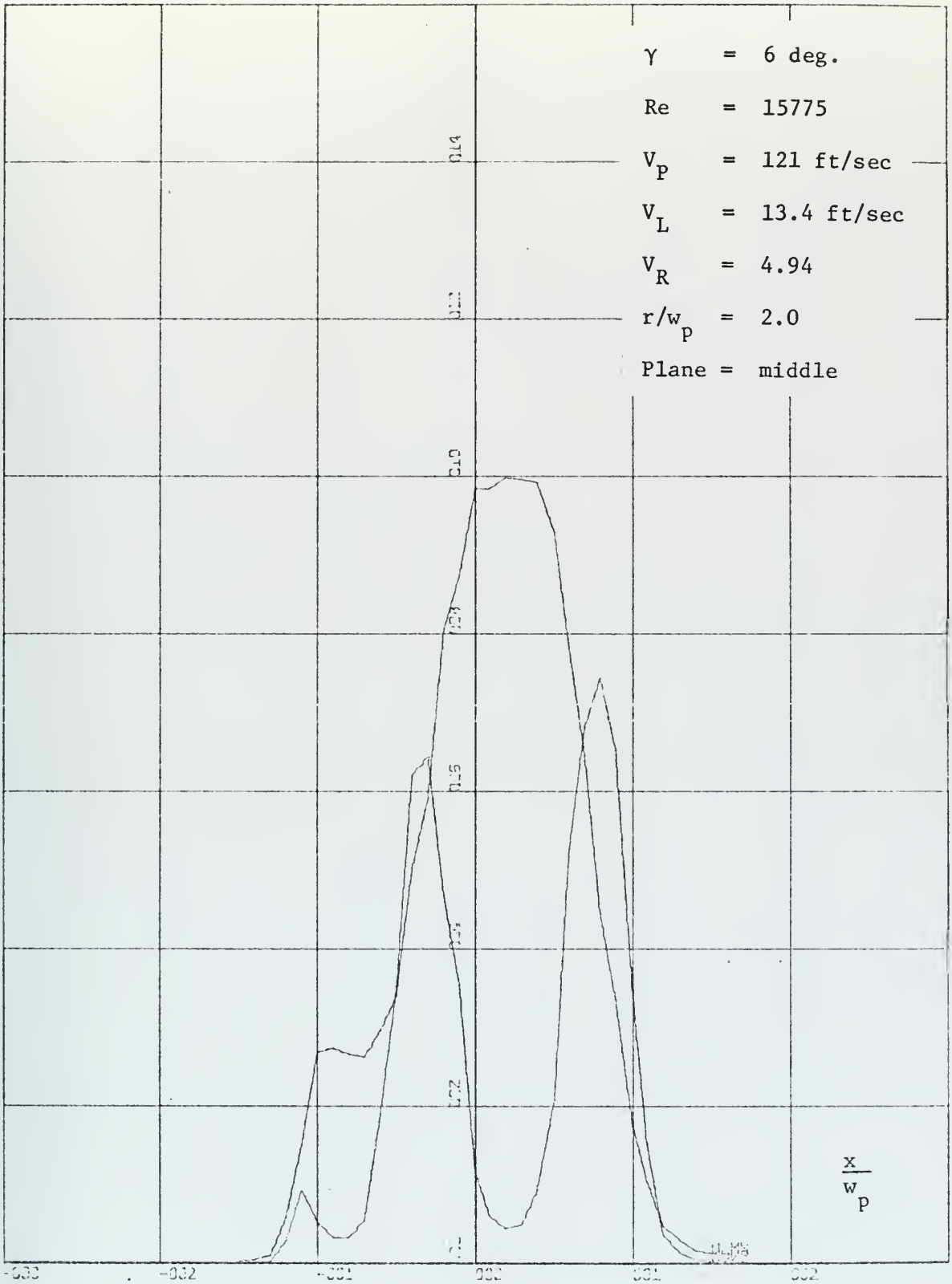

Figure 23. Mean Velocity and Noise

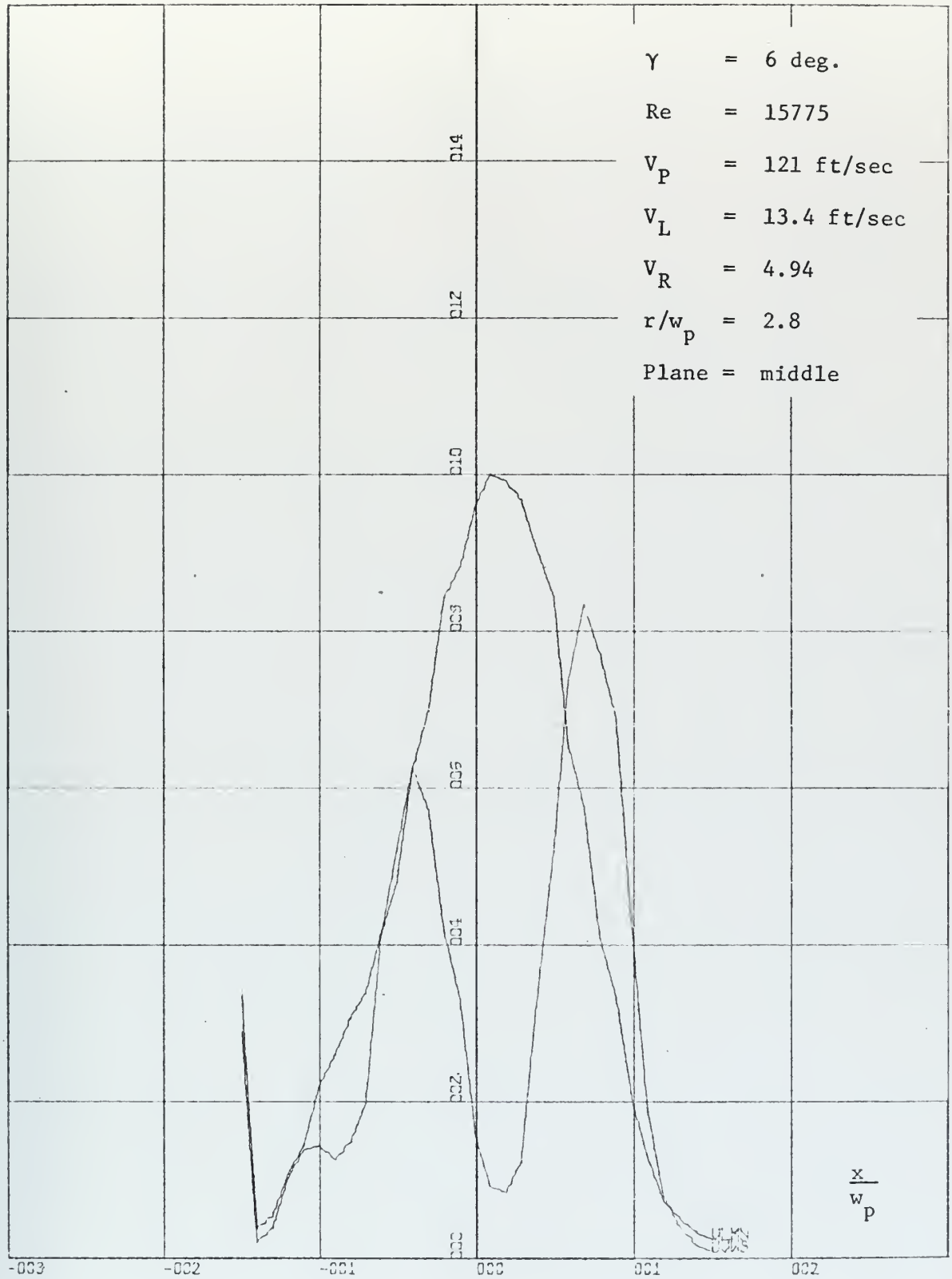

Figure 24. Mean Velocity and Noise

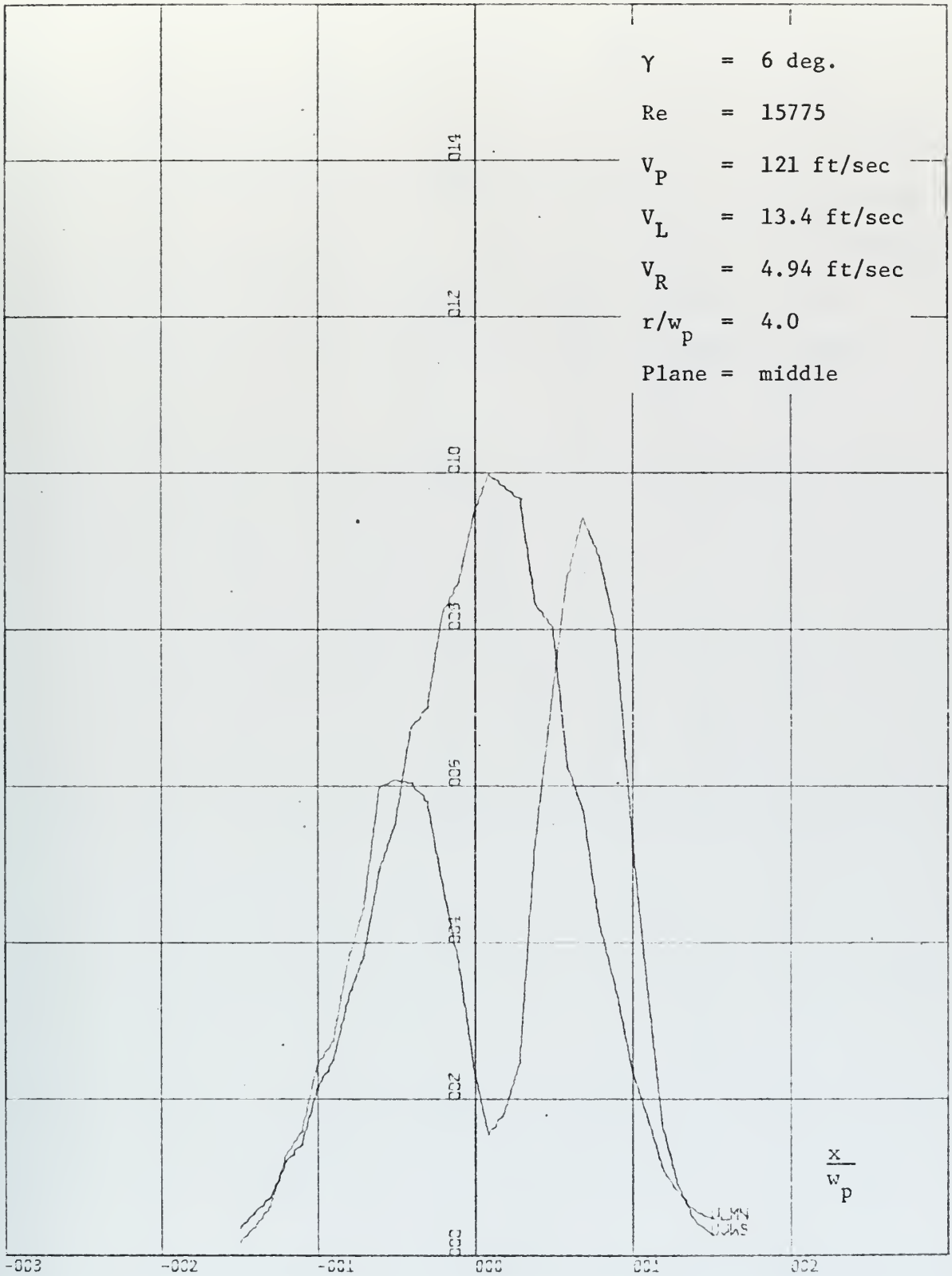

Figure 25. Mean Velocity and Noise

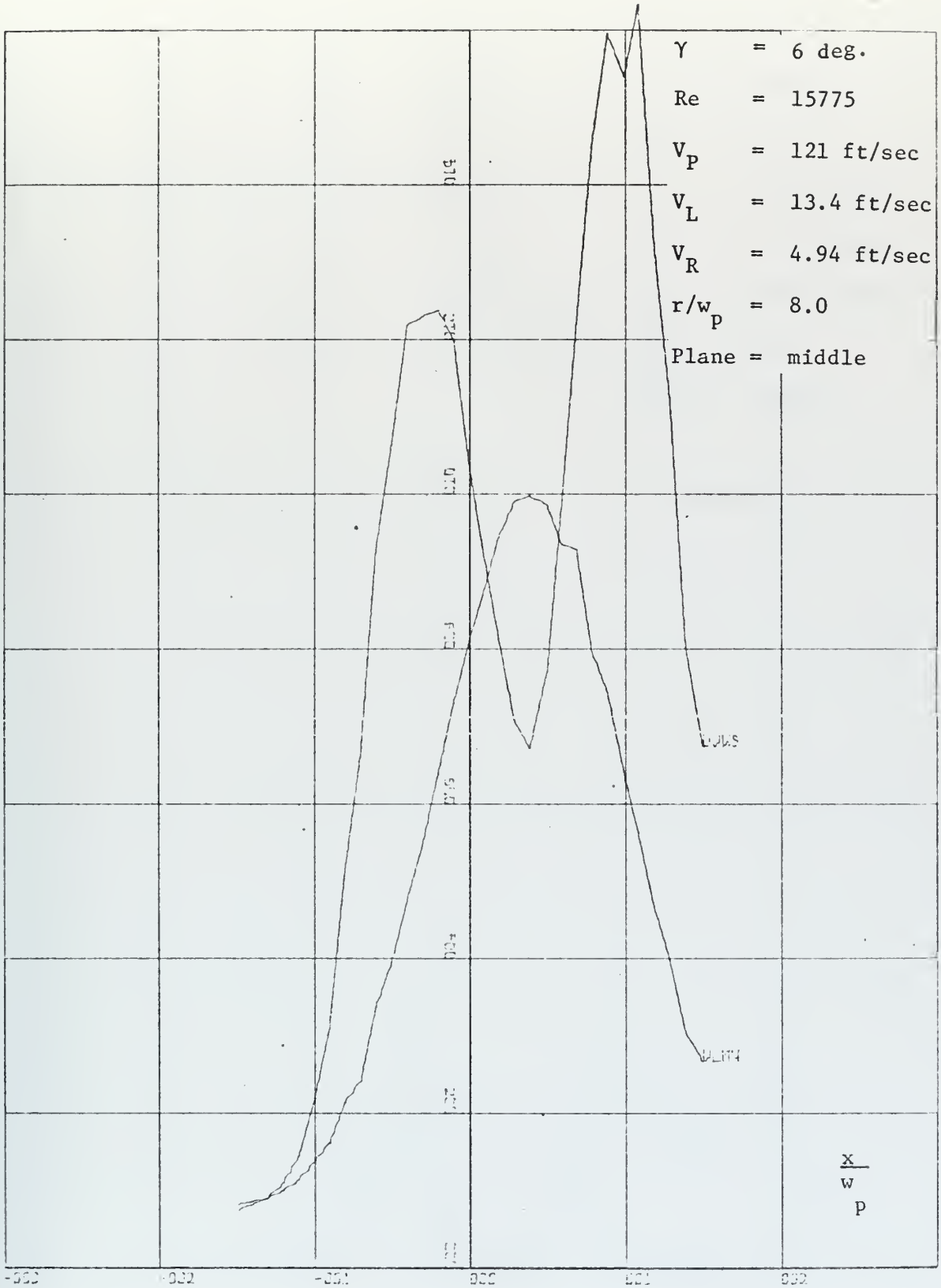

Figure 26. Mean Velocity and Noise

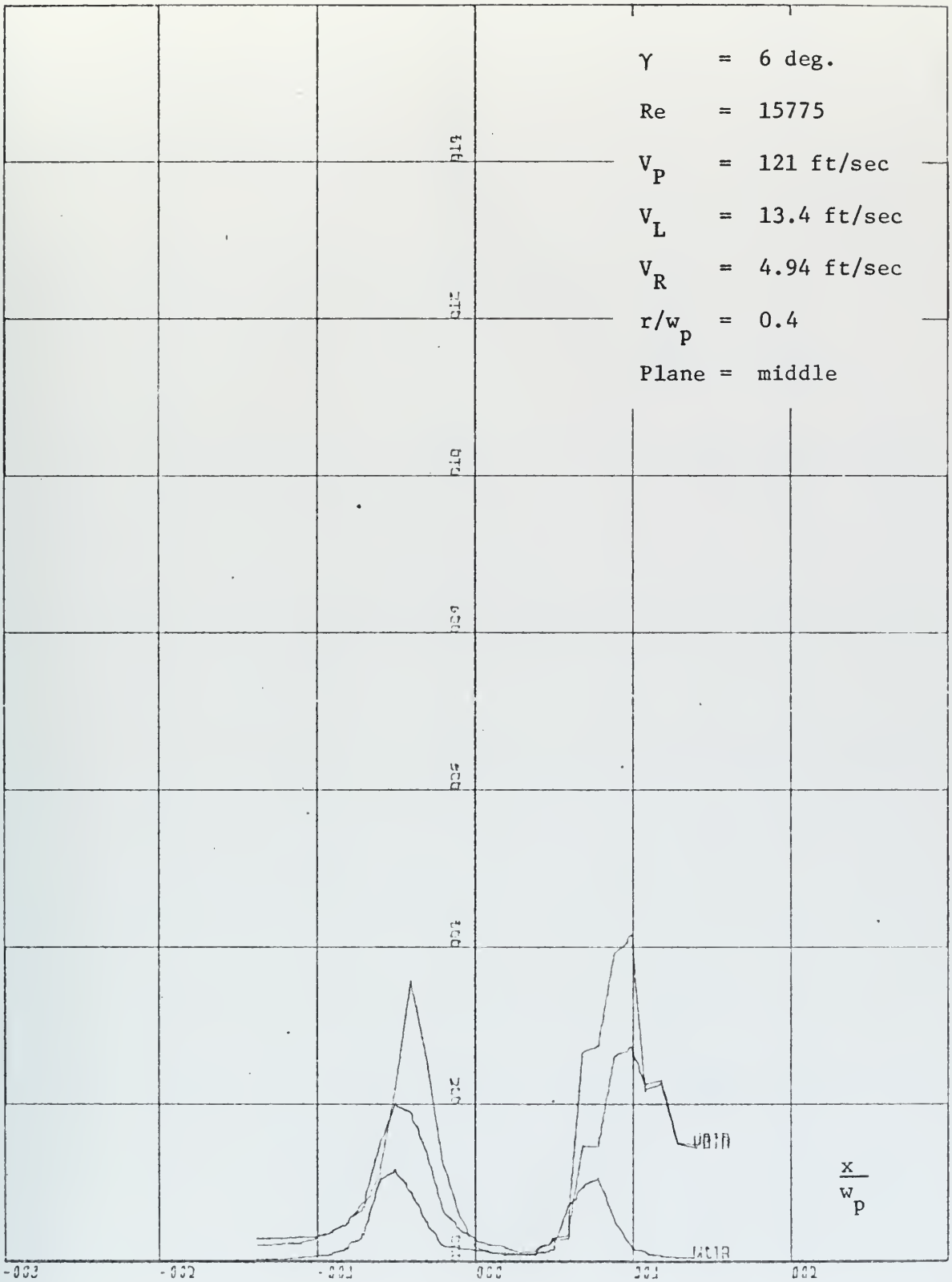

Figure 27. Turbulence Components

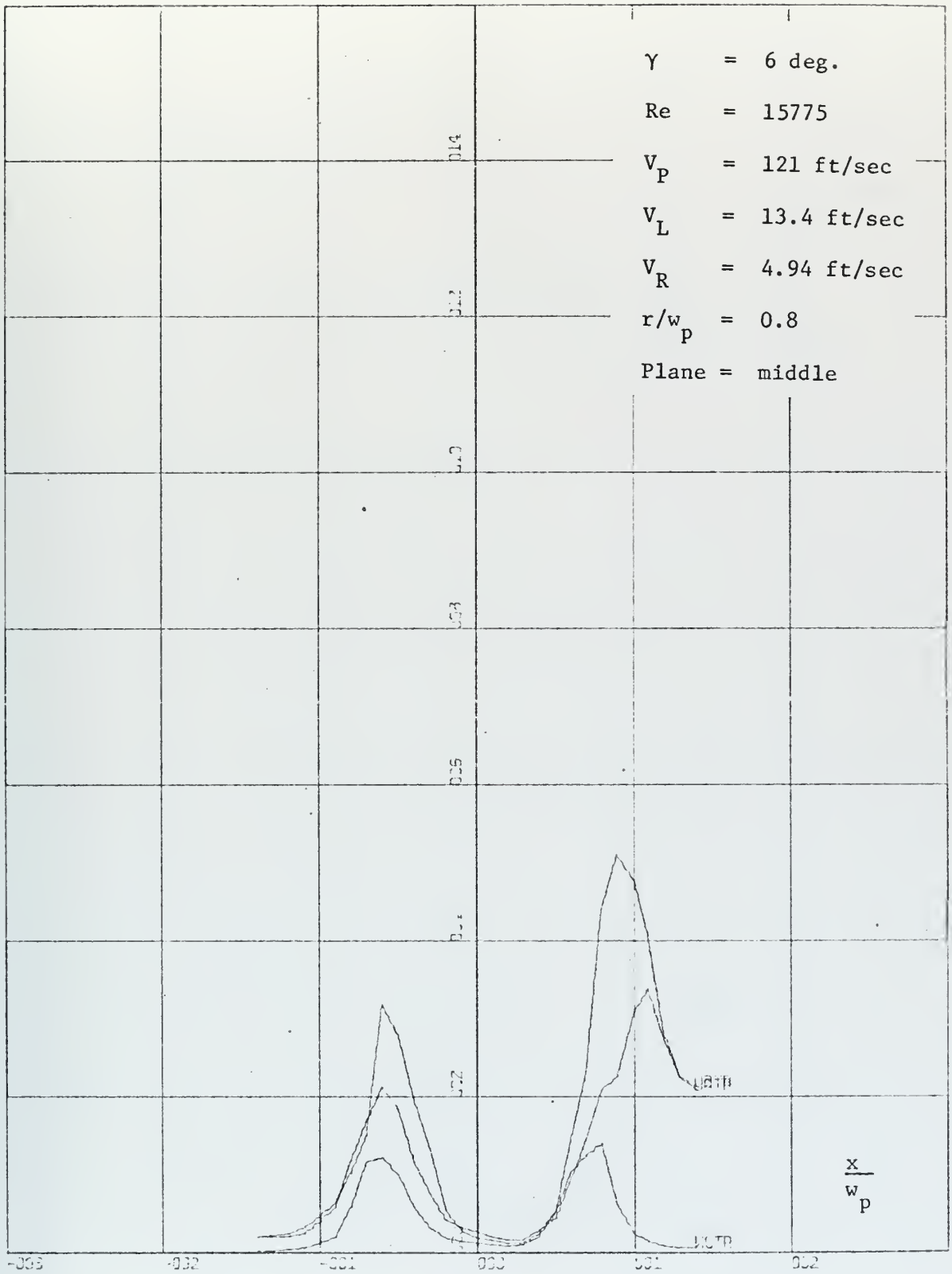

Figure 28. Turbulence Components

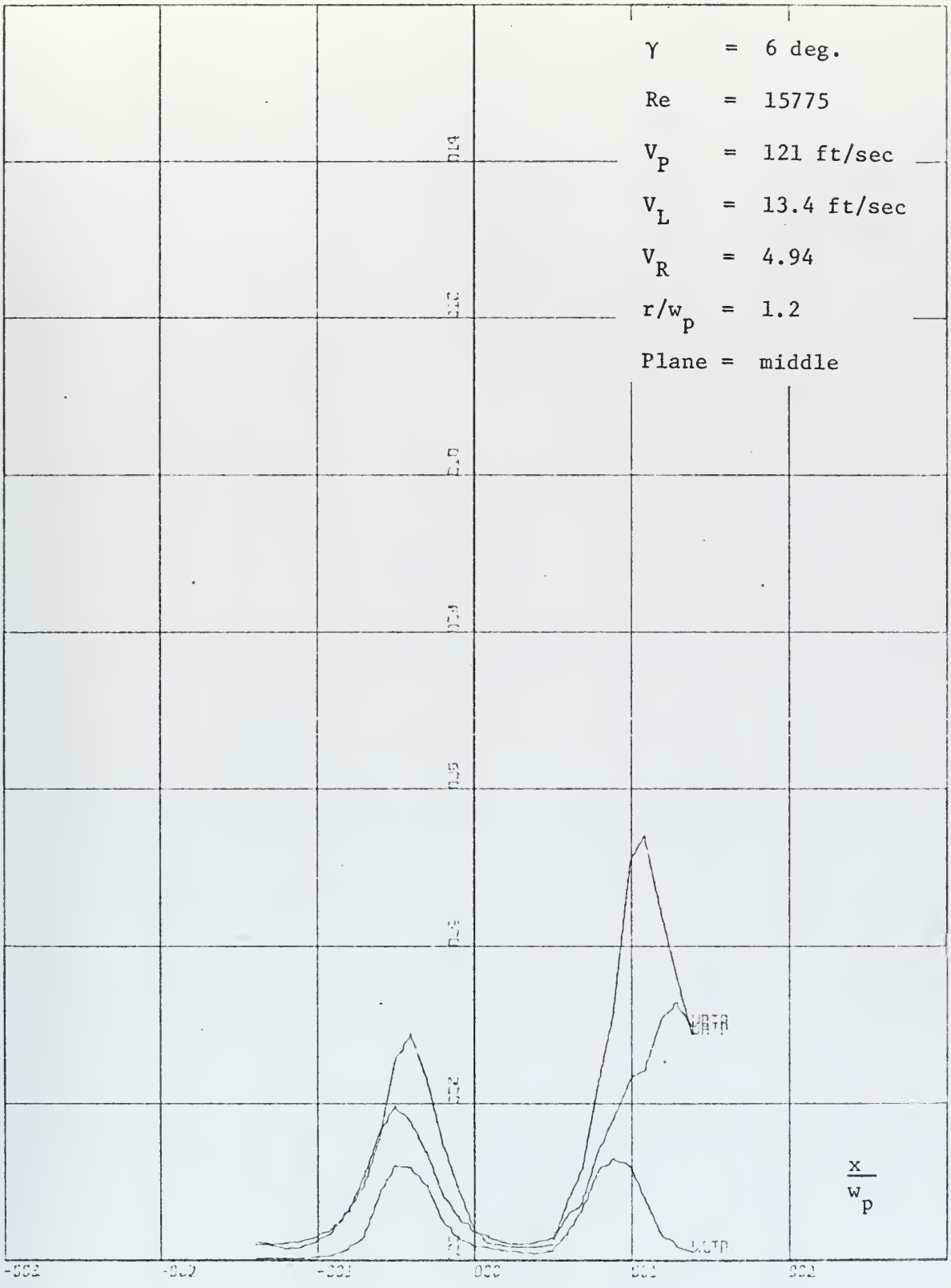

Figure 29. Turbulence Components

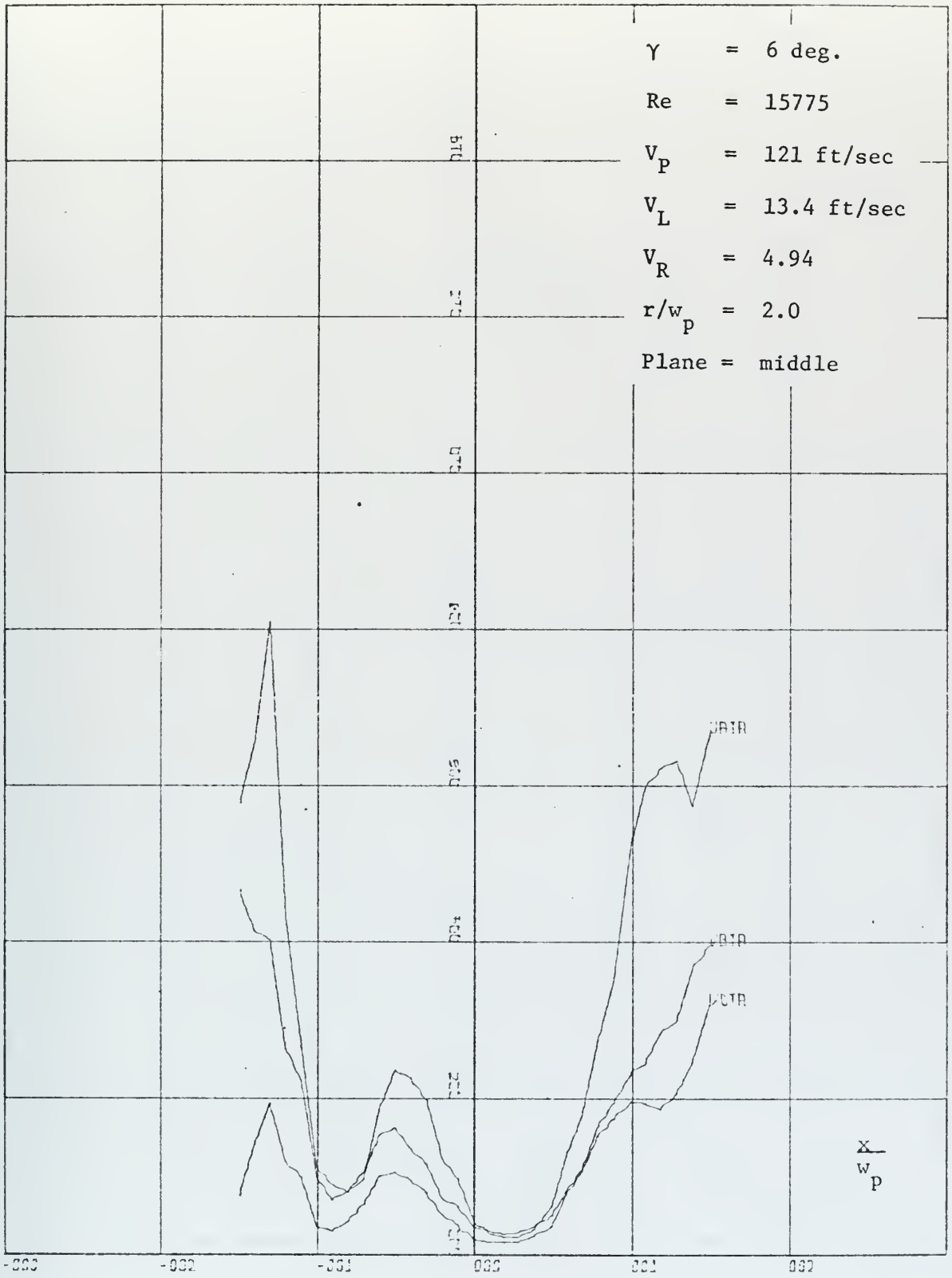

Figure 30. Turbulence Components

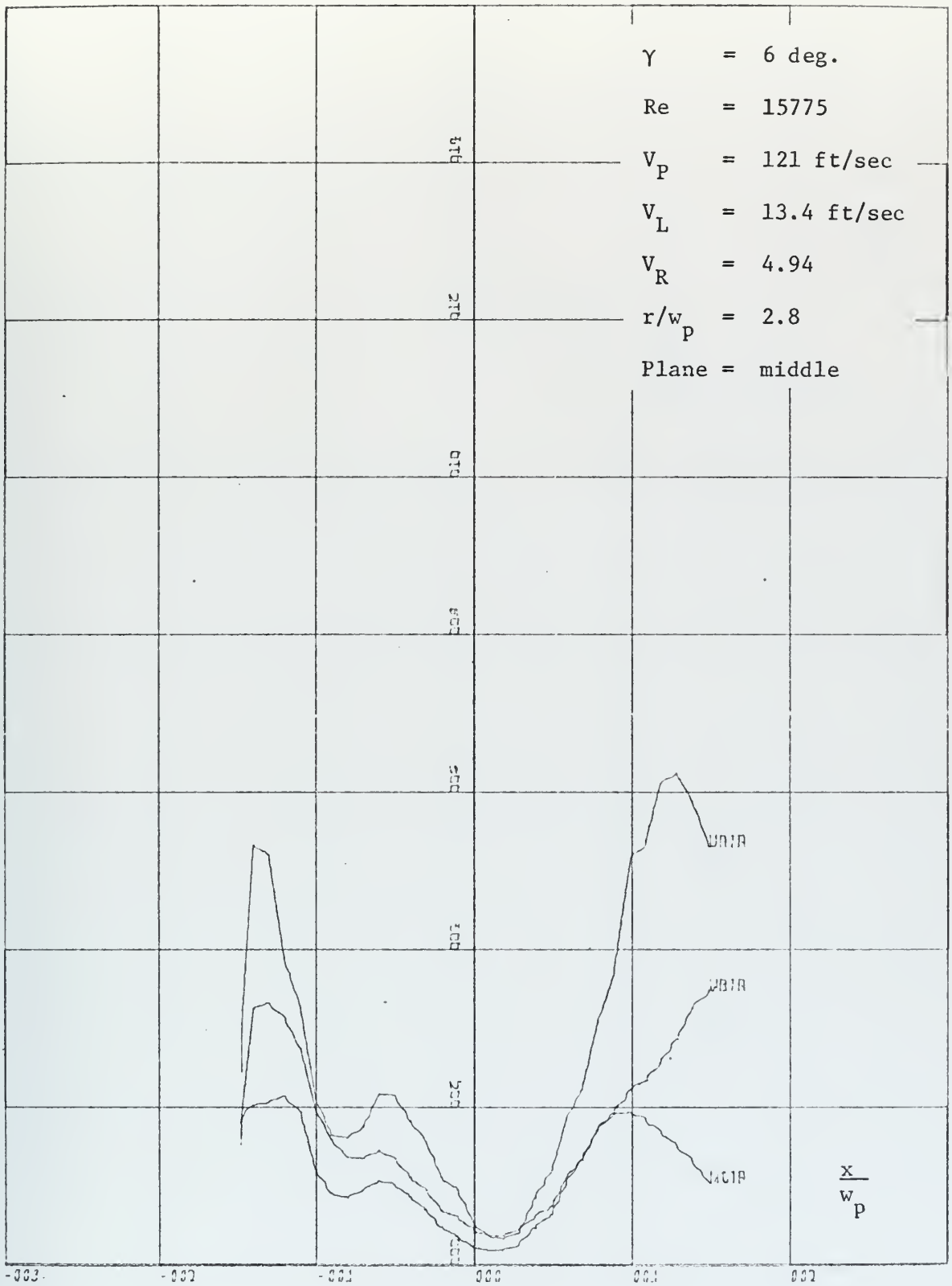

Figure 31. Turbulence Components

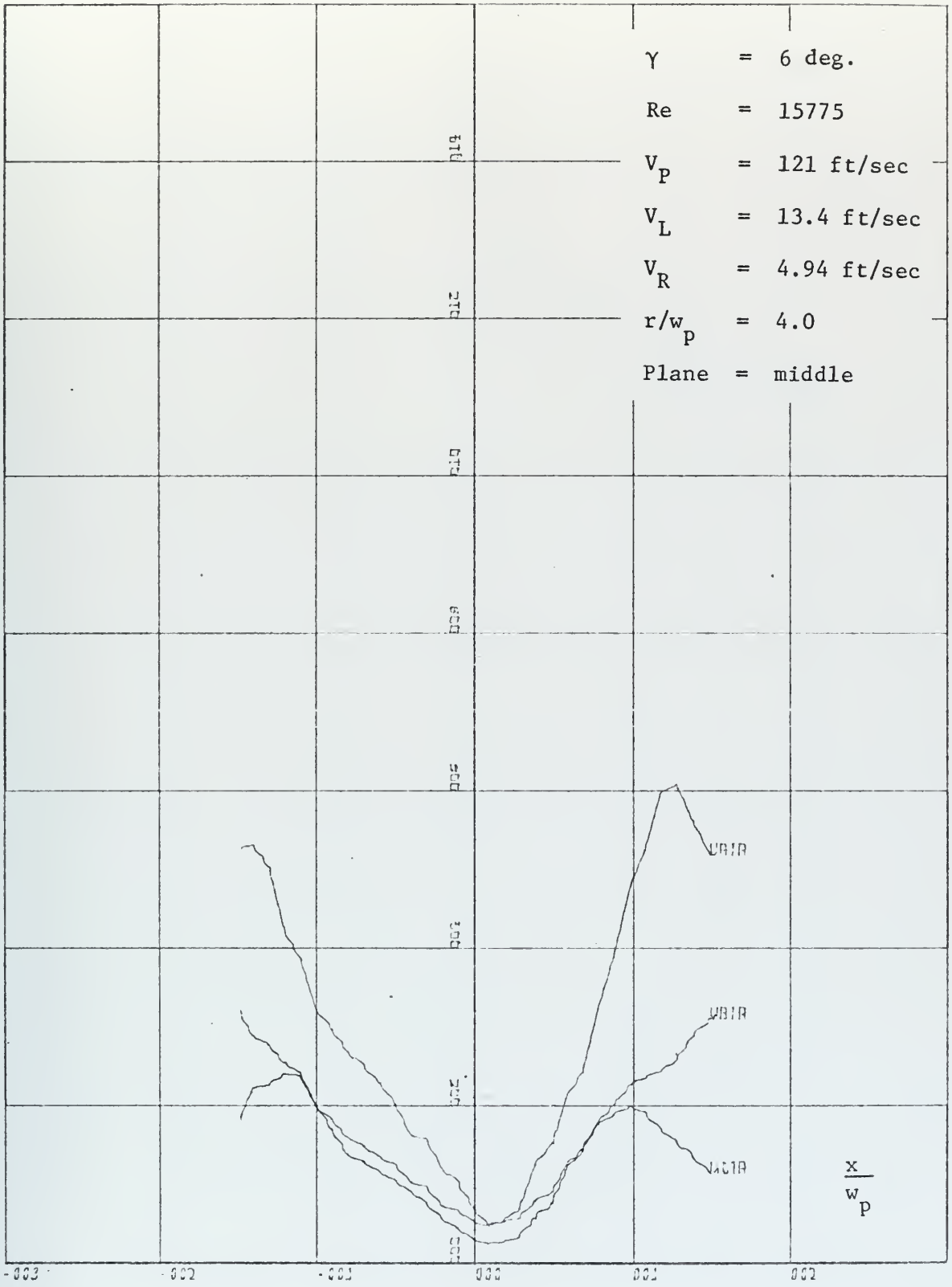

Figure 32. Turbulence Components

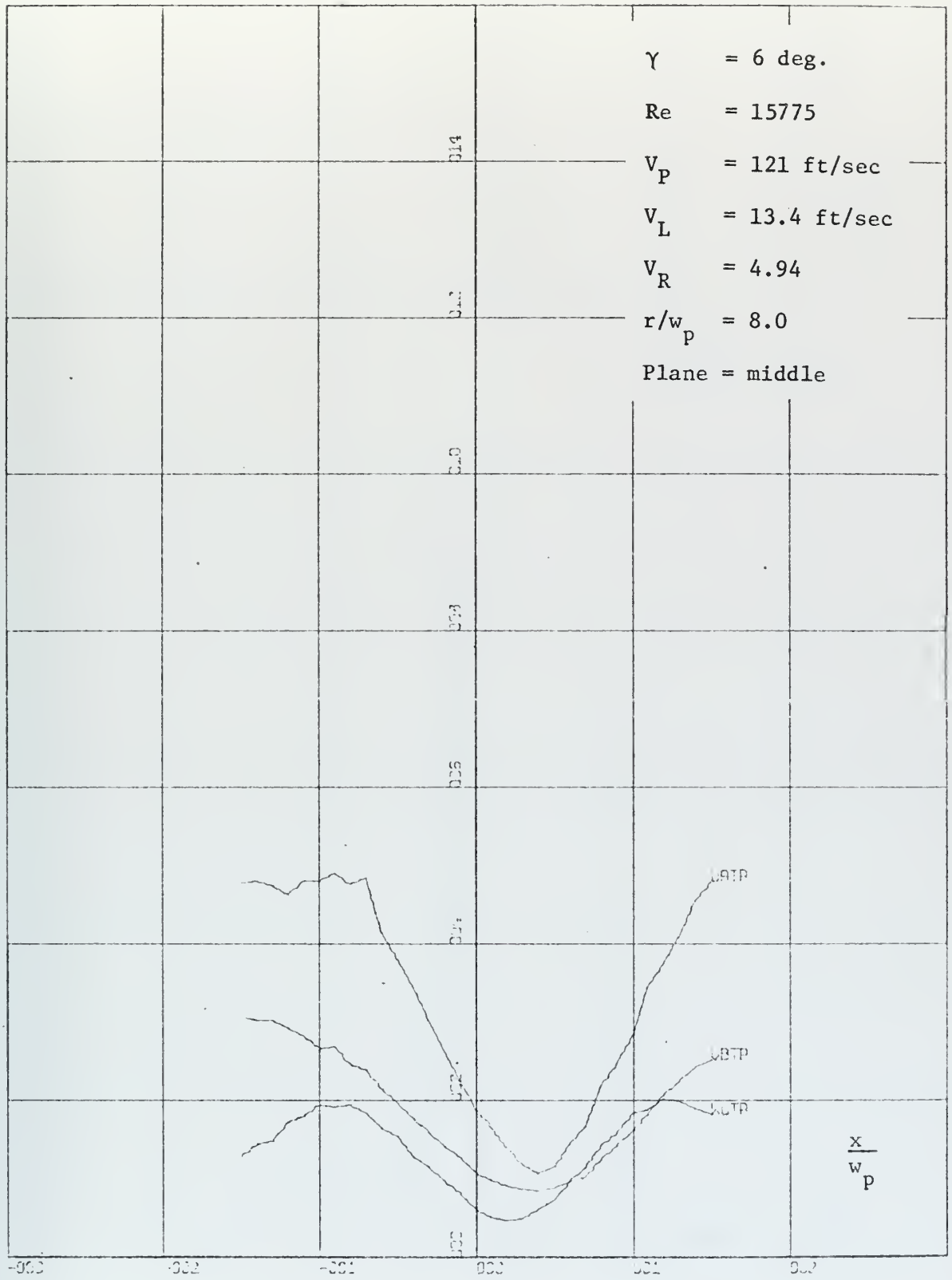

Figure 33. Turbulence Components

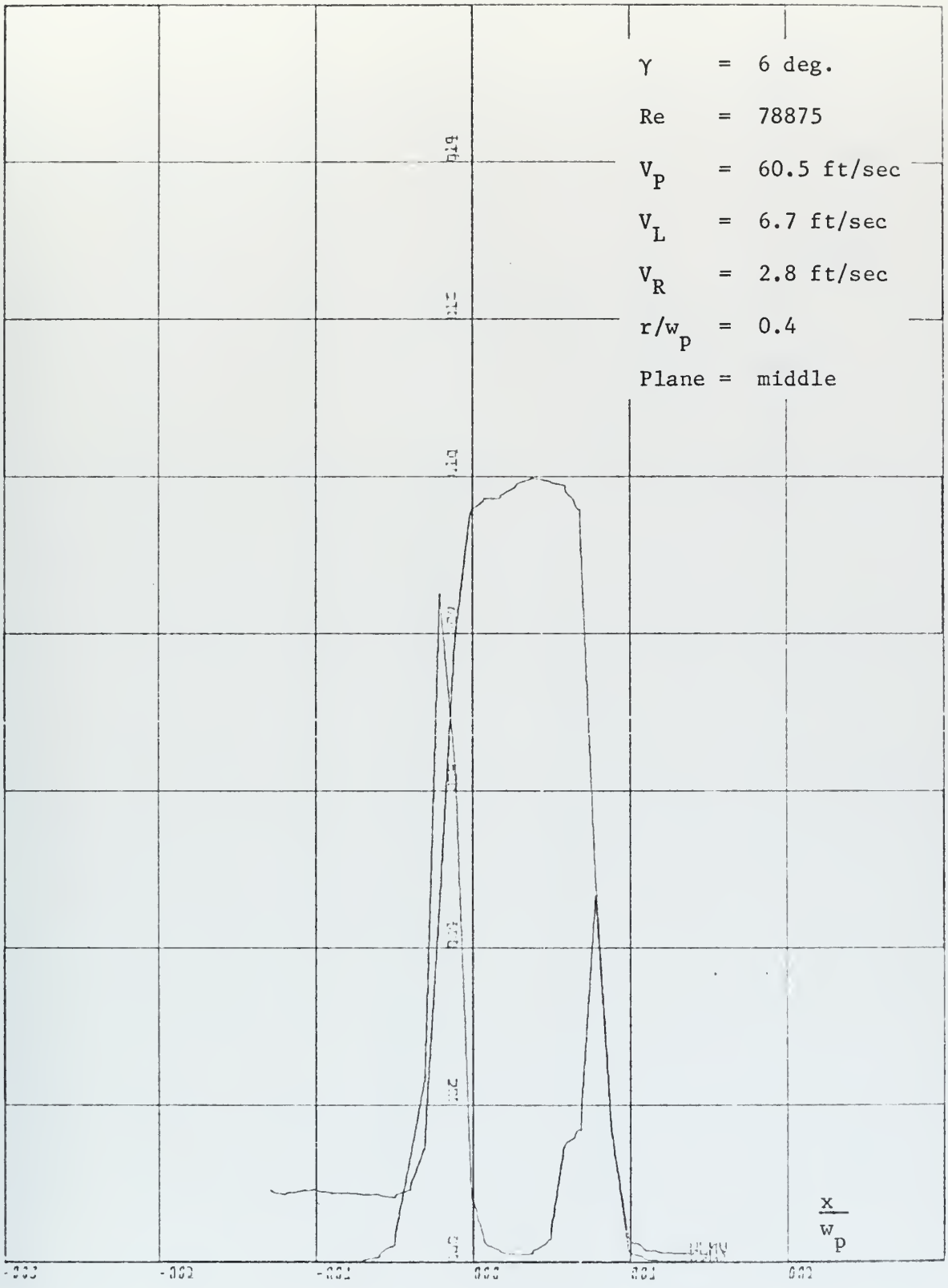

Figure 34. Mean Velocity and Noise

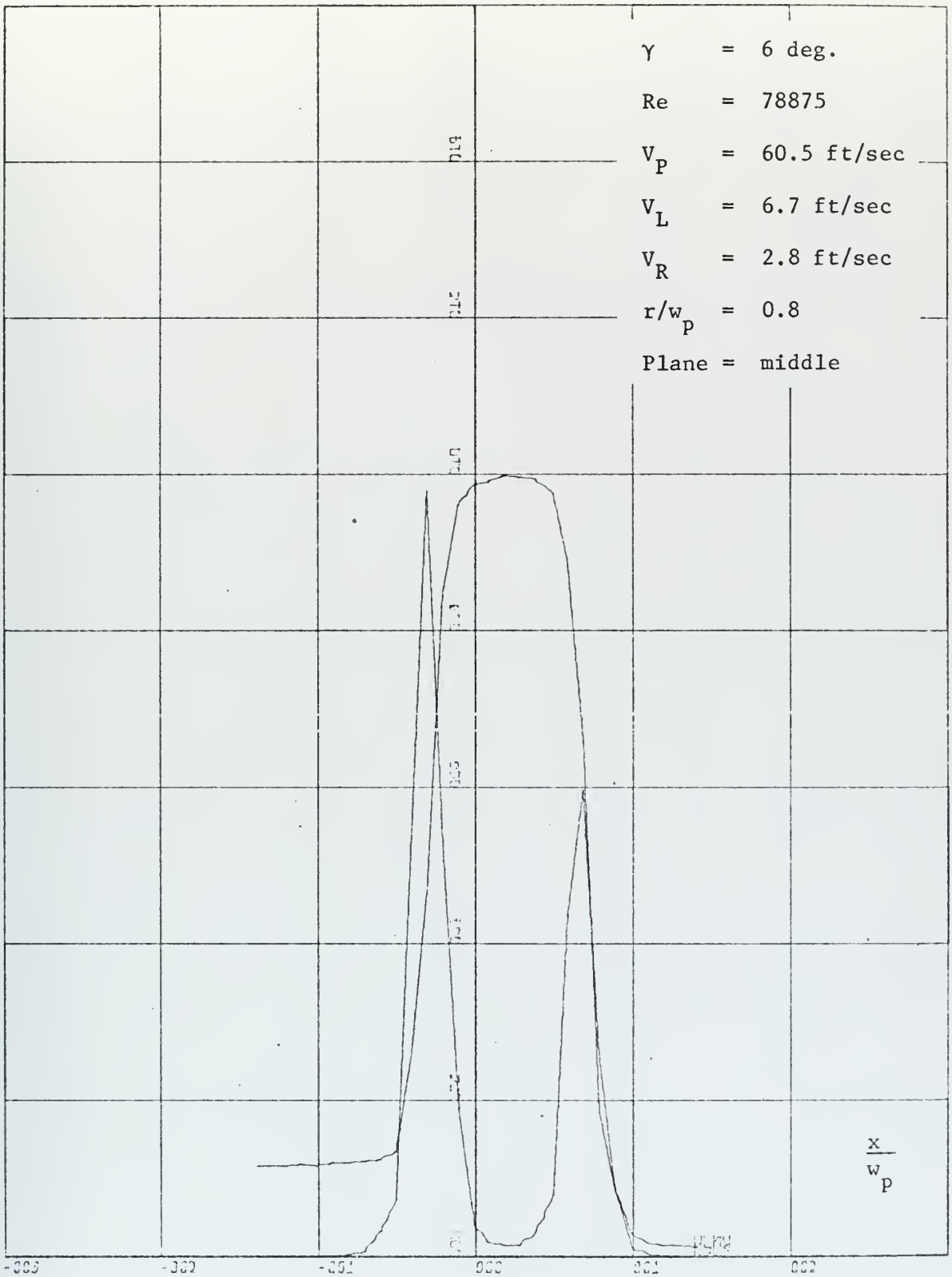

Figure 35. Mean Velocity and Noise

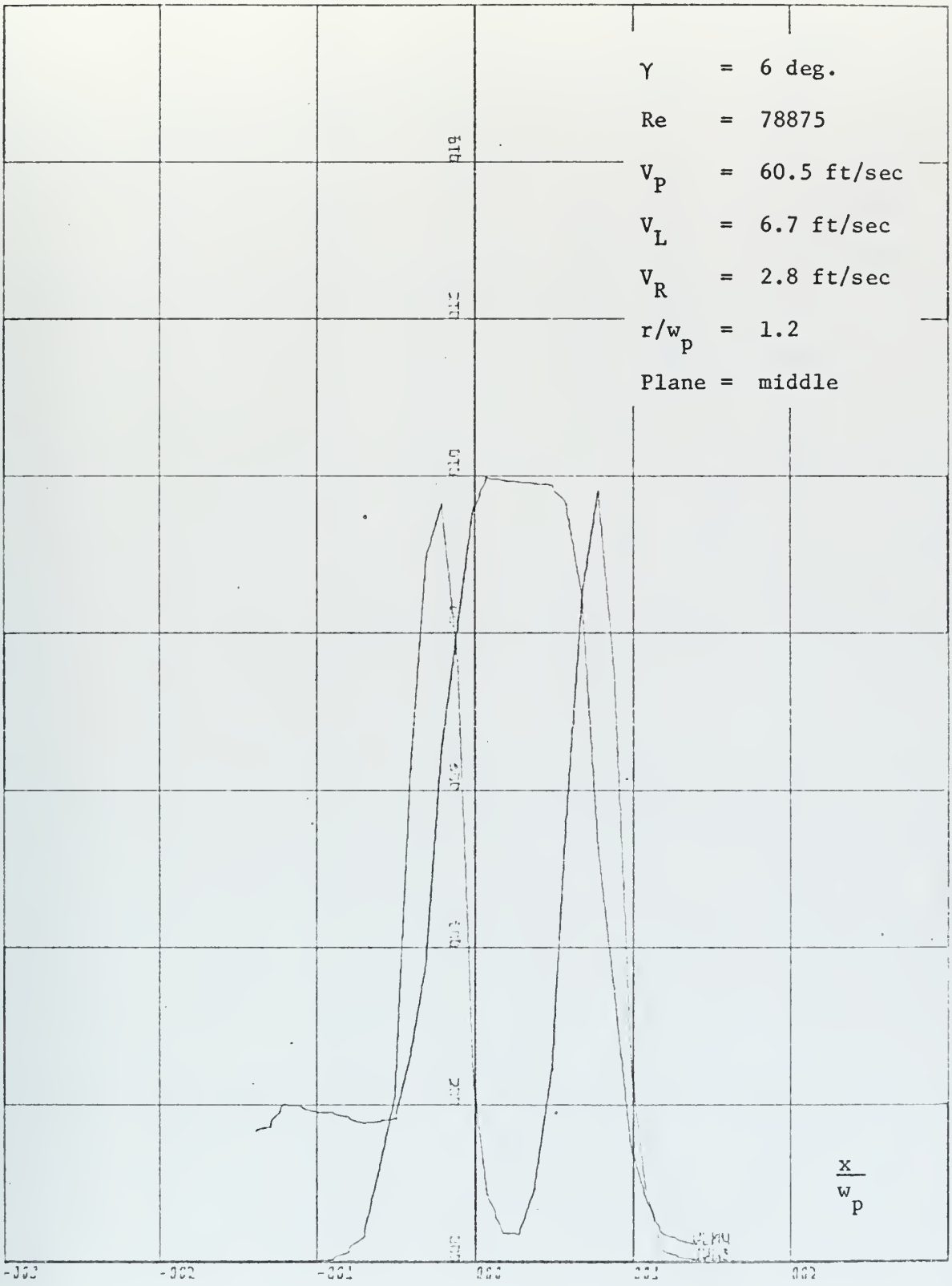

Figure 36. Mean Velocity and Noise

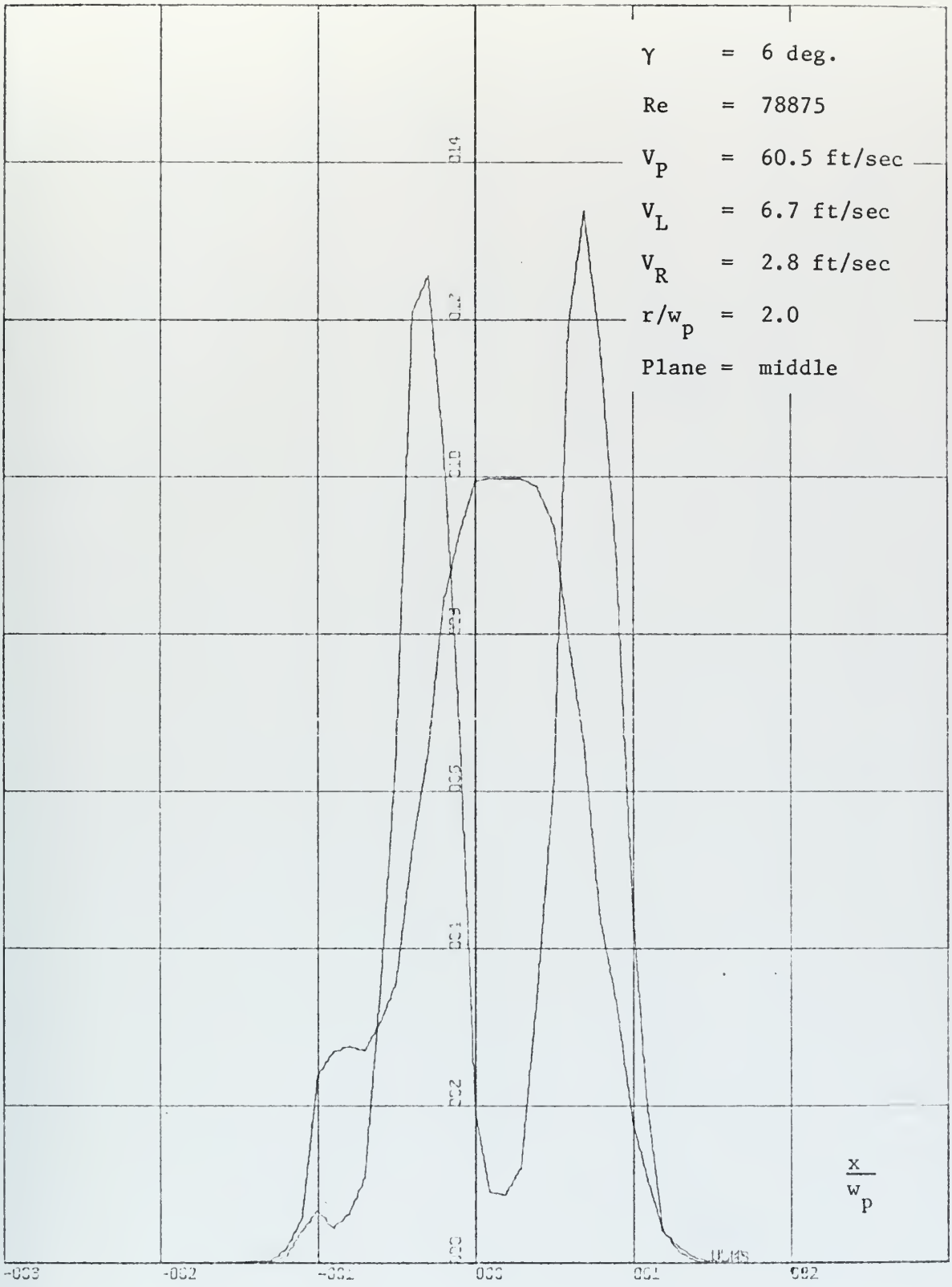

Figure 37. Mean Velocity and Noise

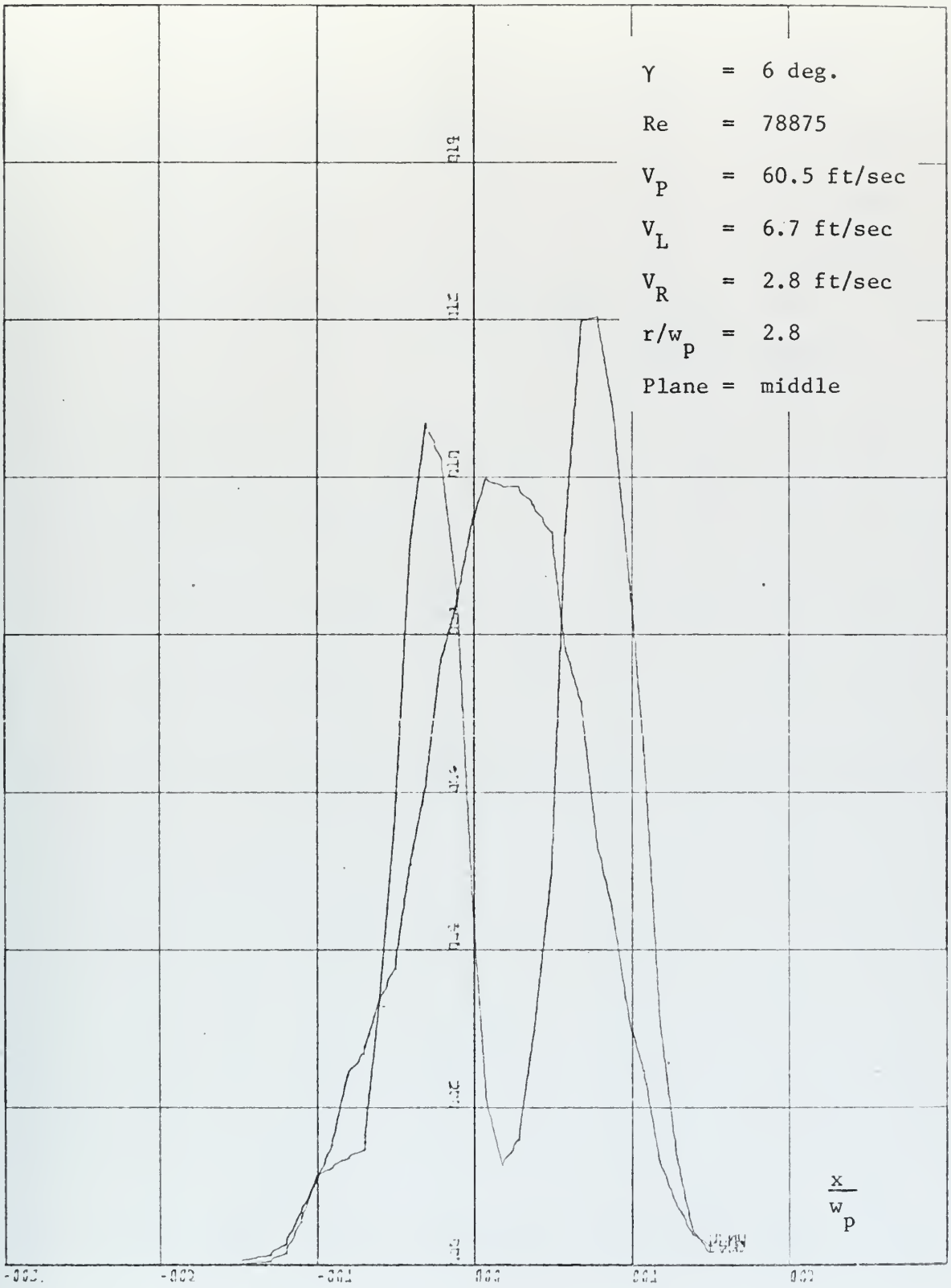

Figure 38. Mean Velocity and Noise

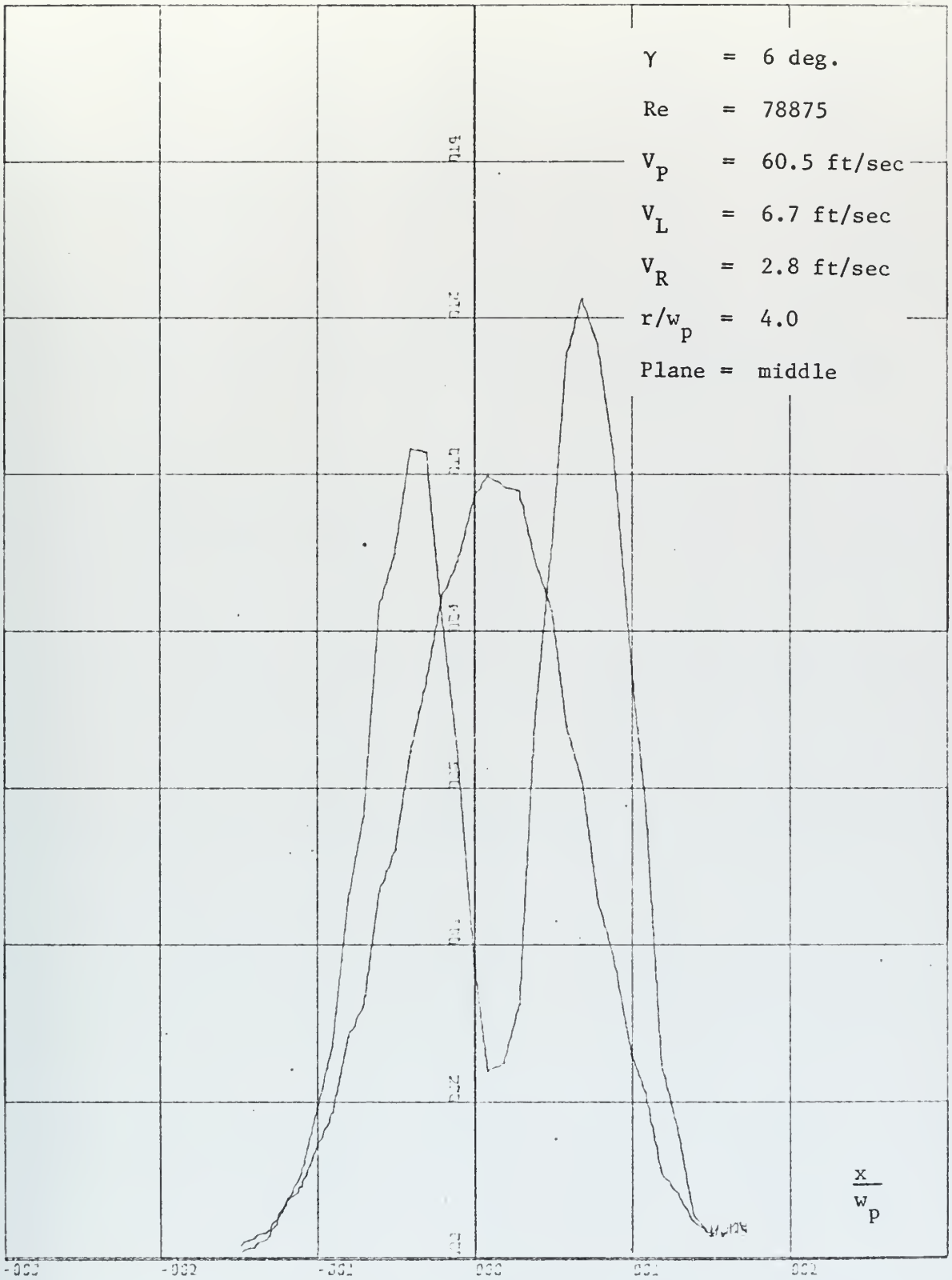

Figure 39. Mean Velocity and Noise

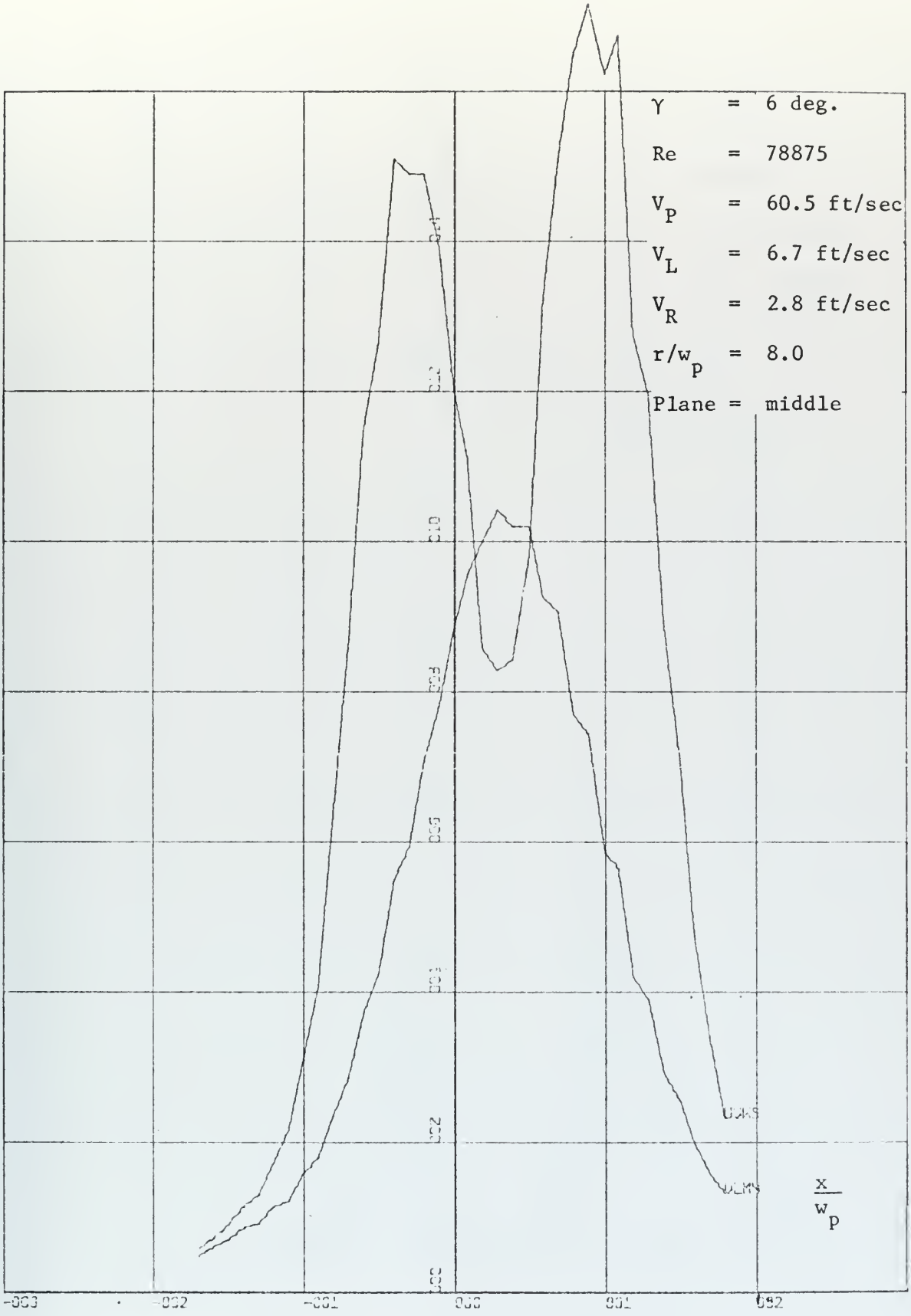

Figure 40. Mean Velocity and Noise

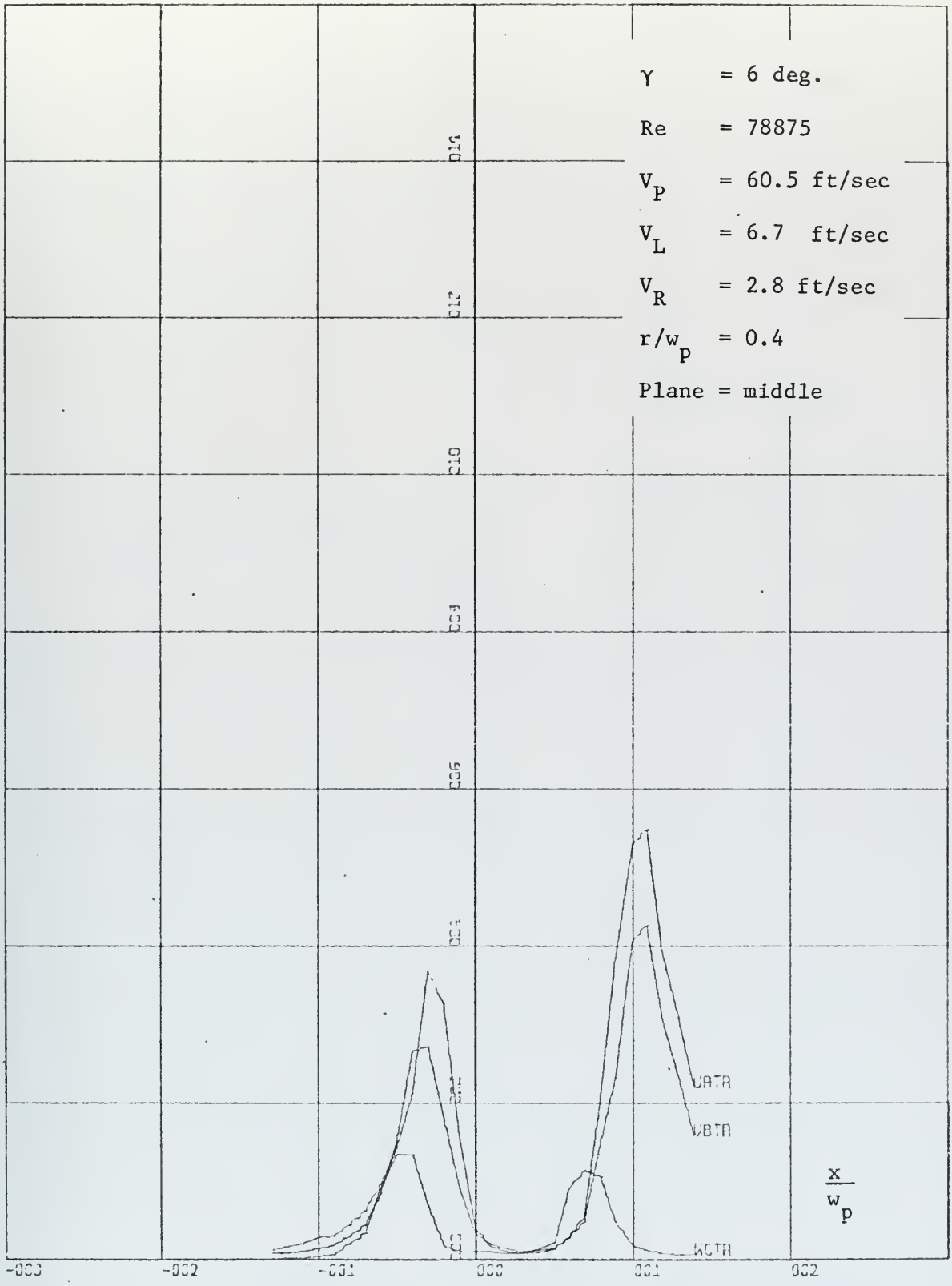

Figure 41. Turbulence Components

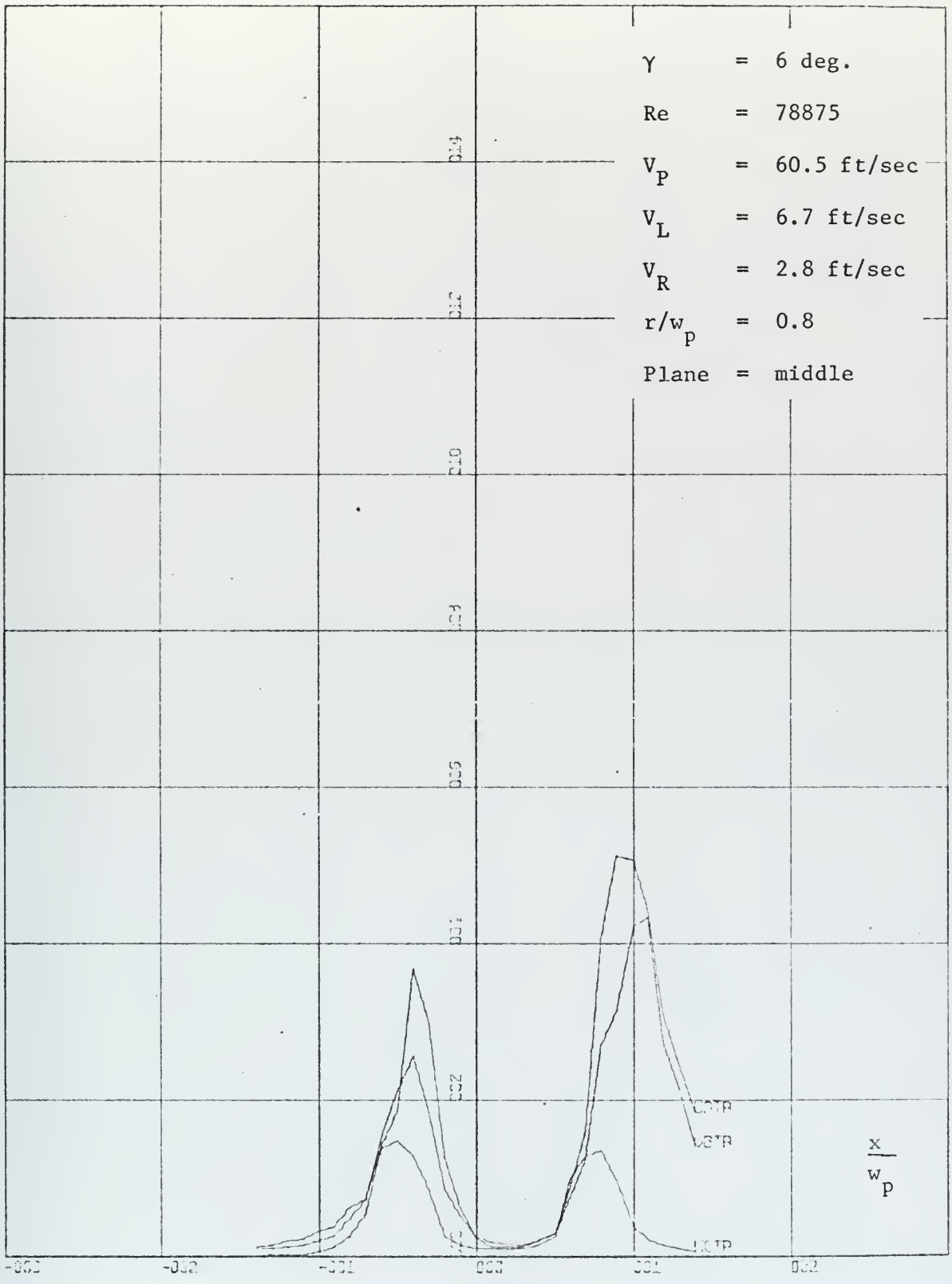

Figure 42. Turbulence Components

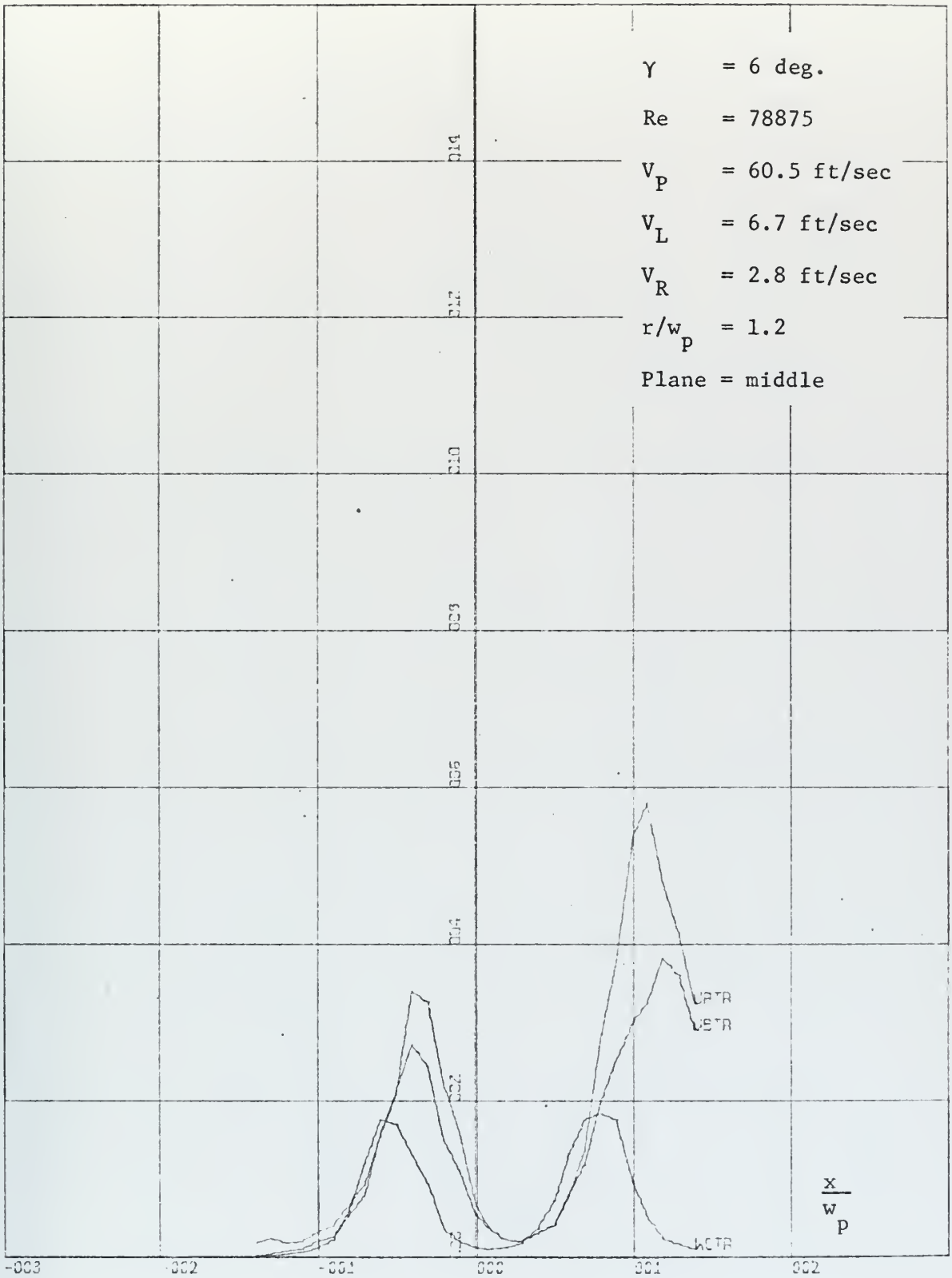

Figure 43. Turbulence Components

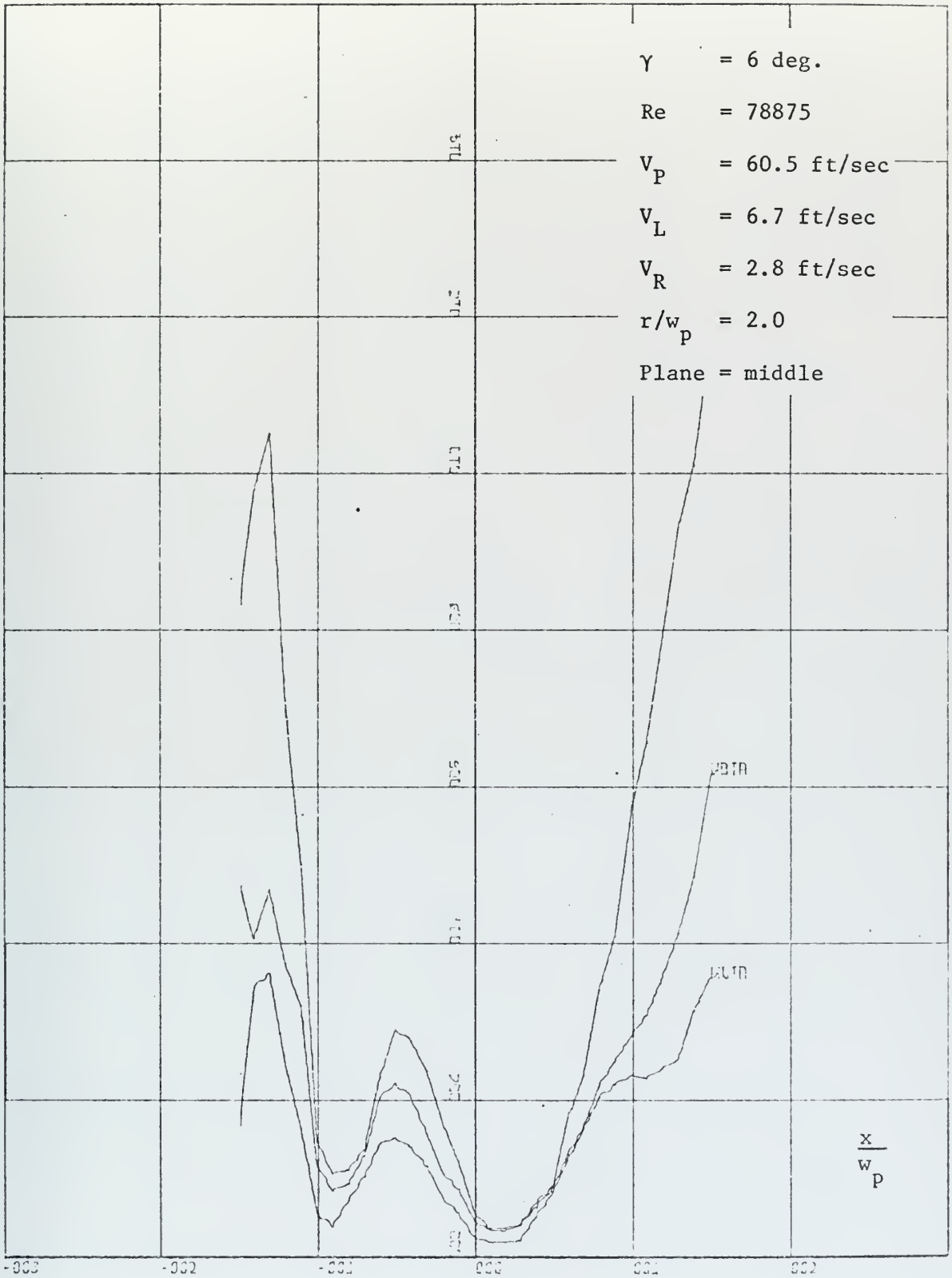

Figure 44. Turbulence Components

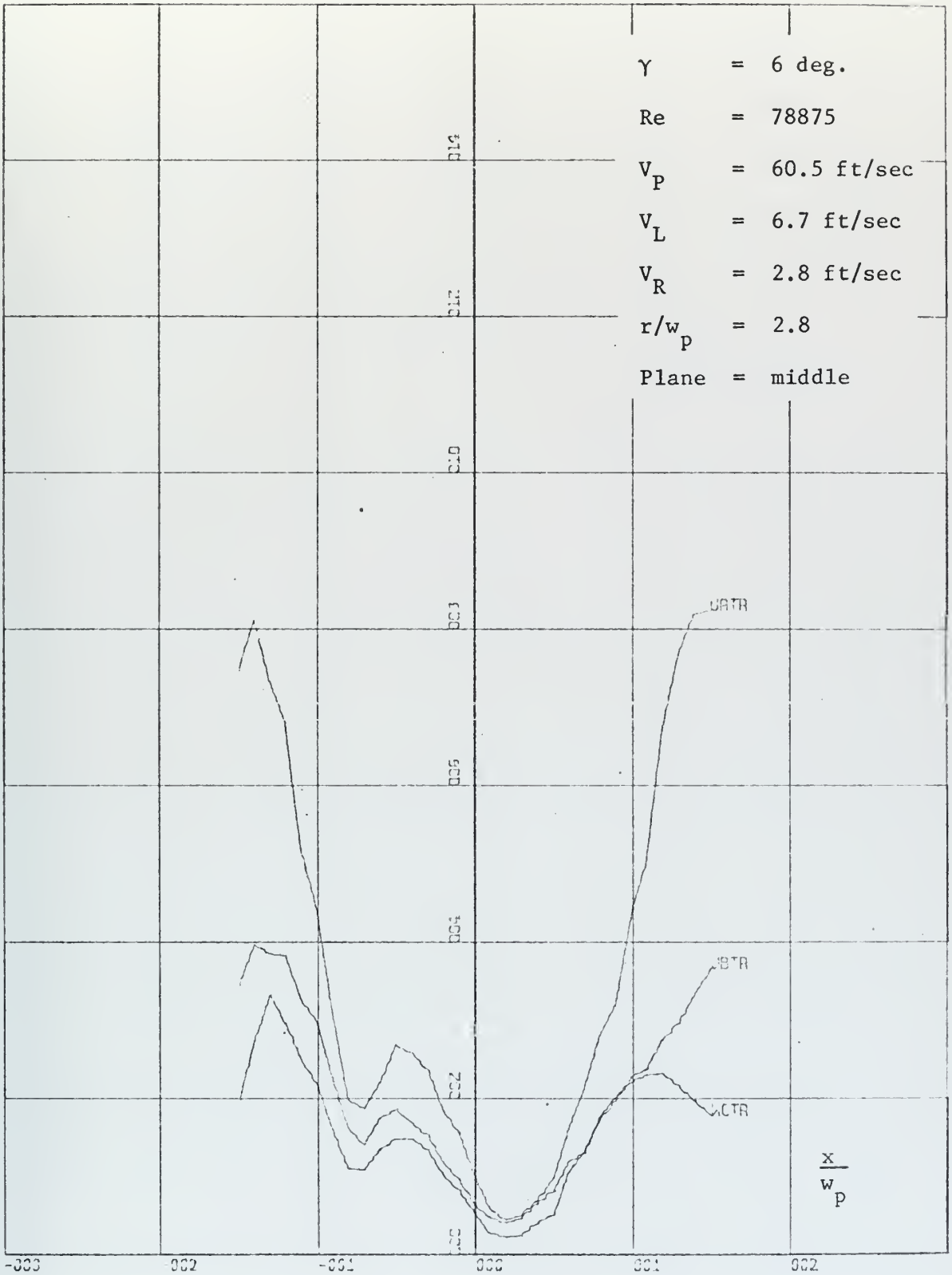

Figure 45. Turbulence Components

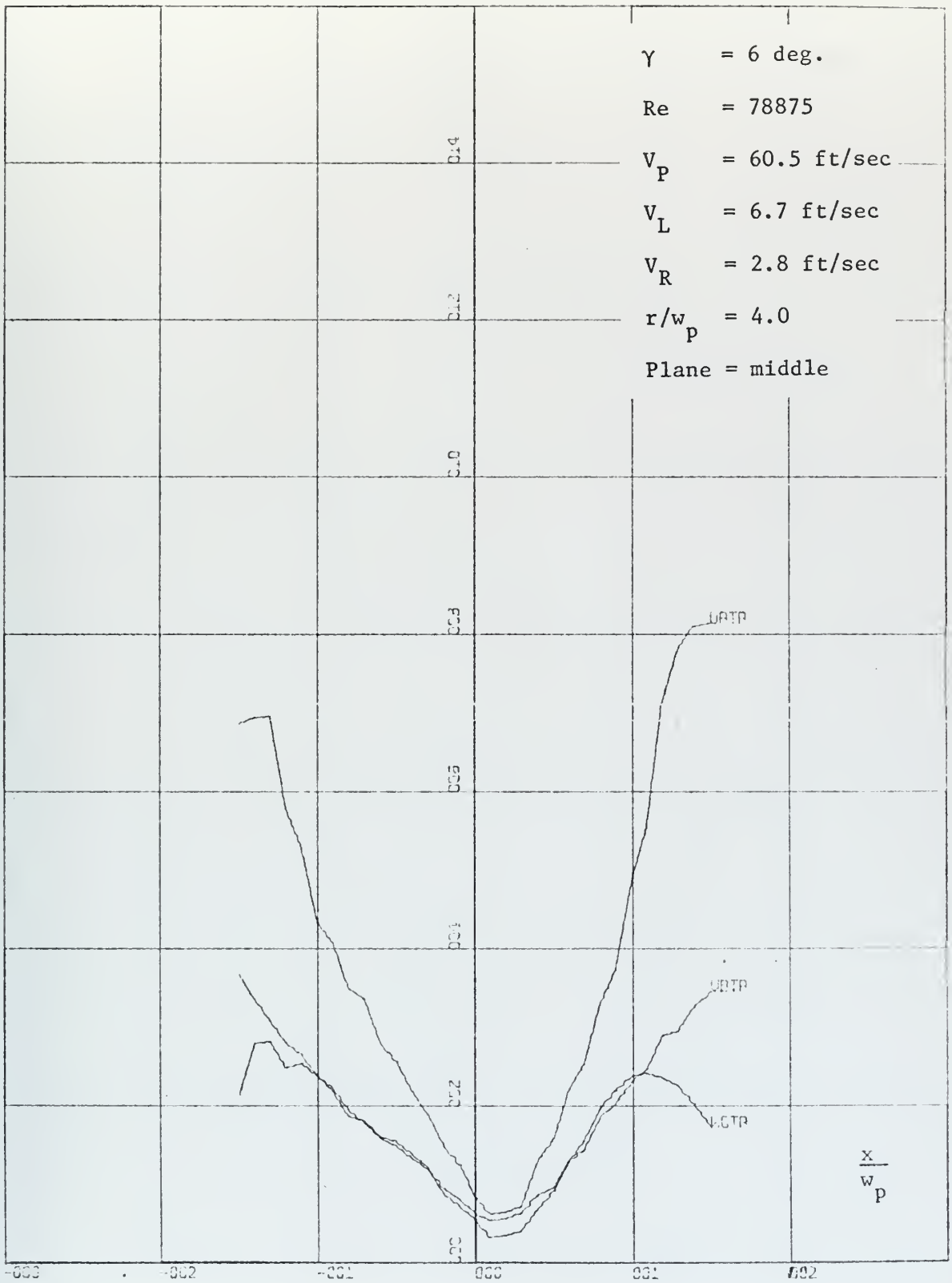

Figure 46. Turbulence Components

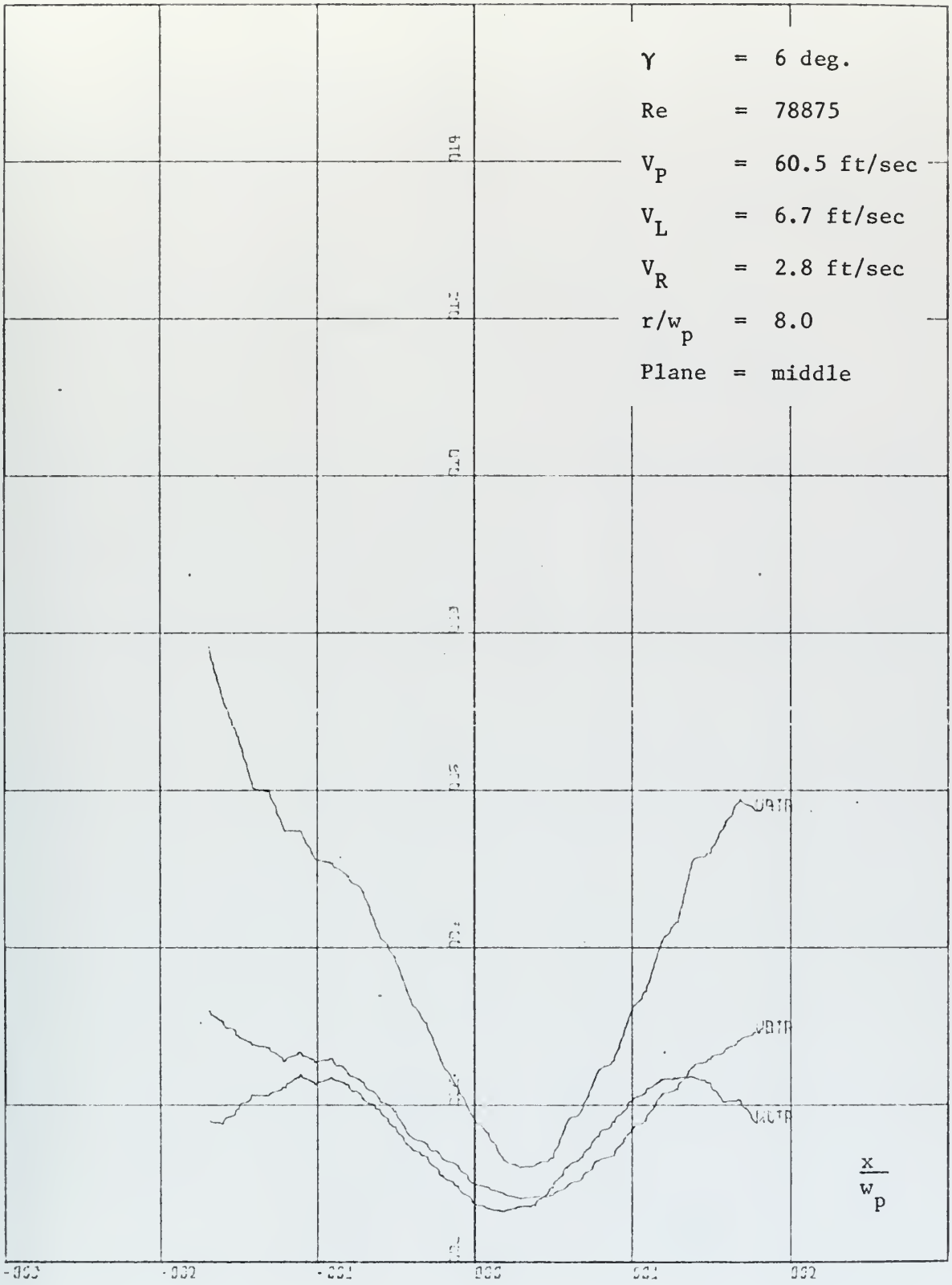

Figure 47. Turbulence Components

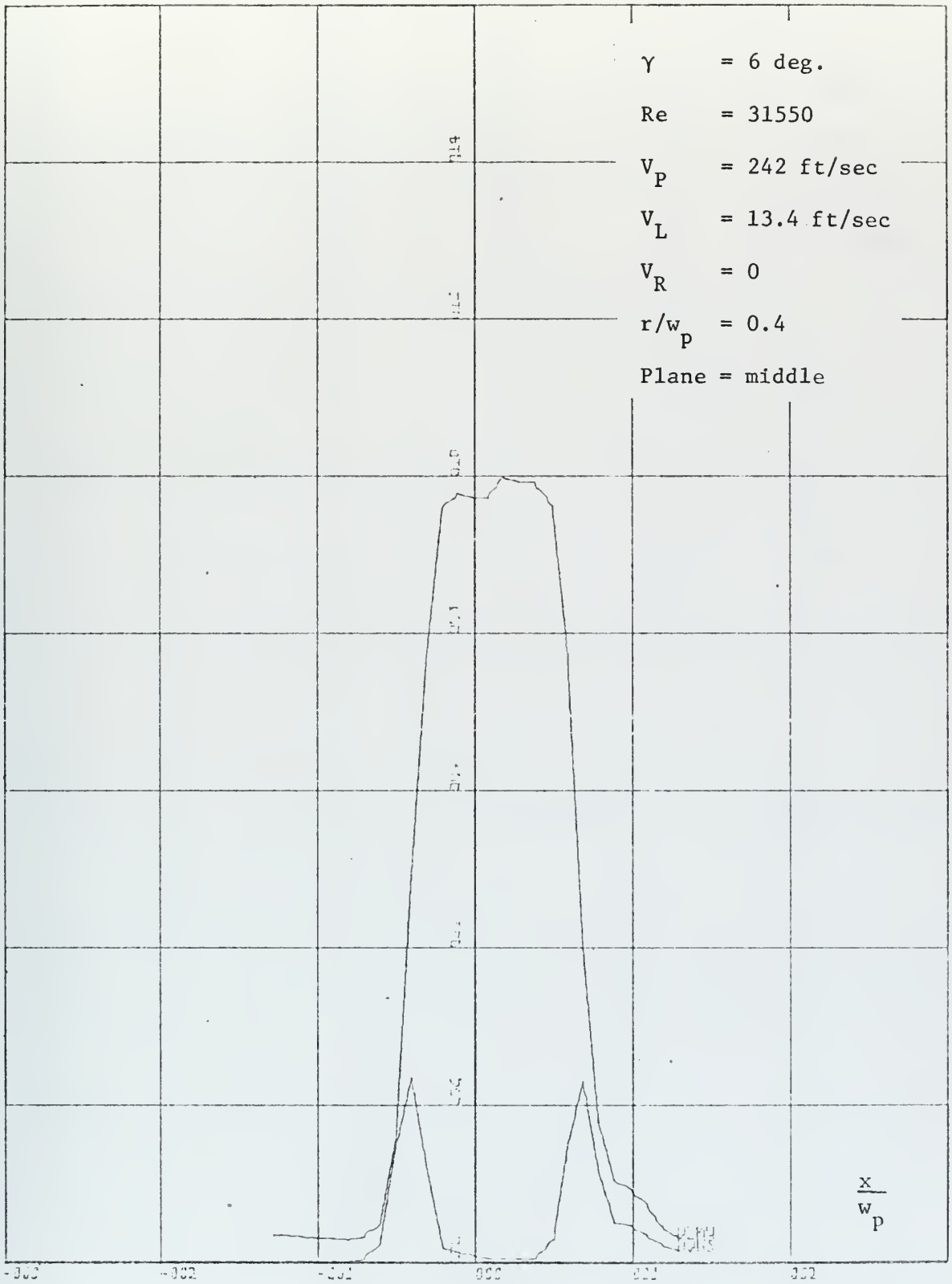

Figure 48. Mean Velocity and Noise

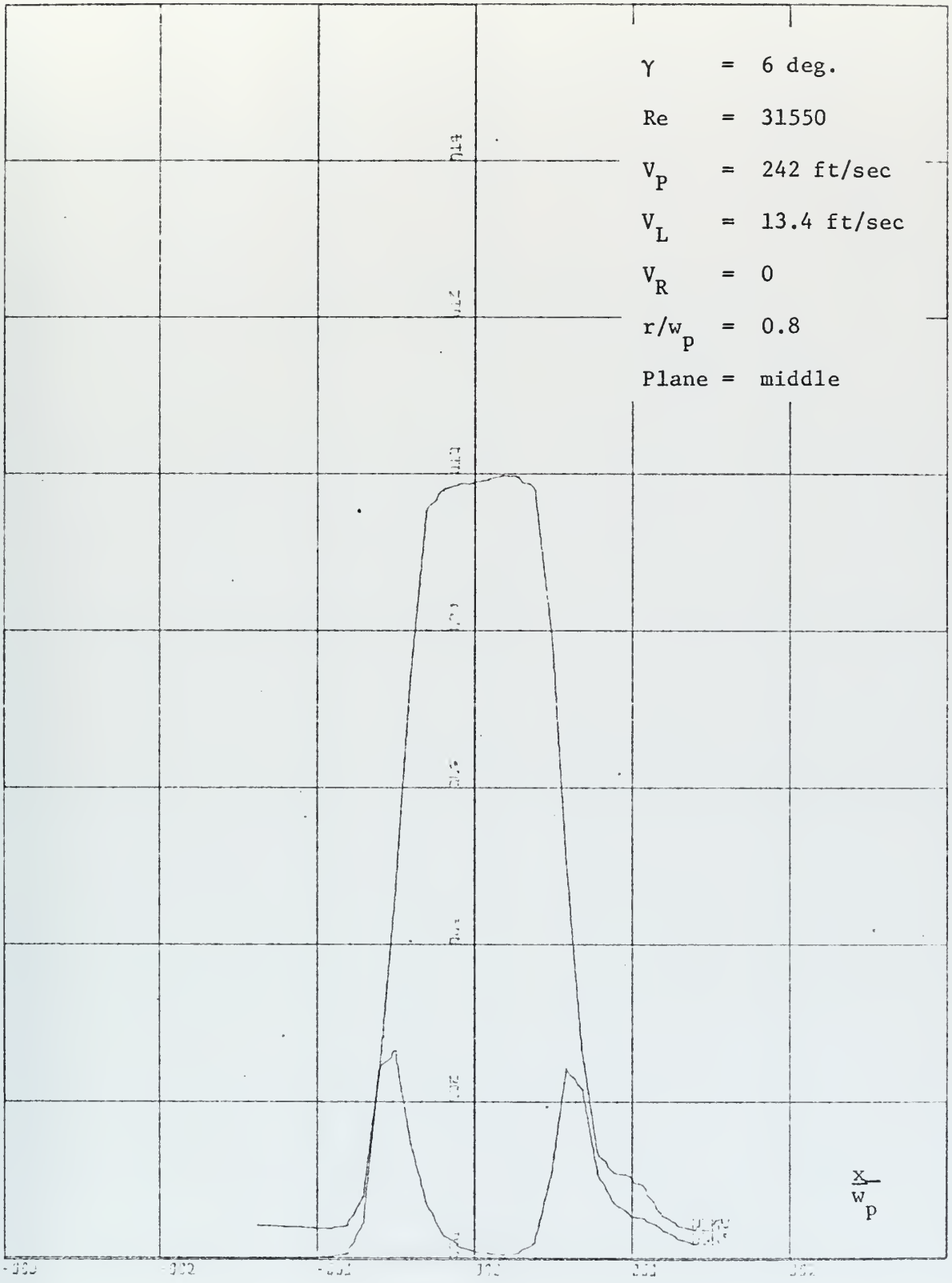

Figure 49. Mean Velocity and Noise

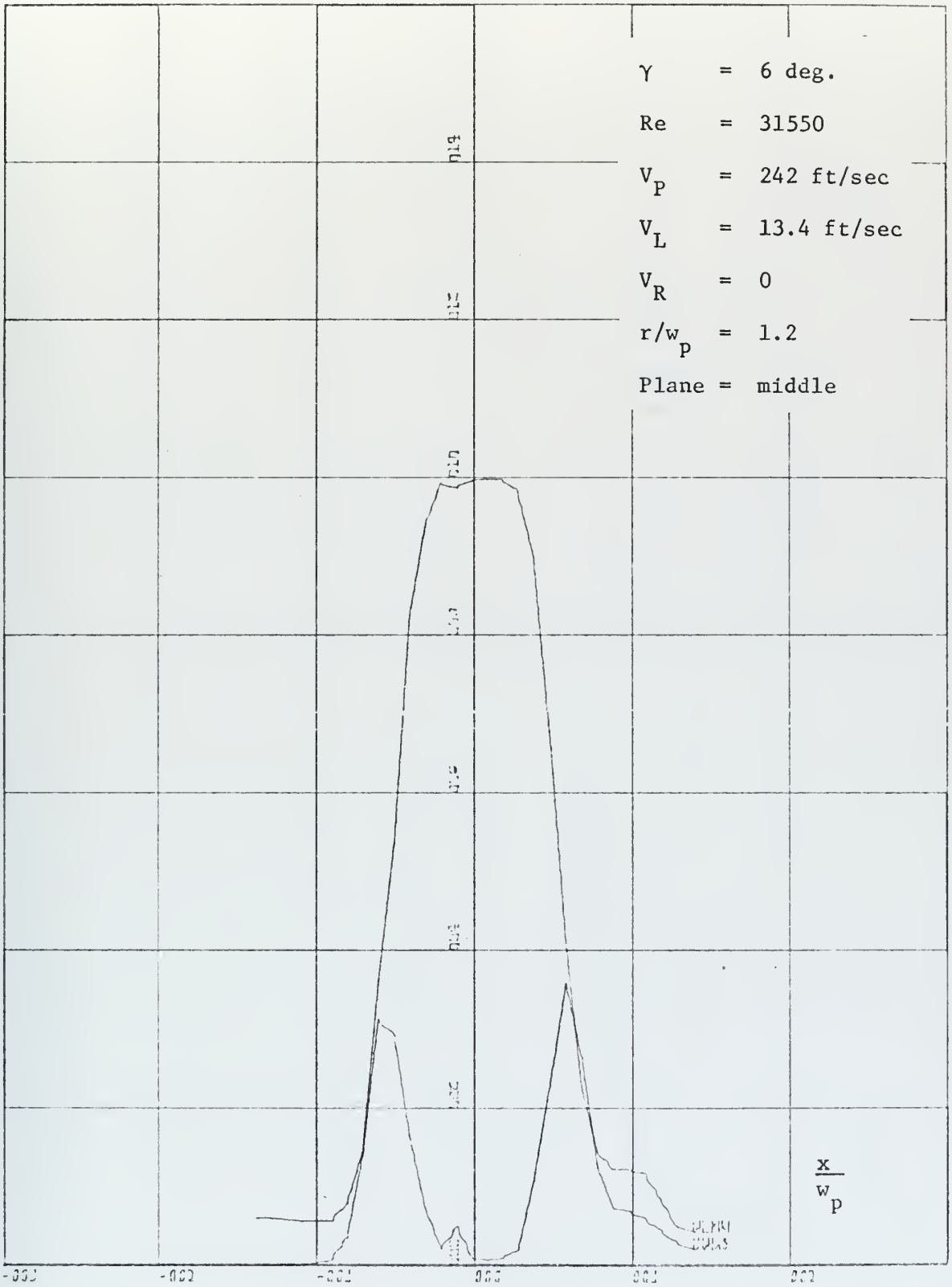

Figure 50. Mean Velocity and Noise

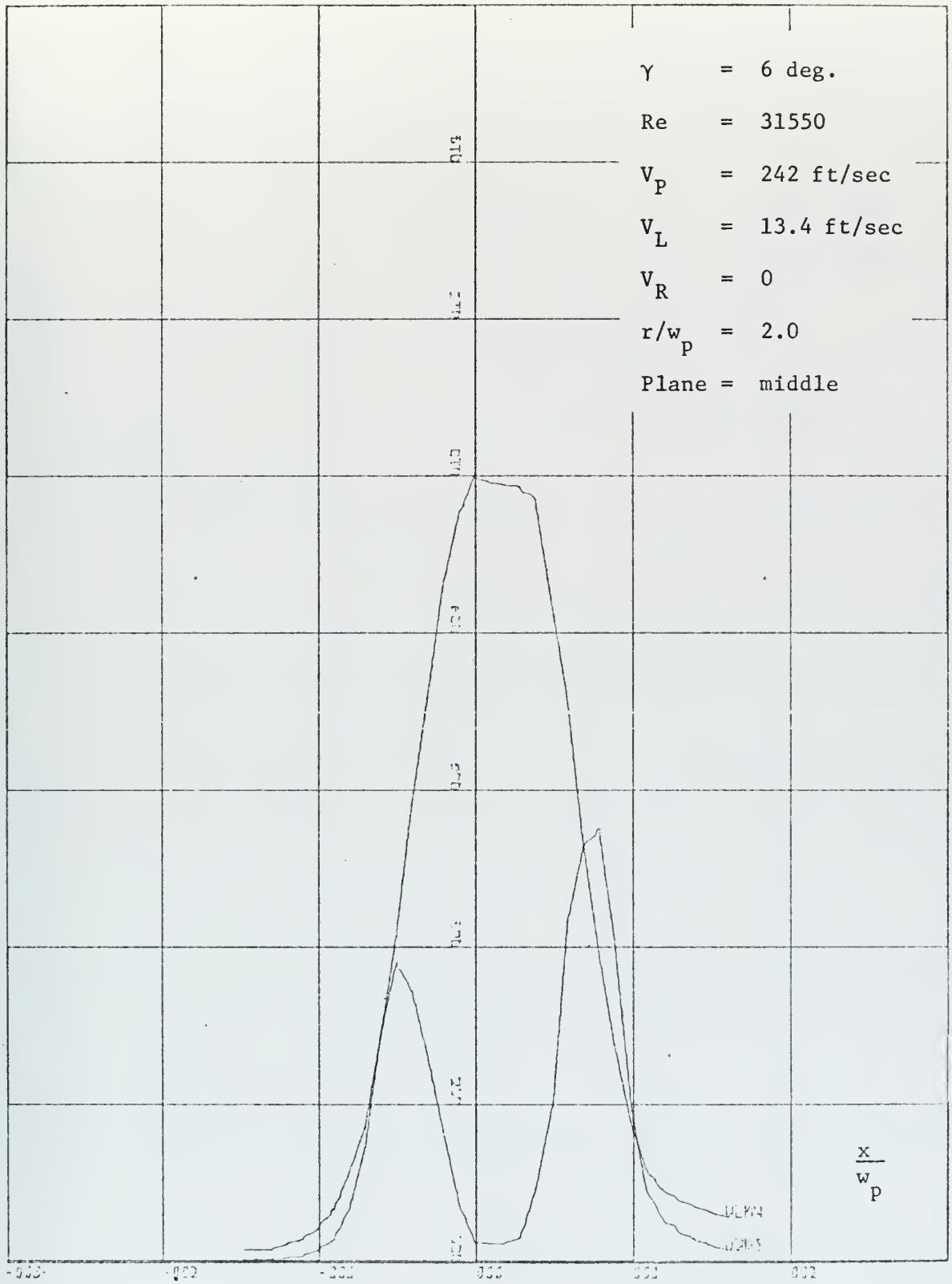

Figure 51. Mean Velocity and Noise

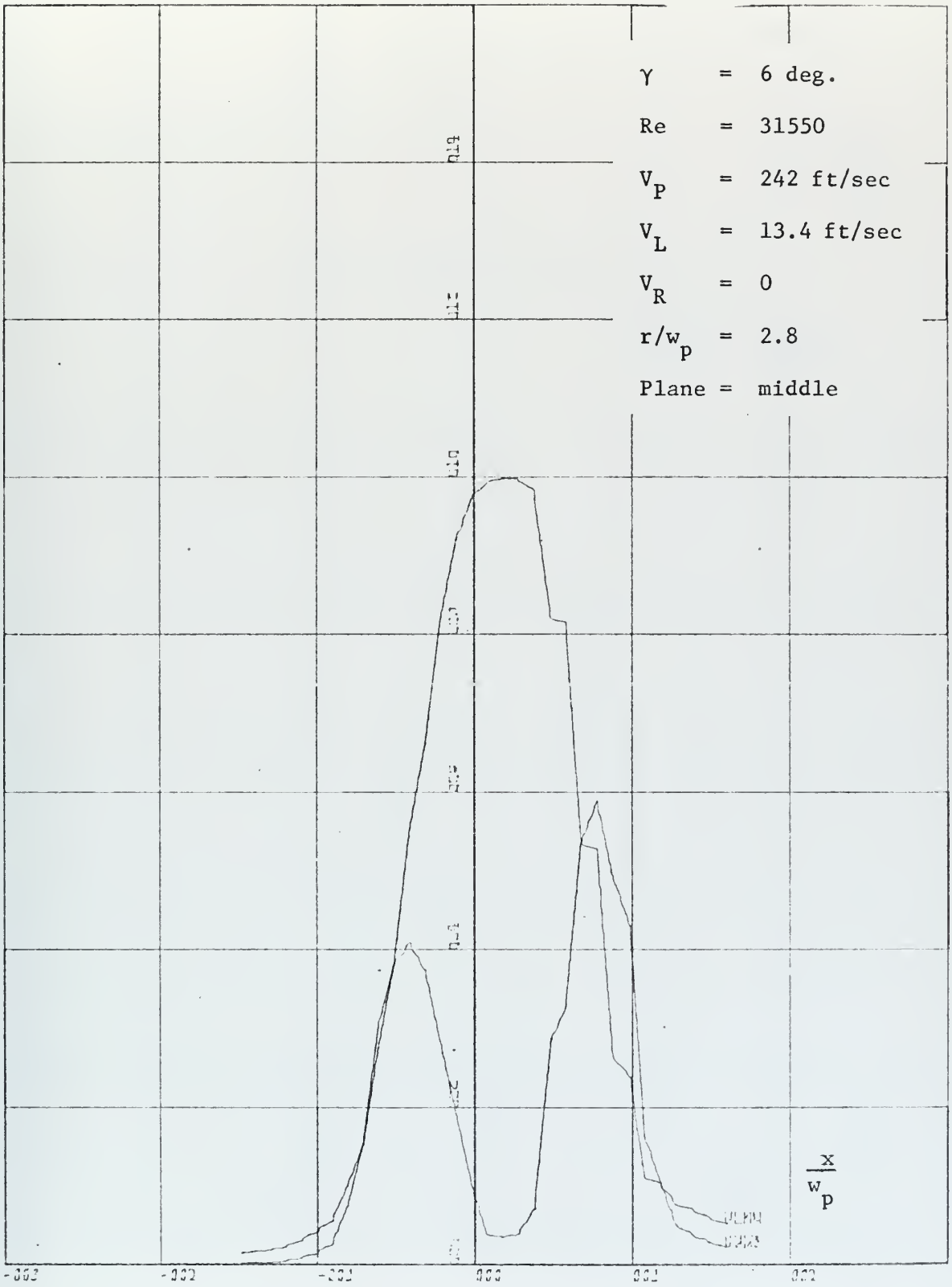

Figure 52. Mean Velocity and Noise

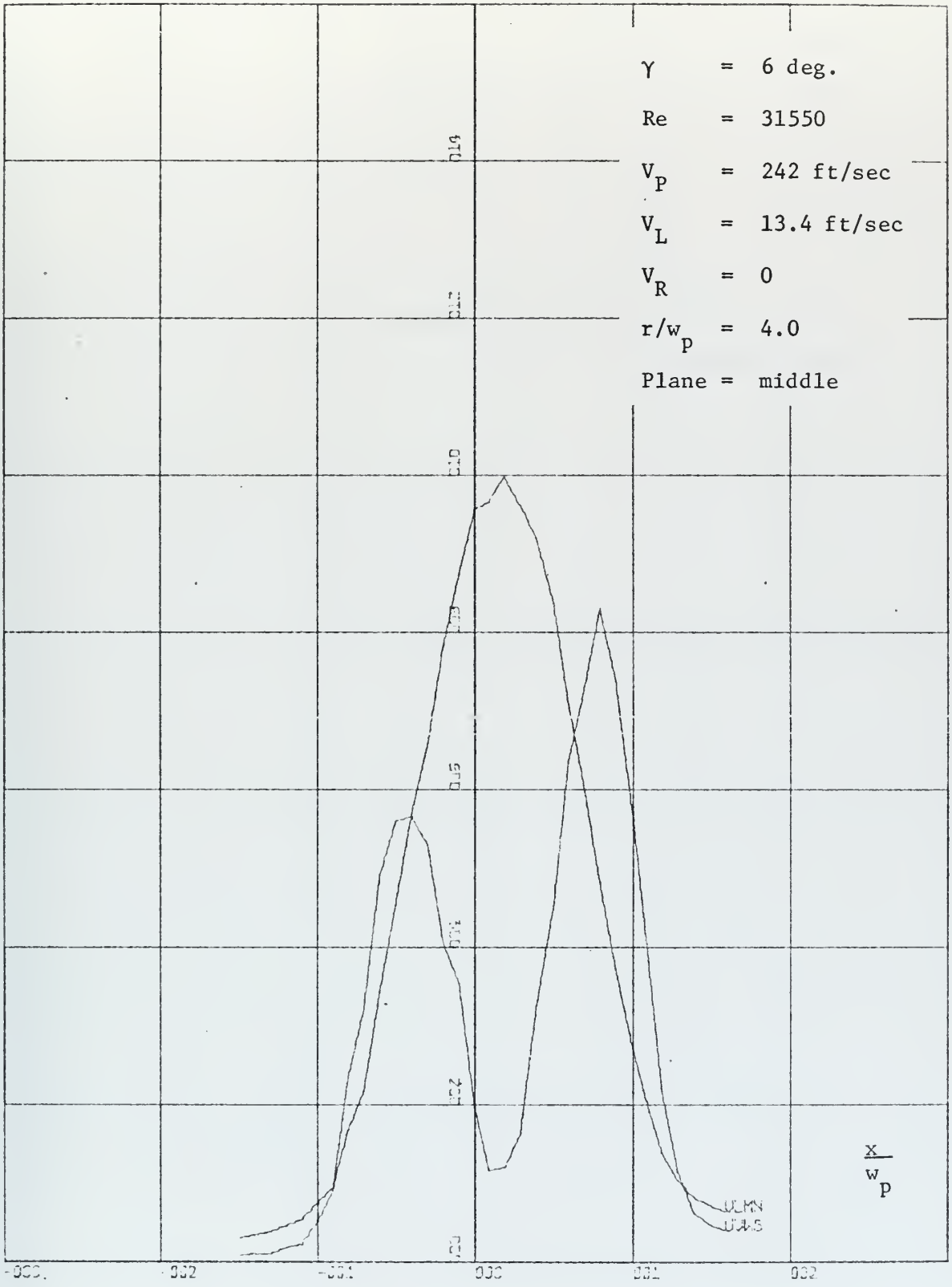

Figure 53. Mean Velocity and Noise

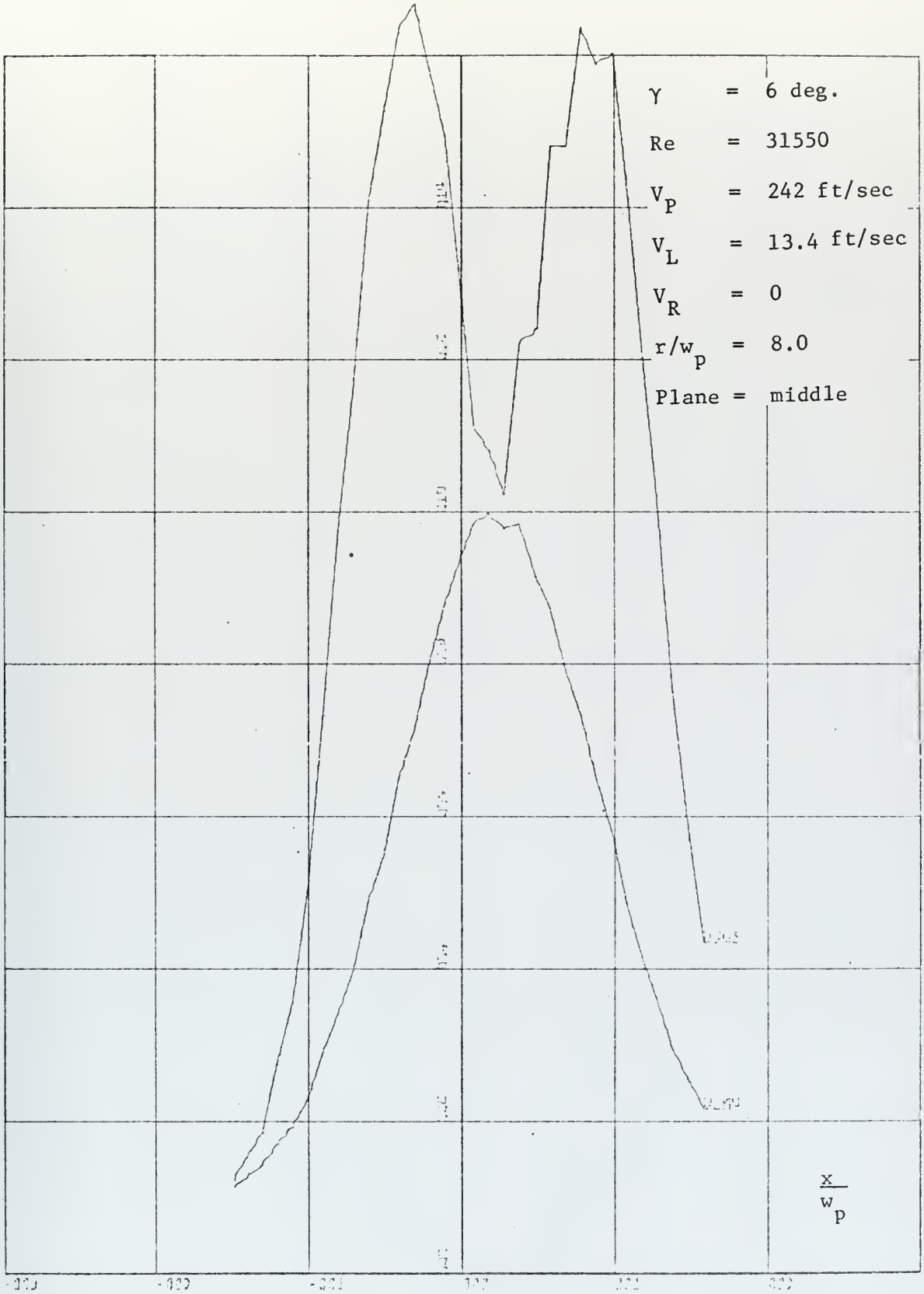

Figure 54. Mean Velocity and Noise

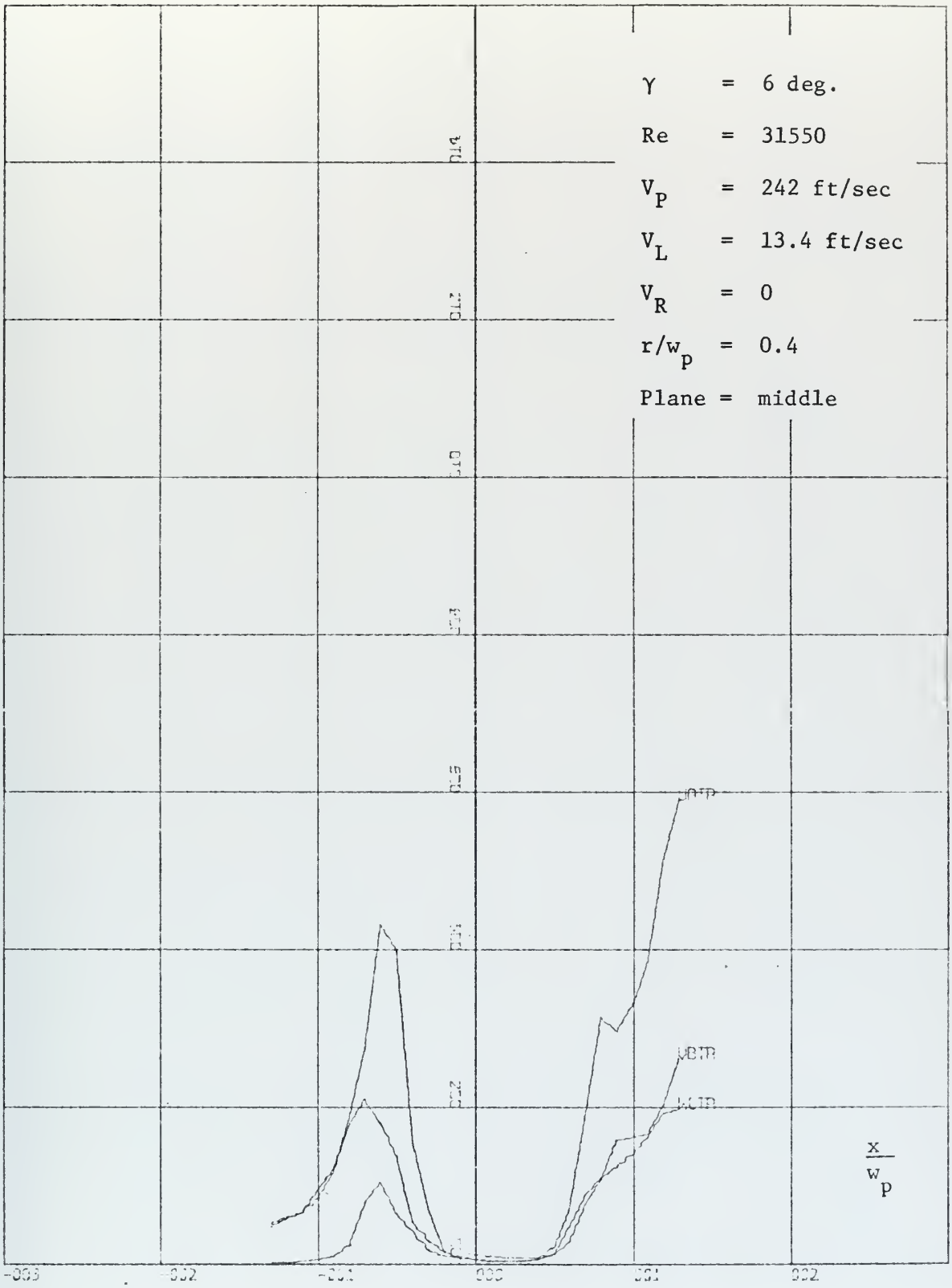

Figure 55. Turbulence Components

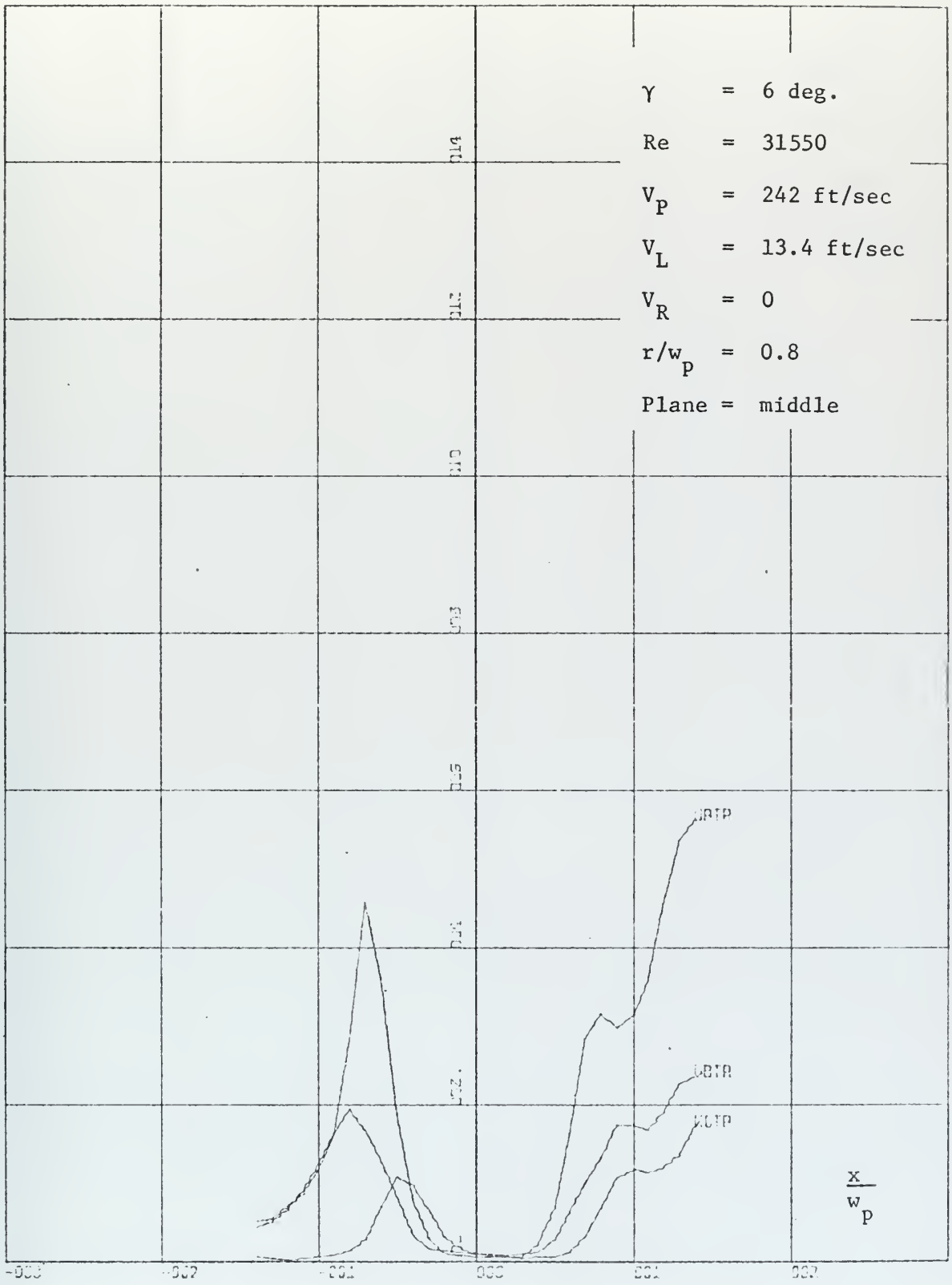

Figure 56. Turbulence Components

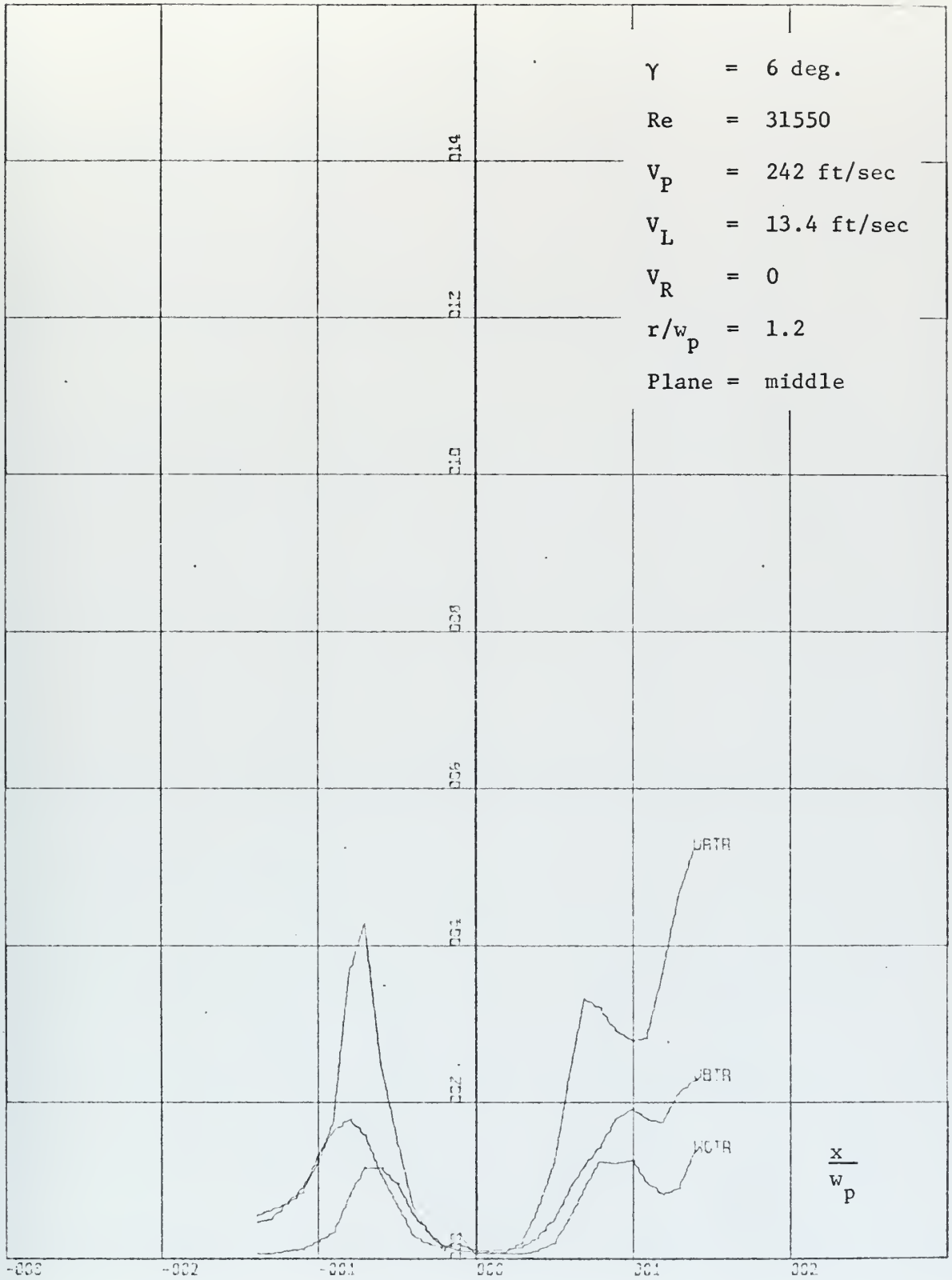

Figure 57. Turbulence Components

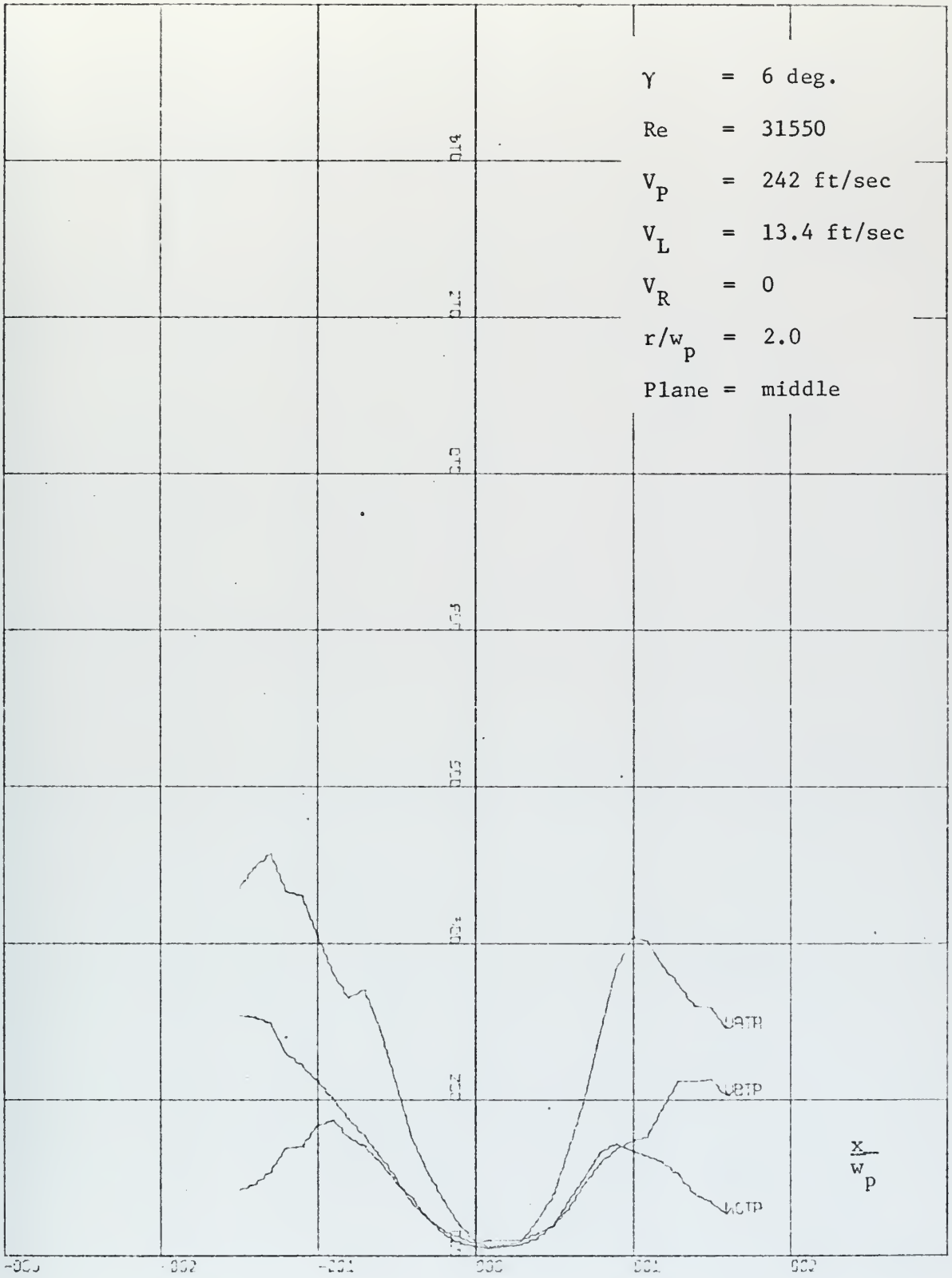

Figure 58. Turbulence Components

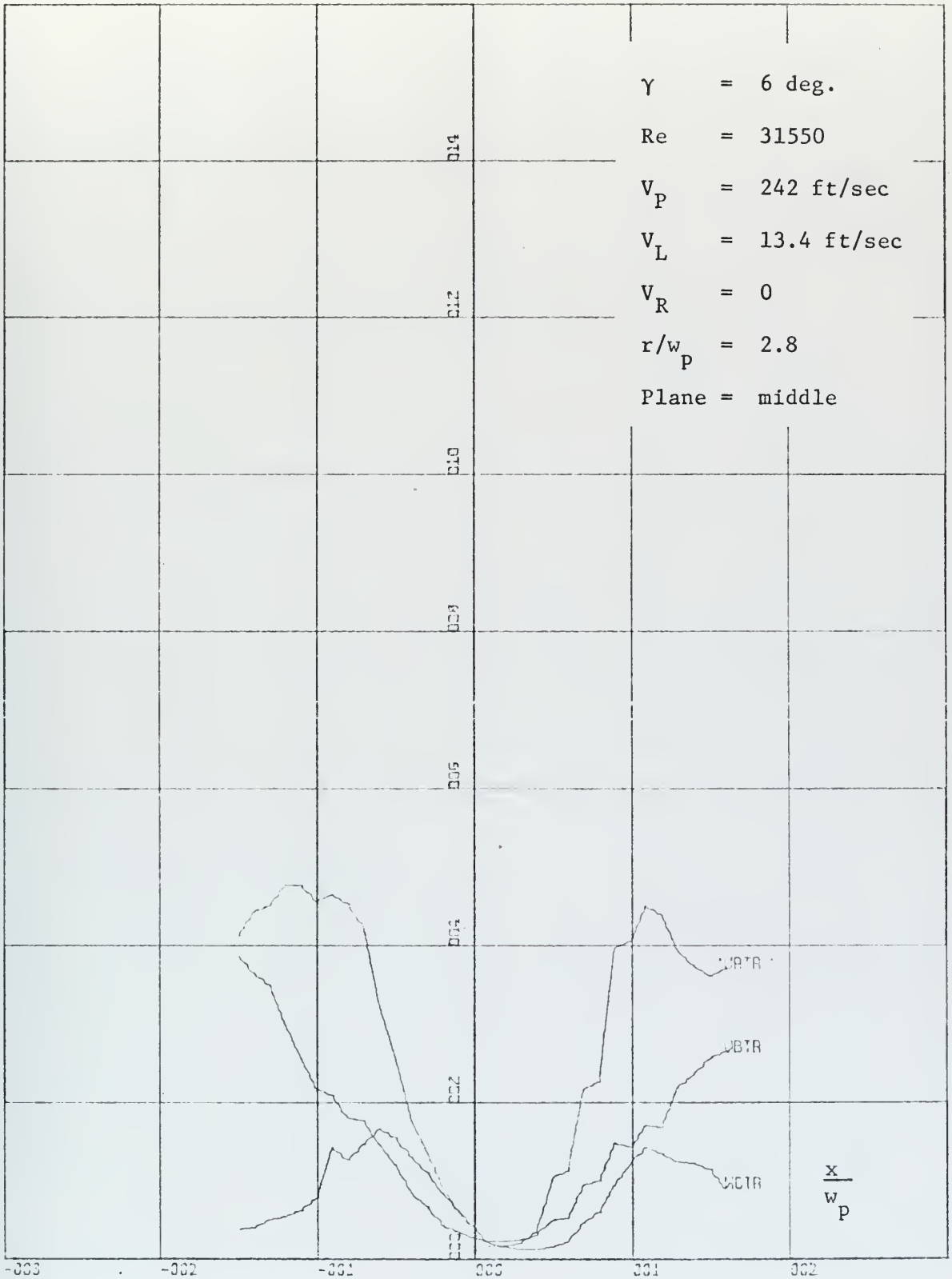

Figure 59. Turbulence Components

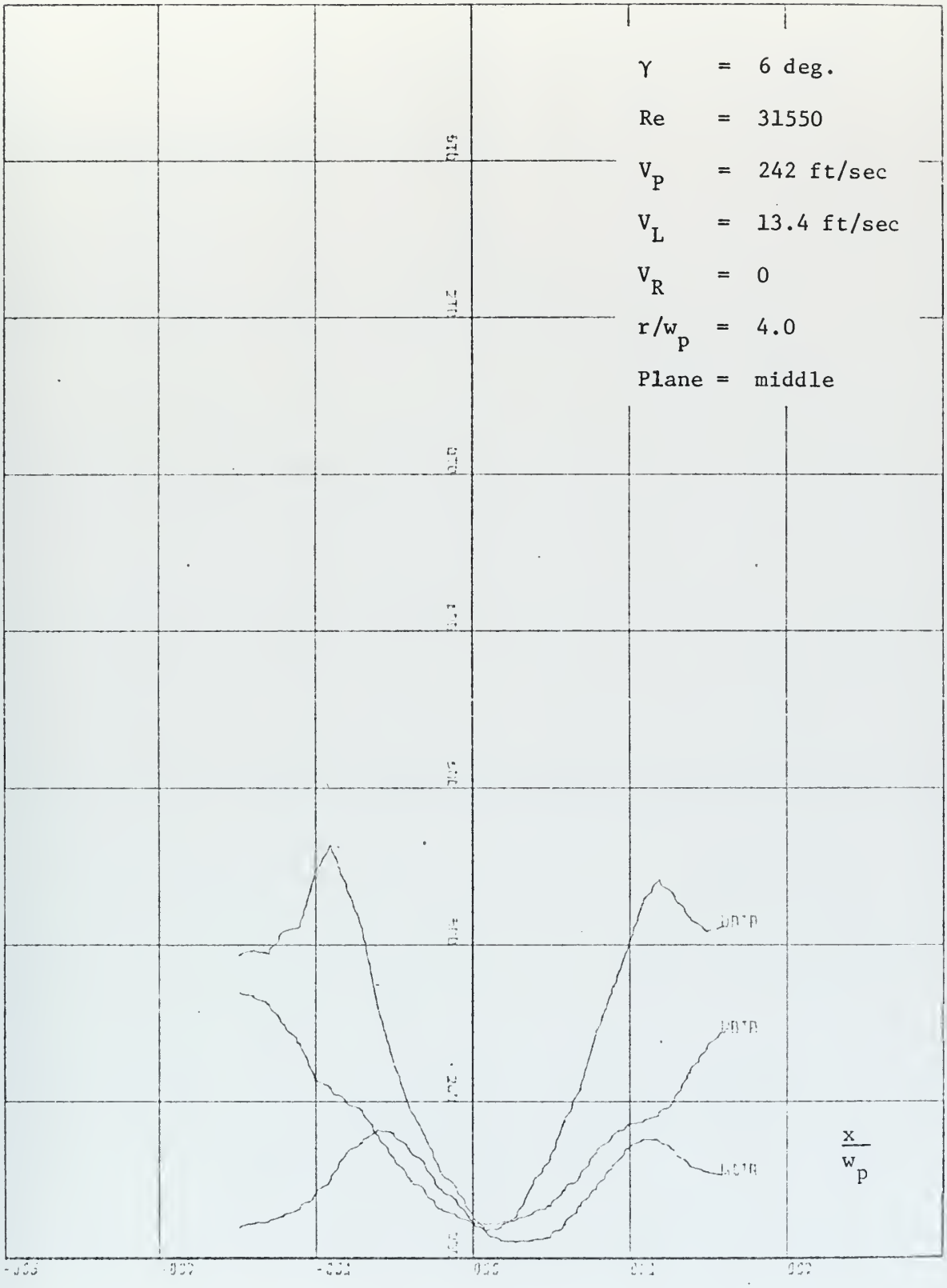

Figure 60. Turbulence Components

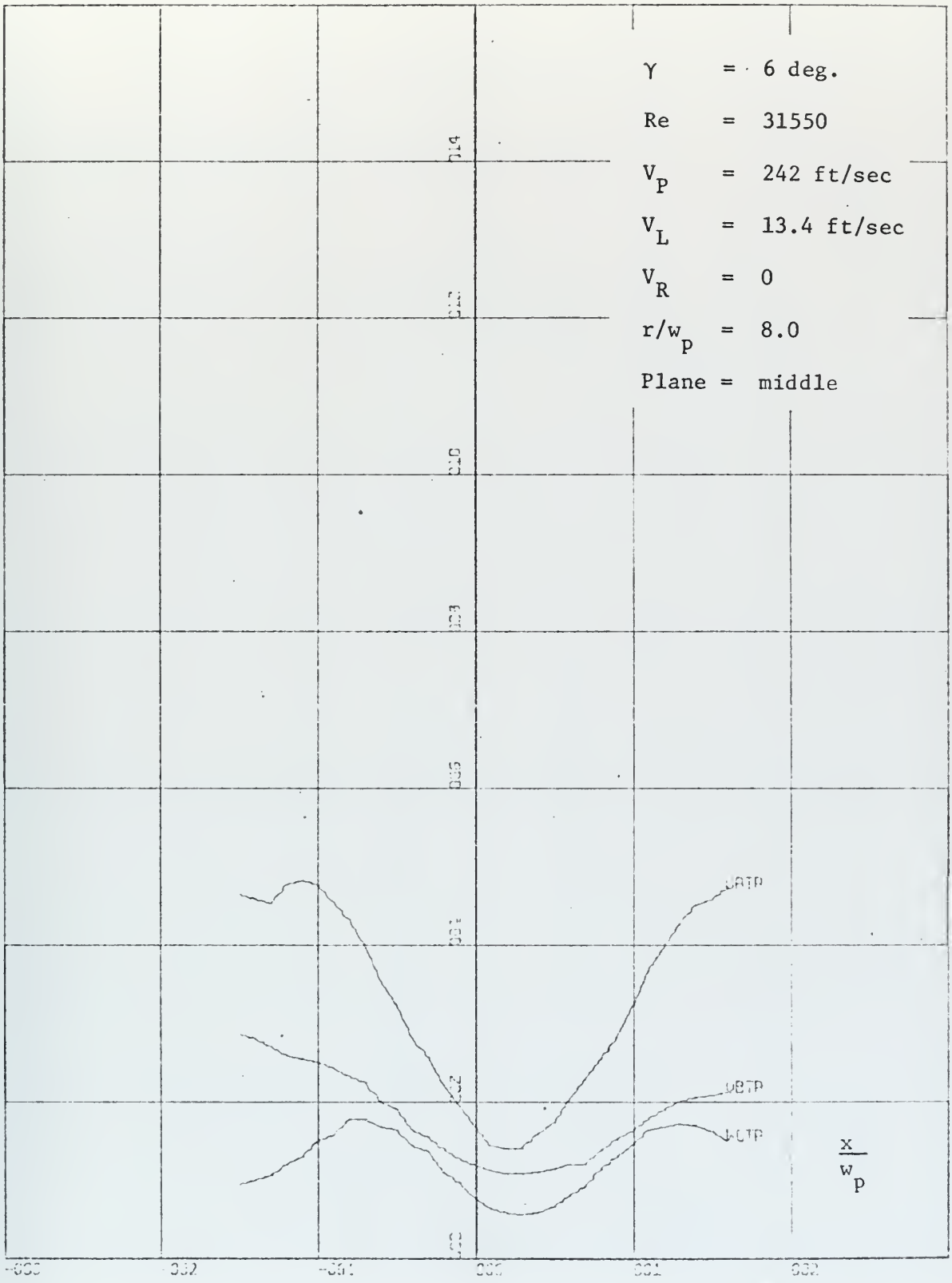

Figure 61. Turbulence Components

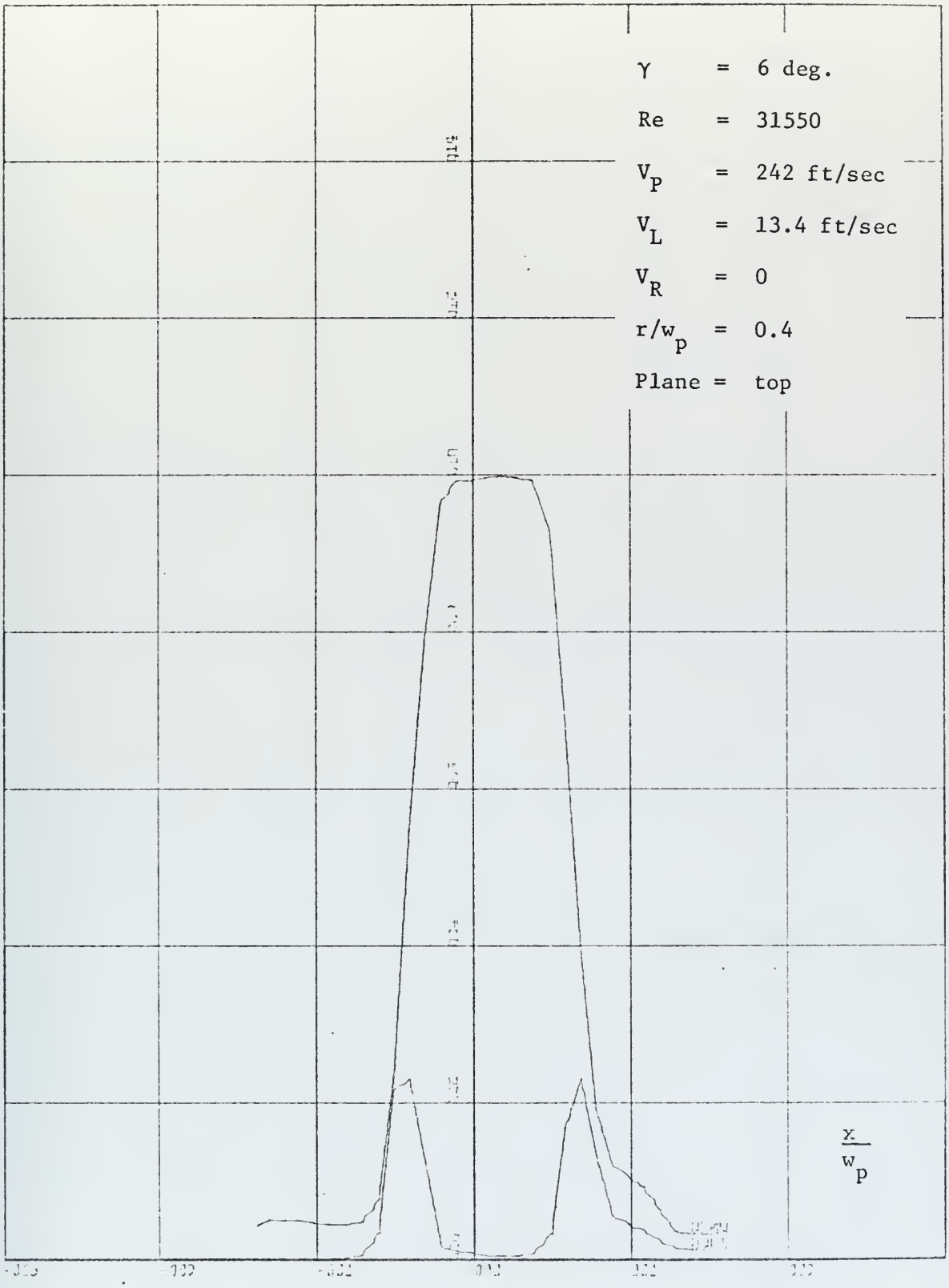

Figure 62. Mean Velocity and Noise

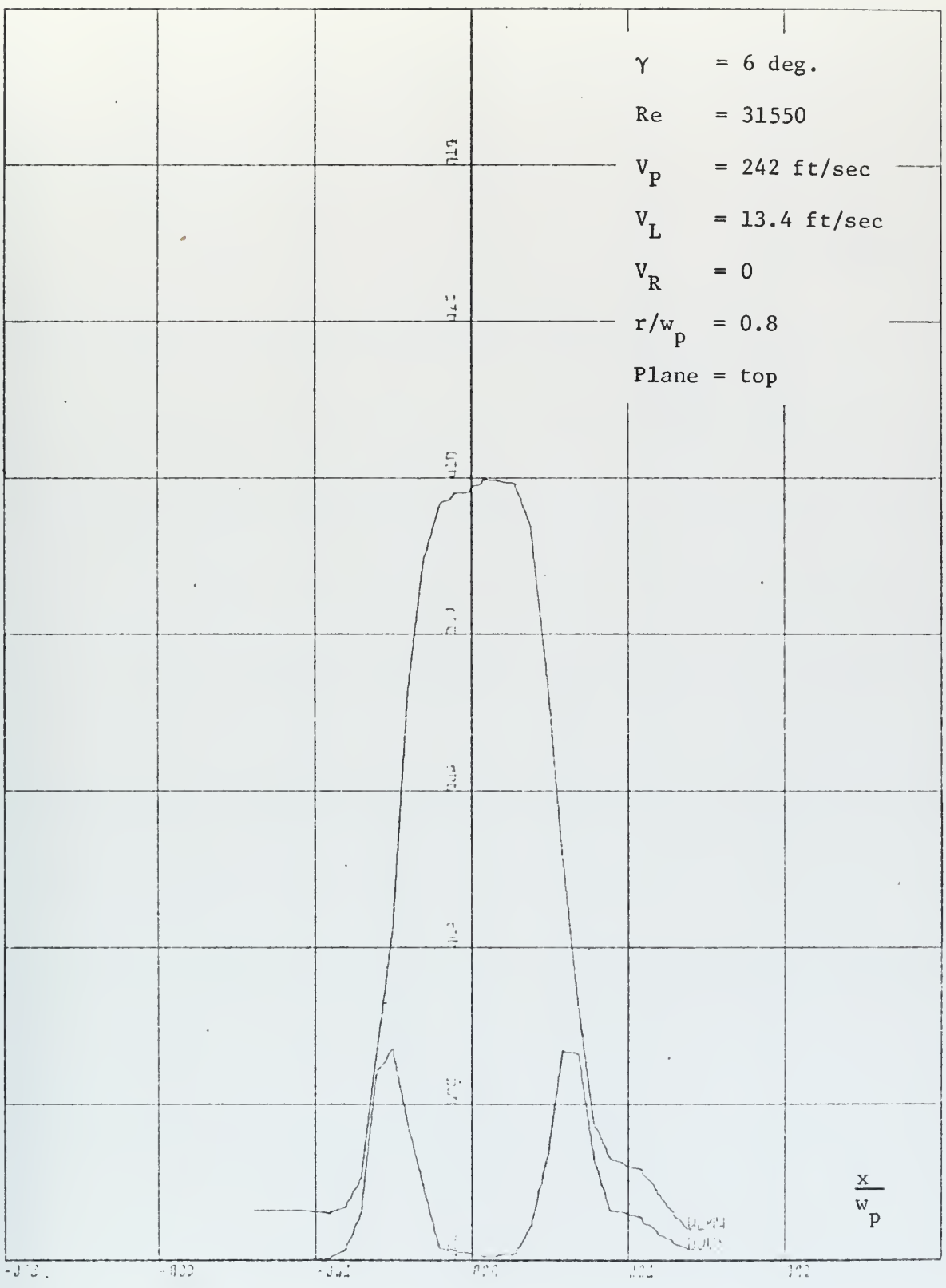

Figure 63. Mean Velocity and Noise

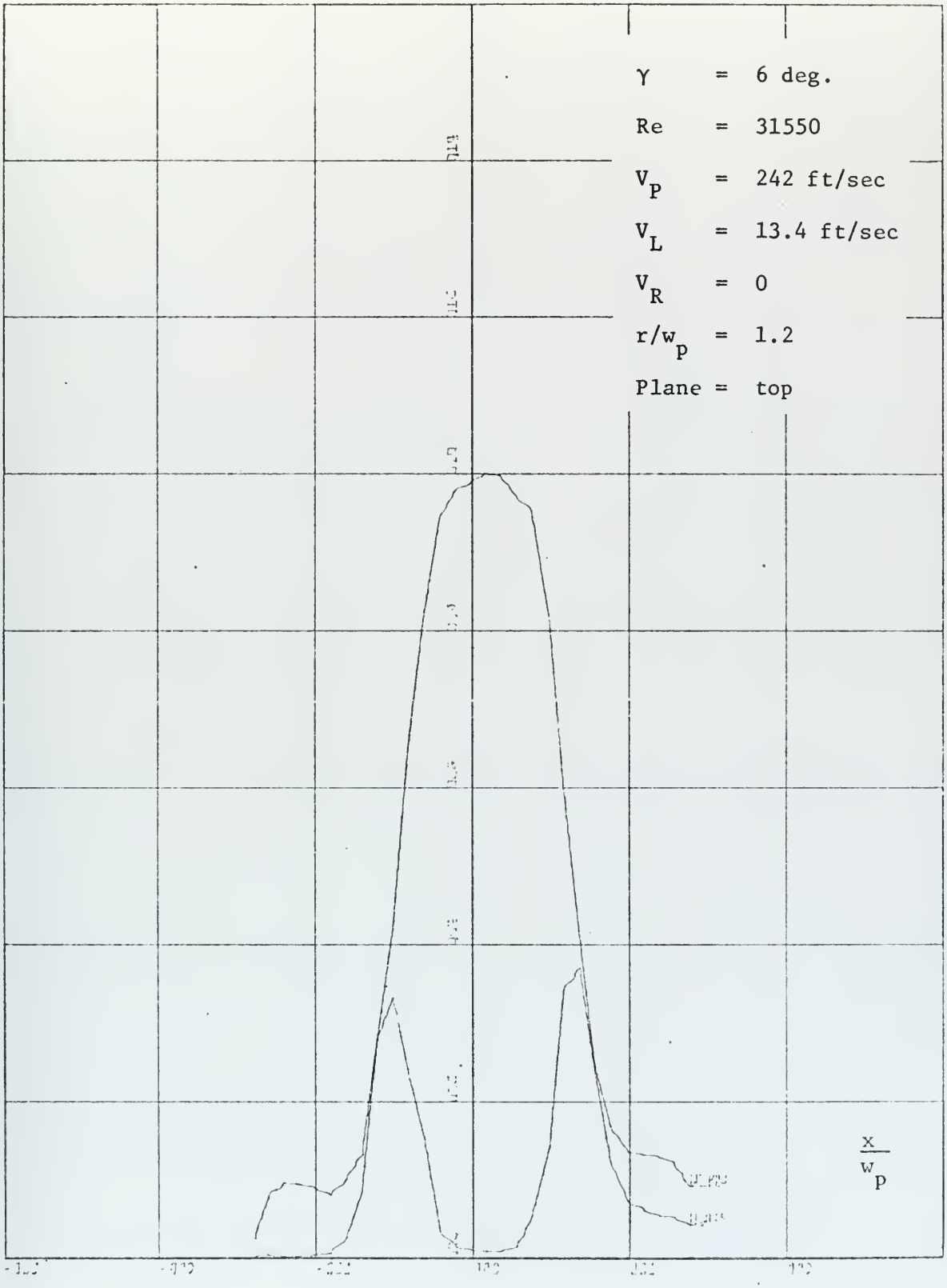

Figure 64. Mean Velocity and Noise

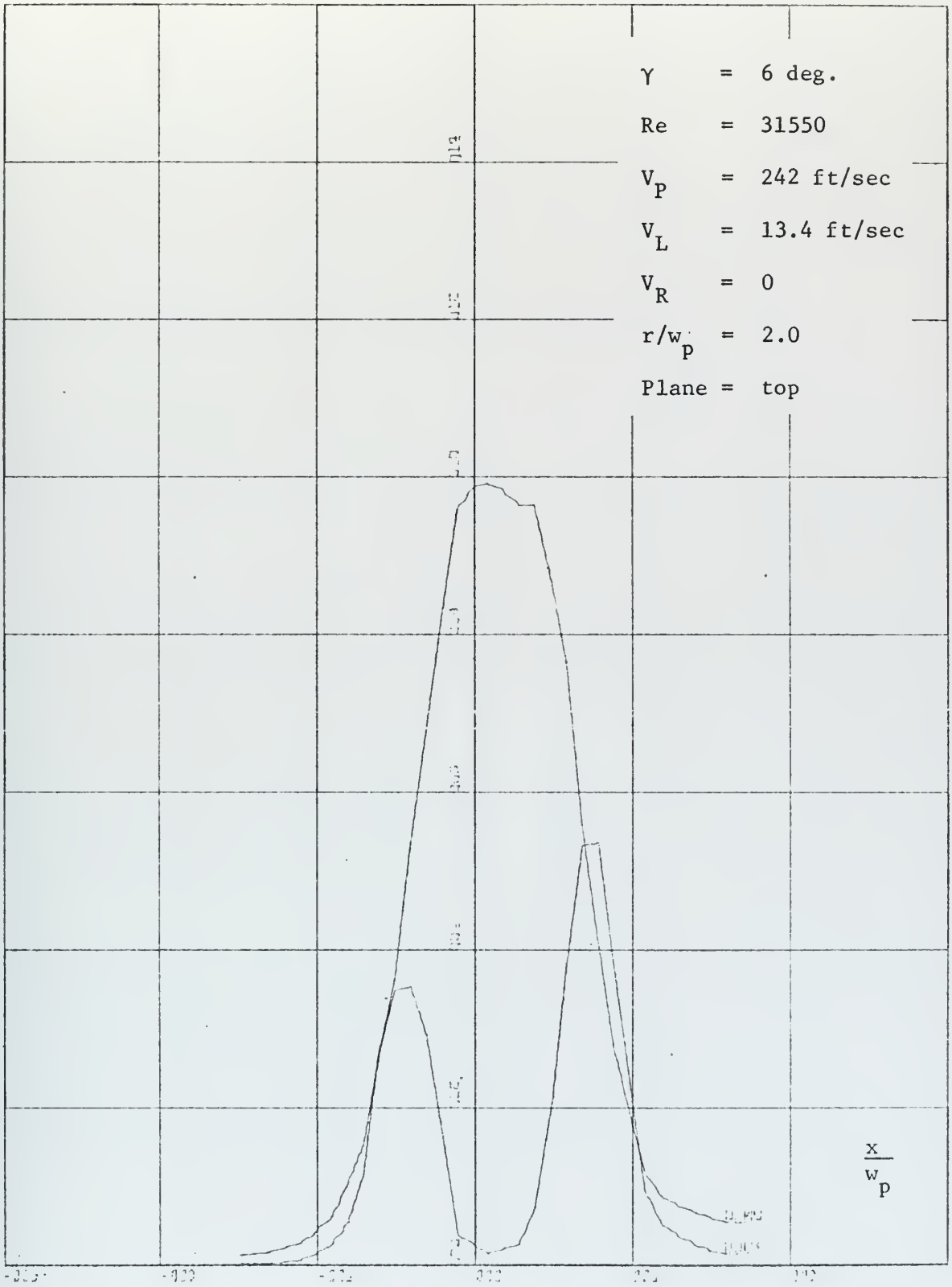

Figure 65. Mean Velocity and Noise

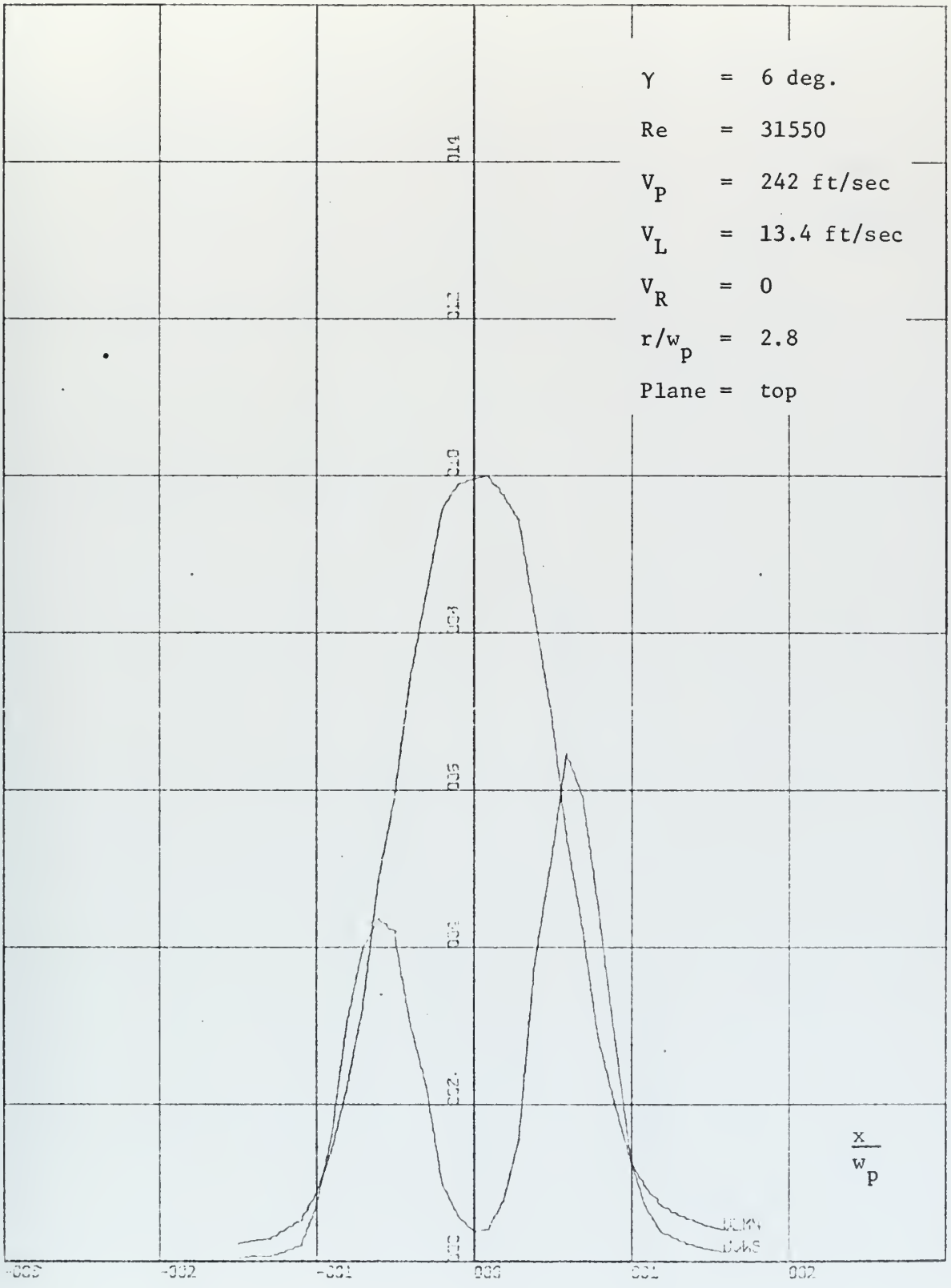

Figure 66. Mean Velocity and Noise

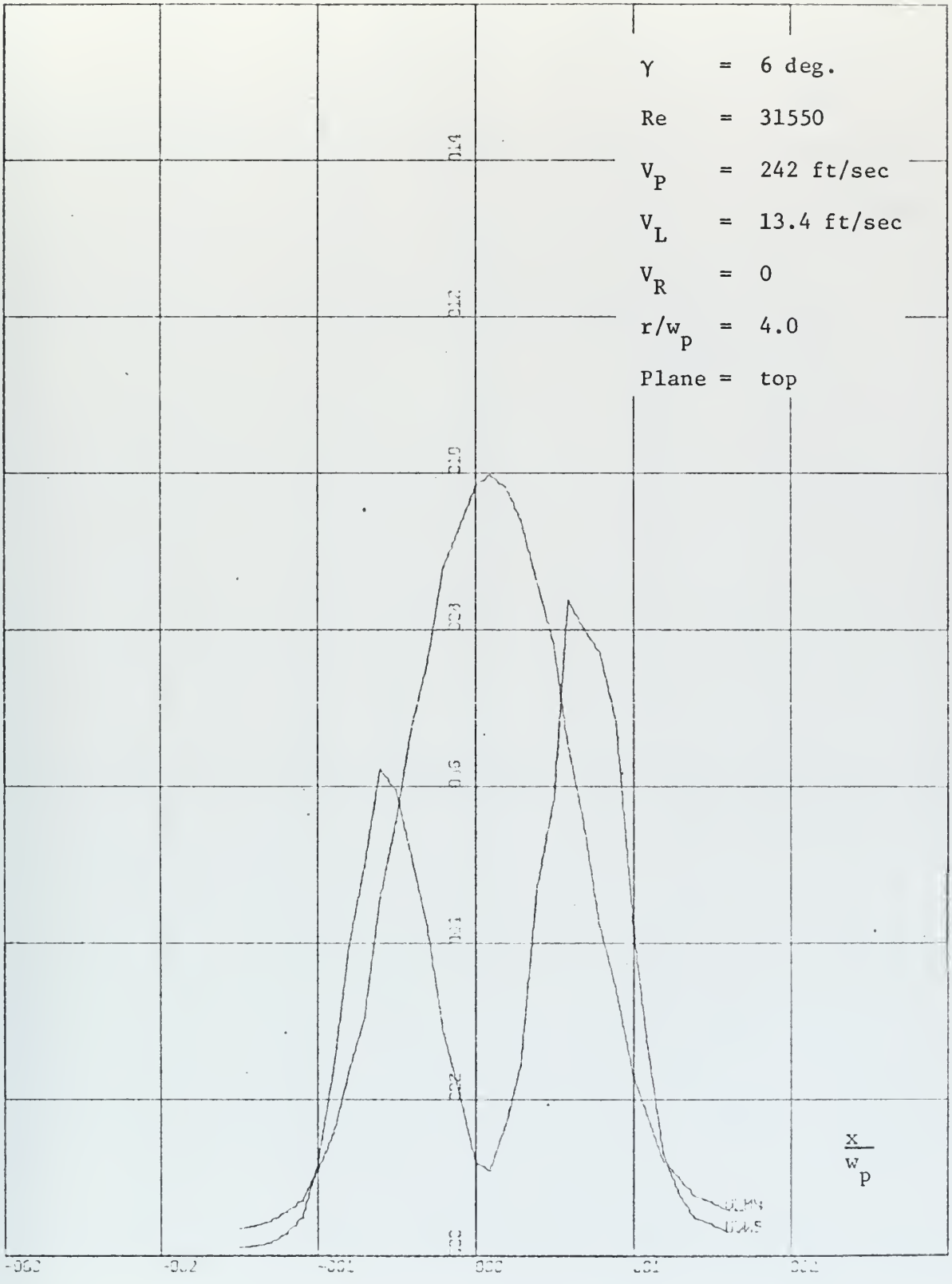

Figure 67. Mean Velocity and Noise

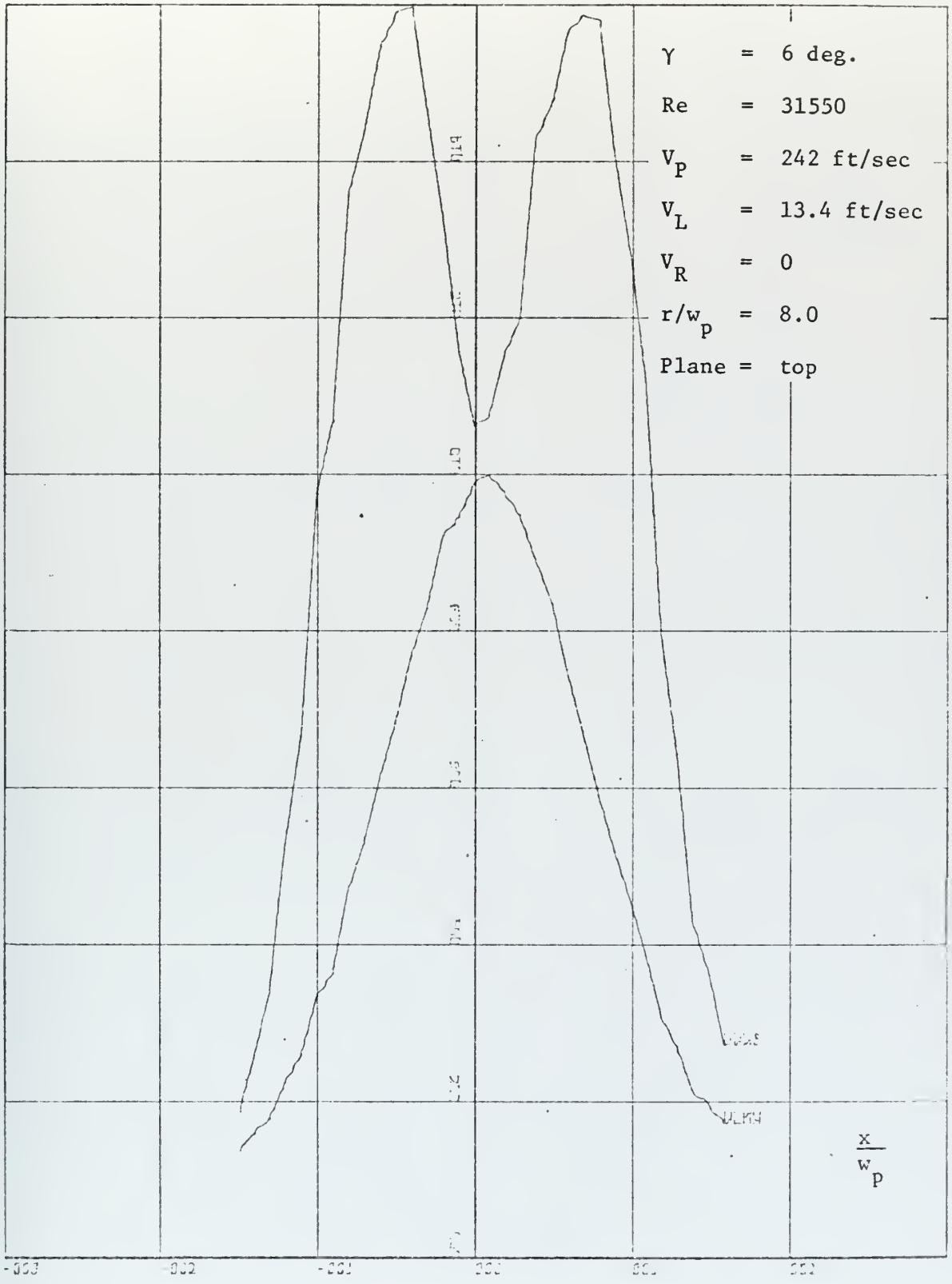

Figure 68. Mean Velocity and Noise

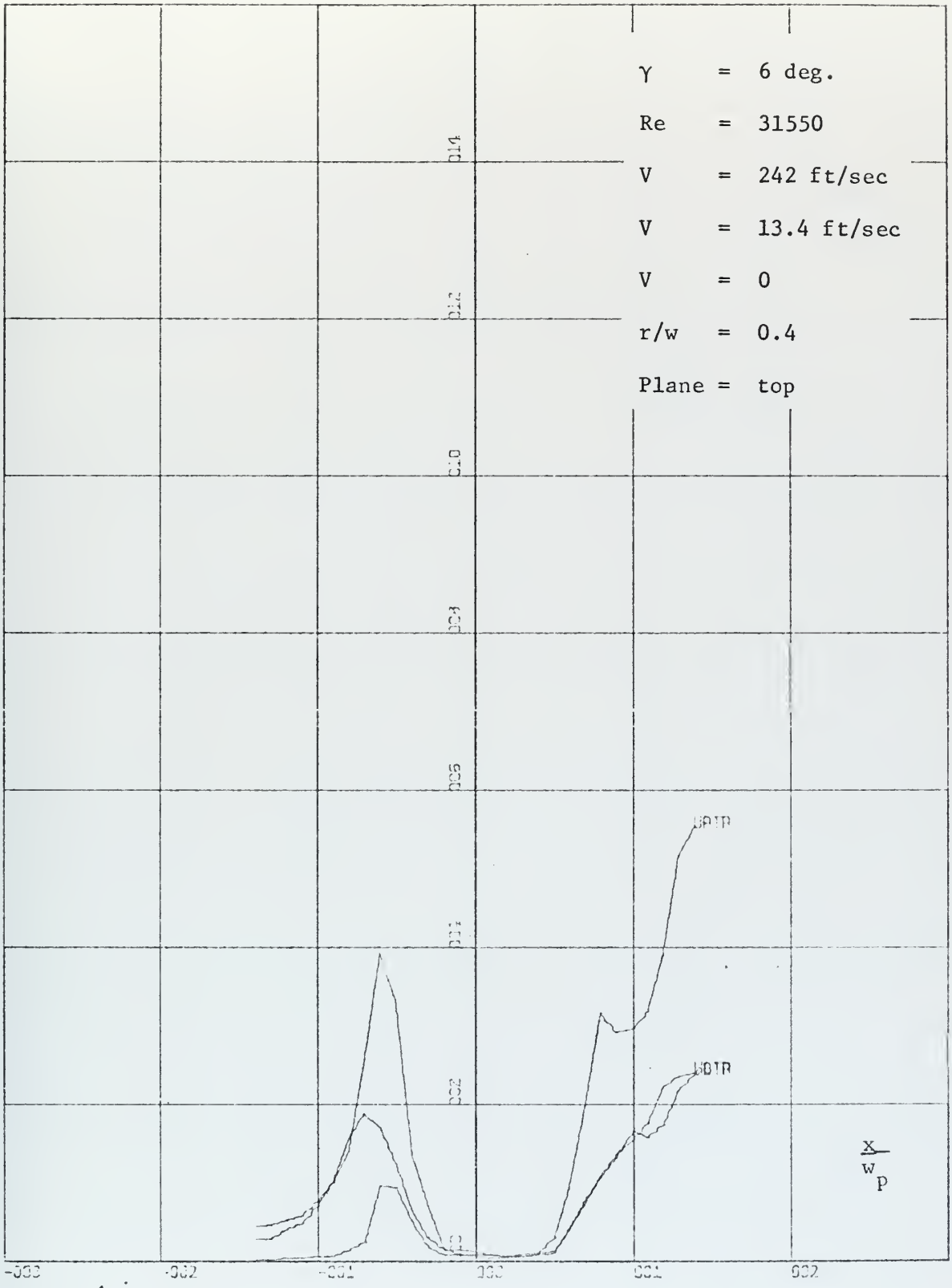

Figure 69. Turbulence Components

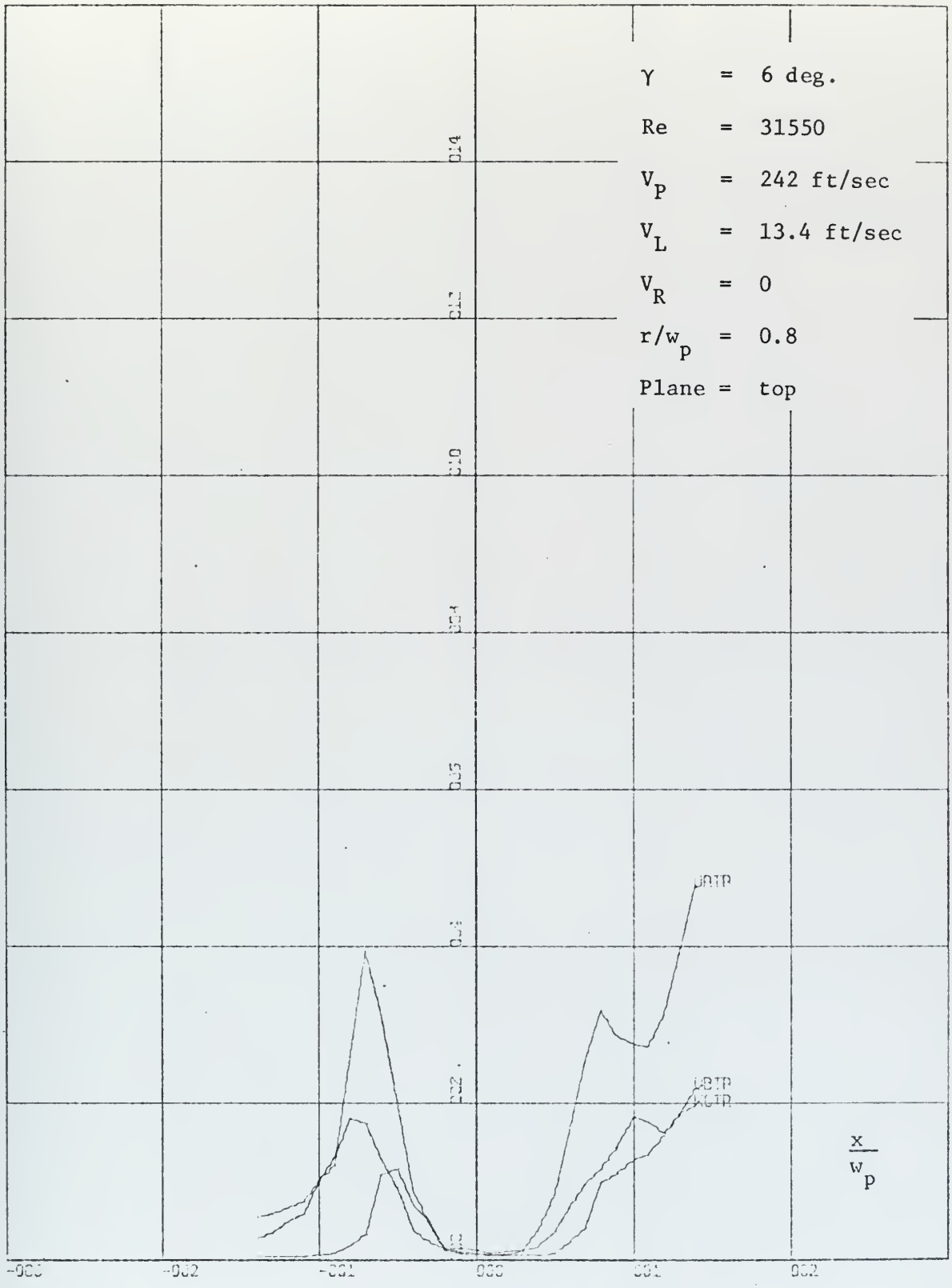

Figure 70. Turbulence Components

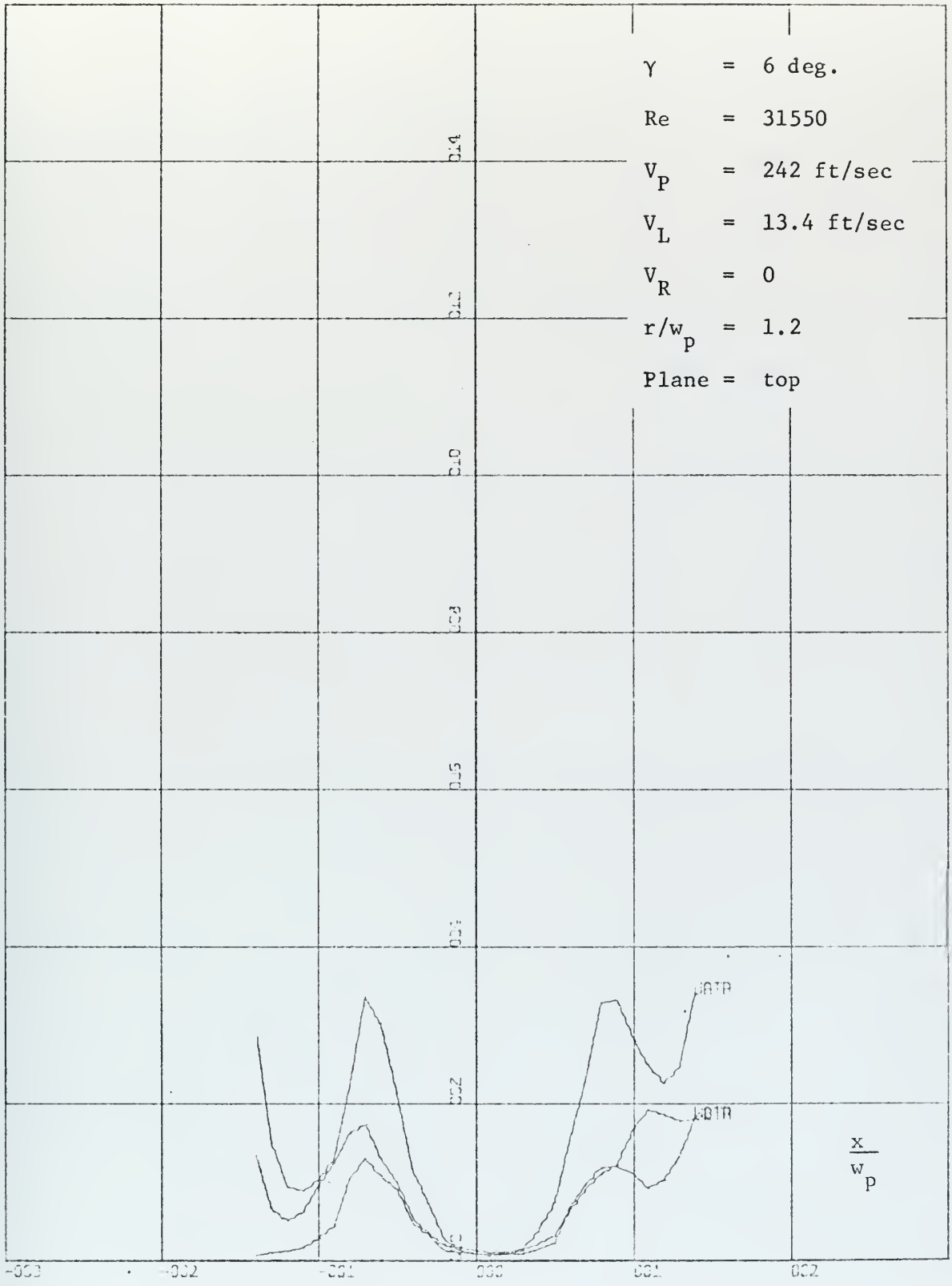

Figure 71. Turbulence Components

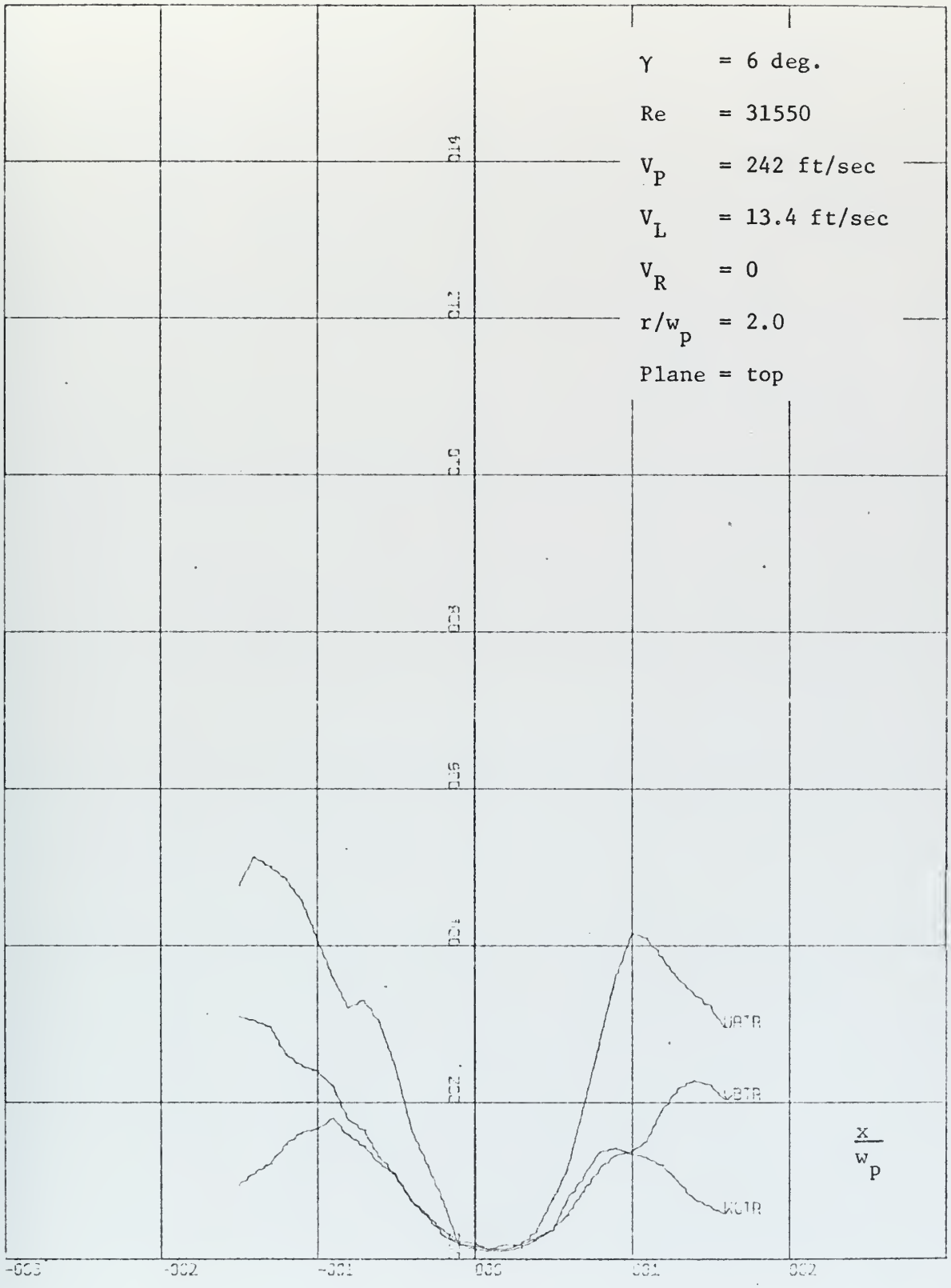

Figure 72. Turbulence Components

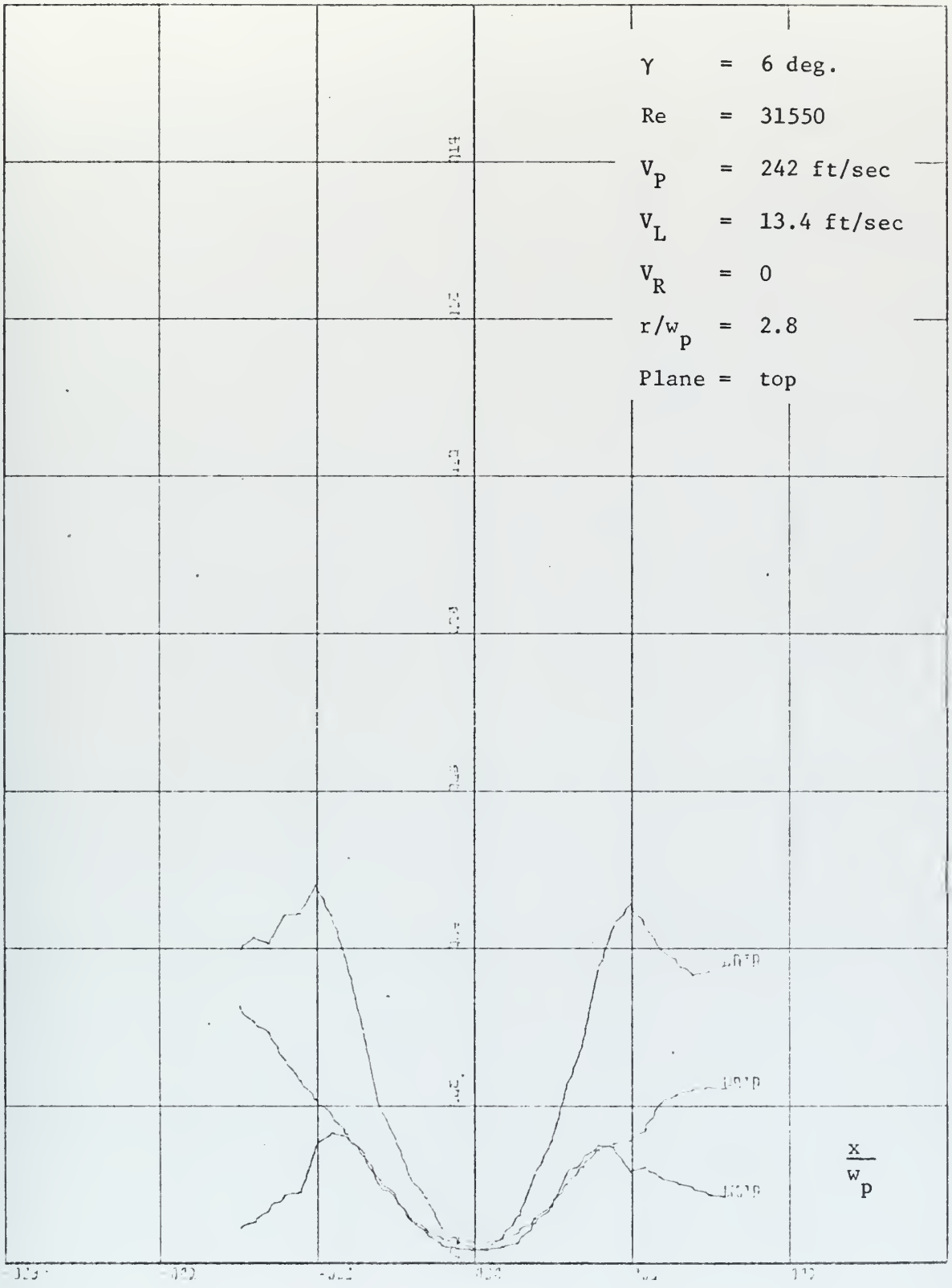

Figure 73. Turbulence Components

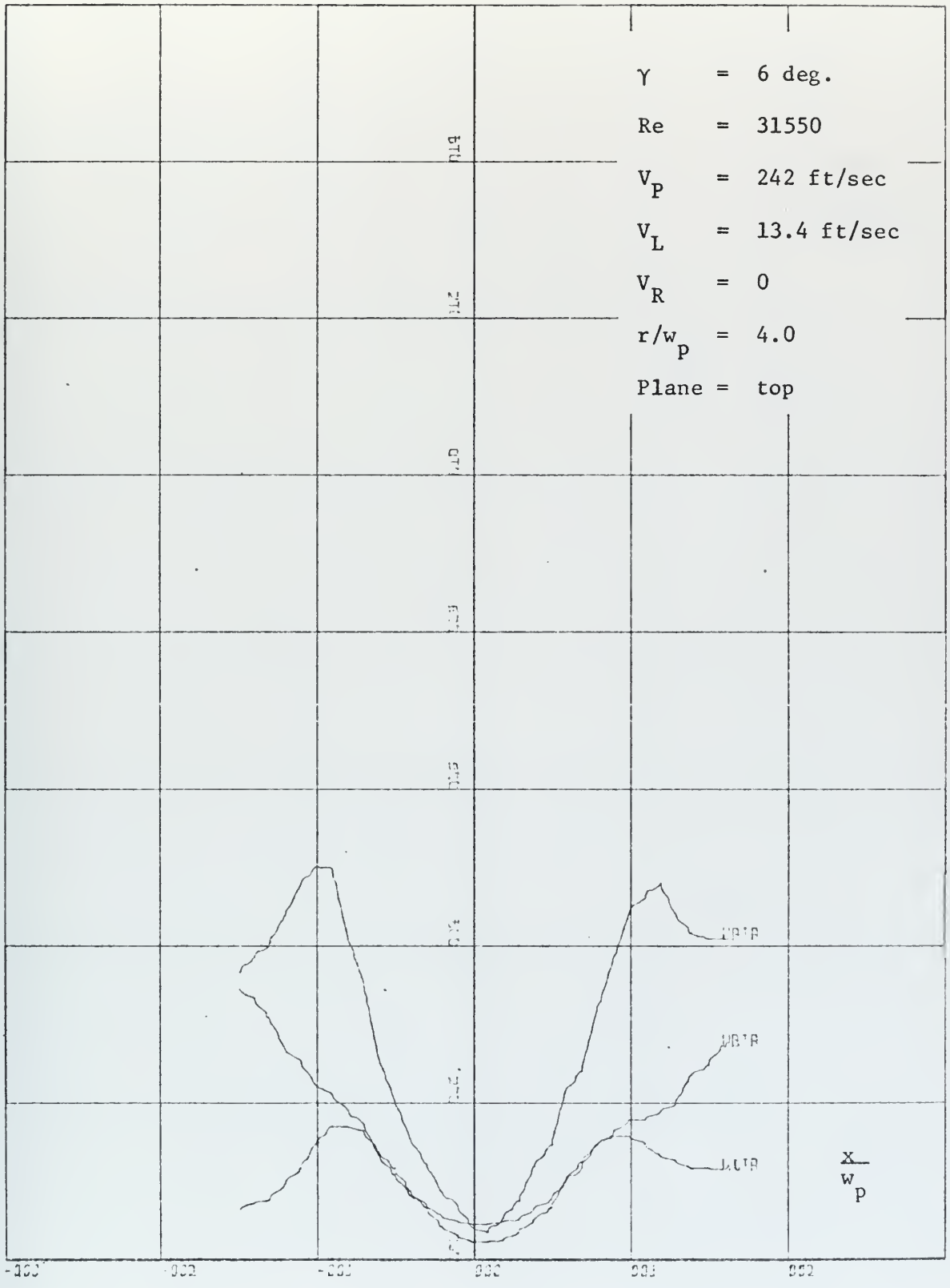

Figure 74. Turbulence Components

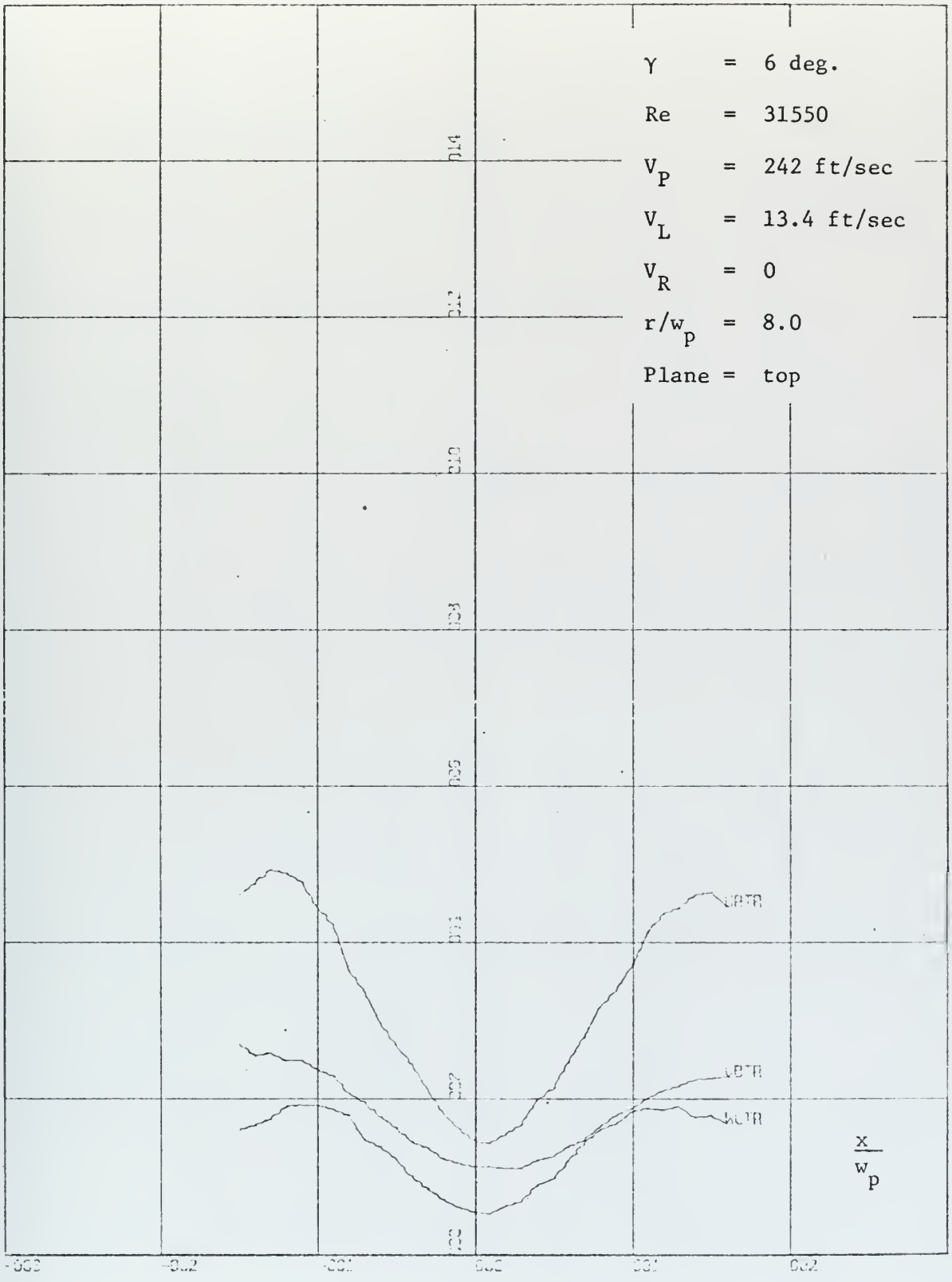

Figure 75. Turbulence Components

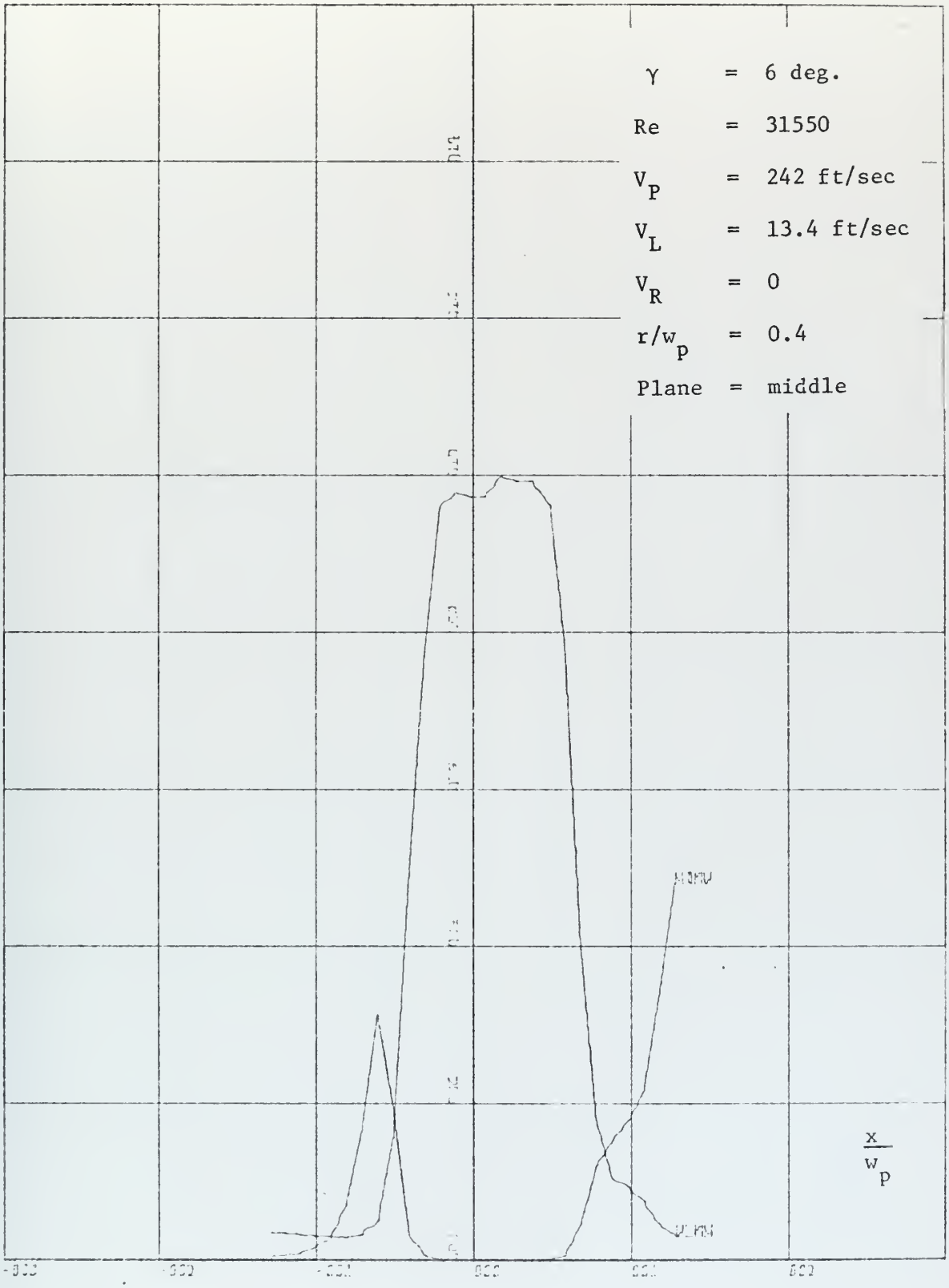

Figure 76. Mean Velocity and Noise

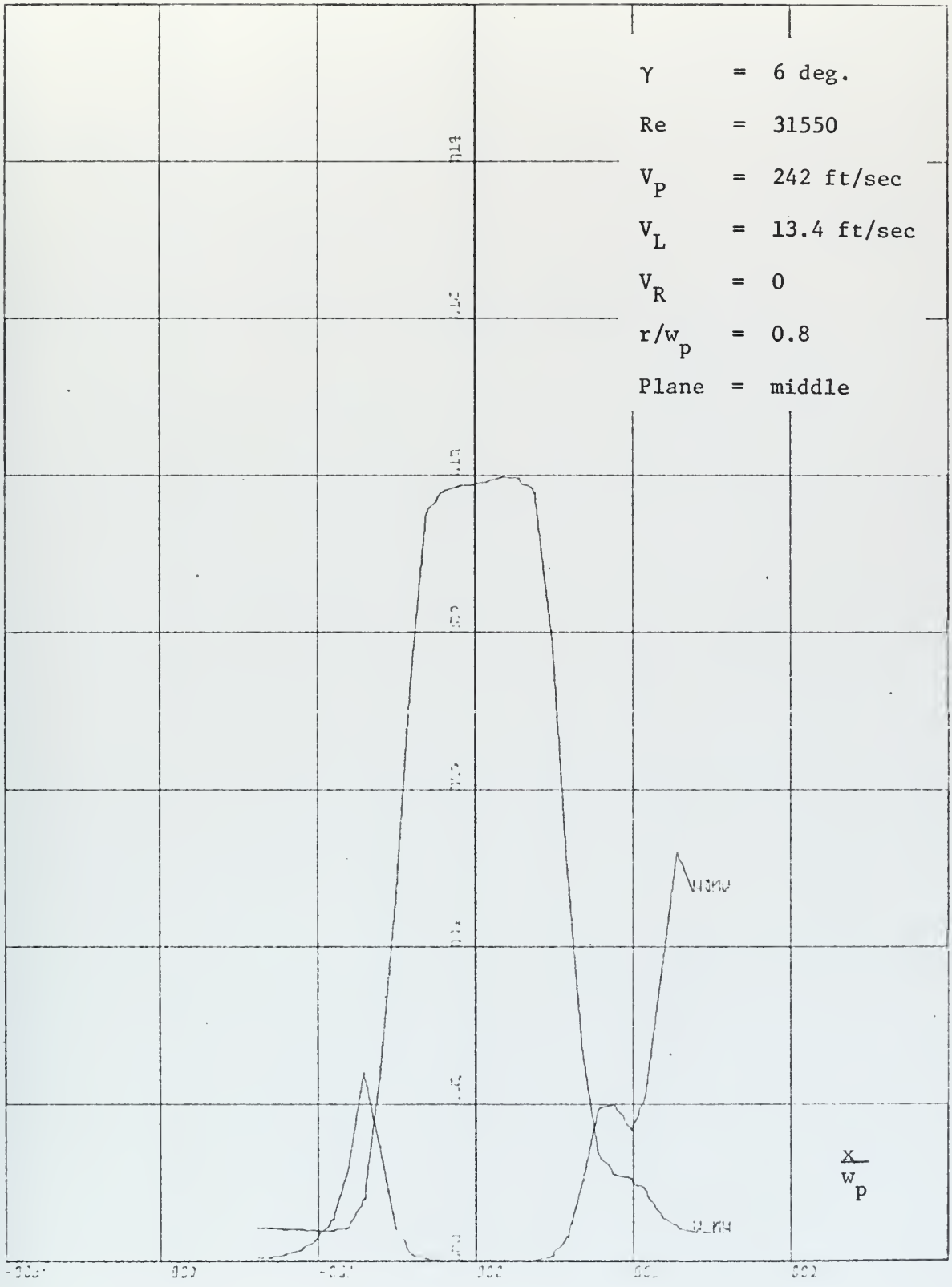

Figure 77. Mean Velocity and Noise

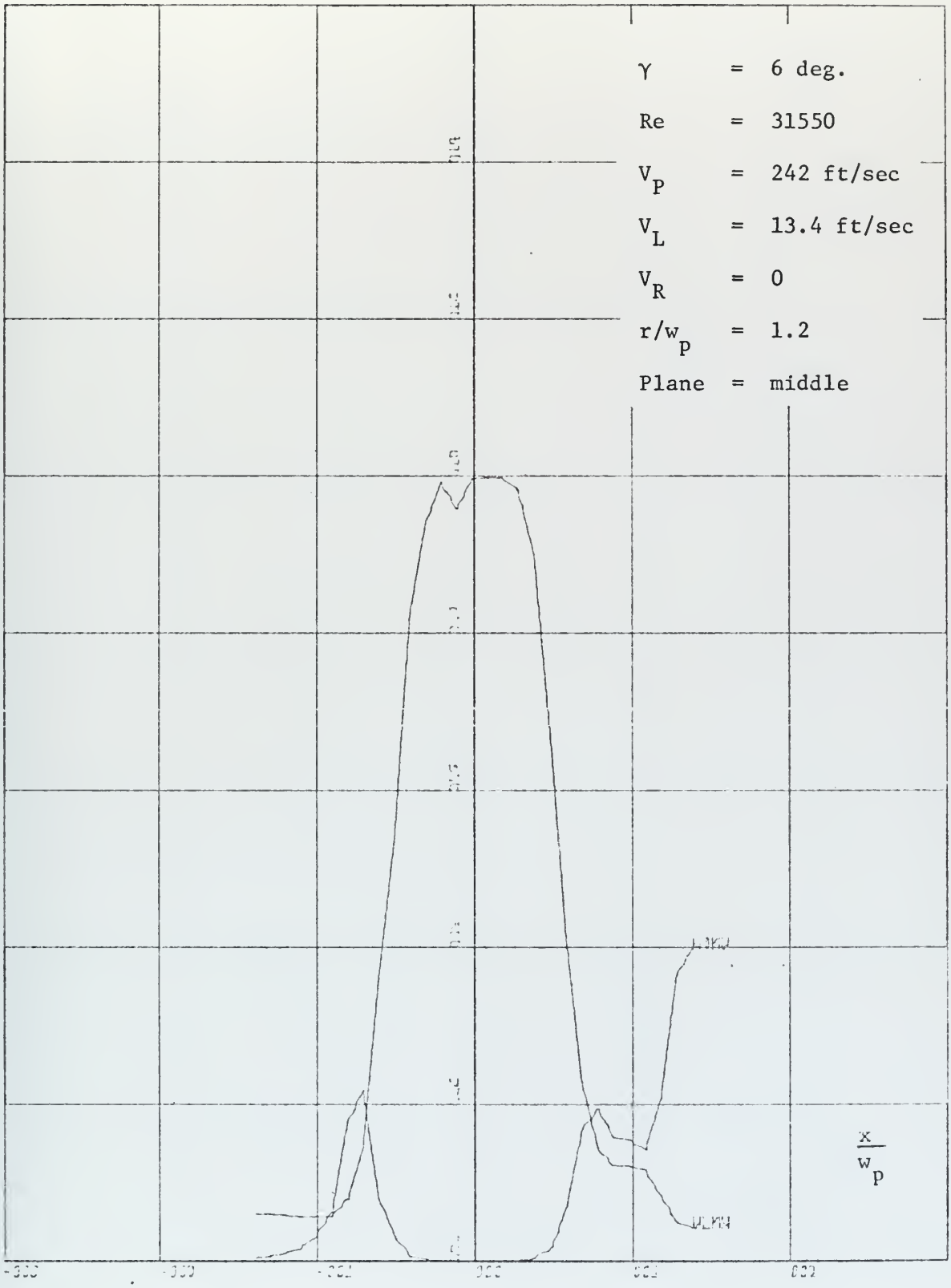

Figure 78. Mean Velocity and Noise

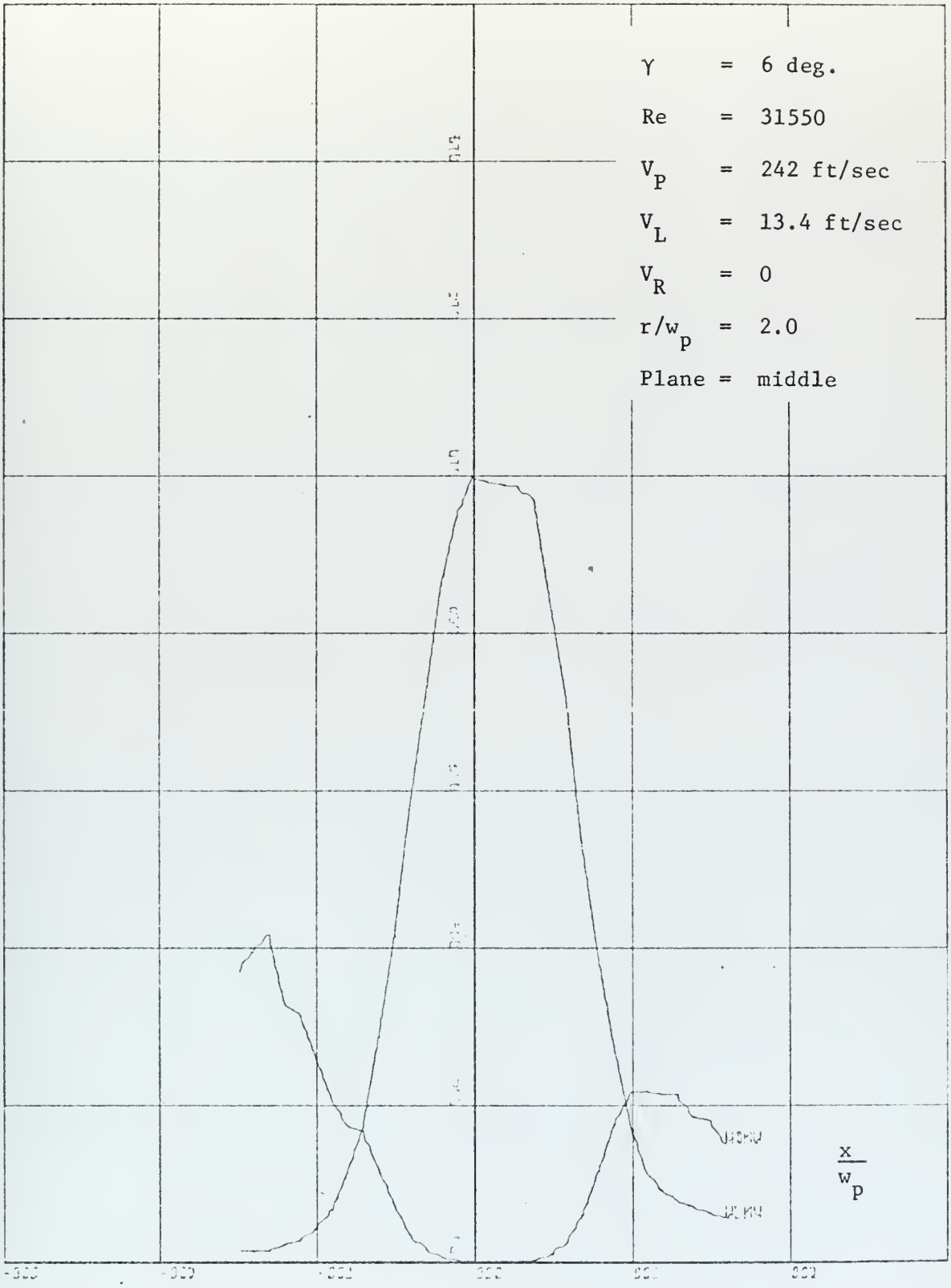

Figure 79. Mean Velocity and Noise

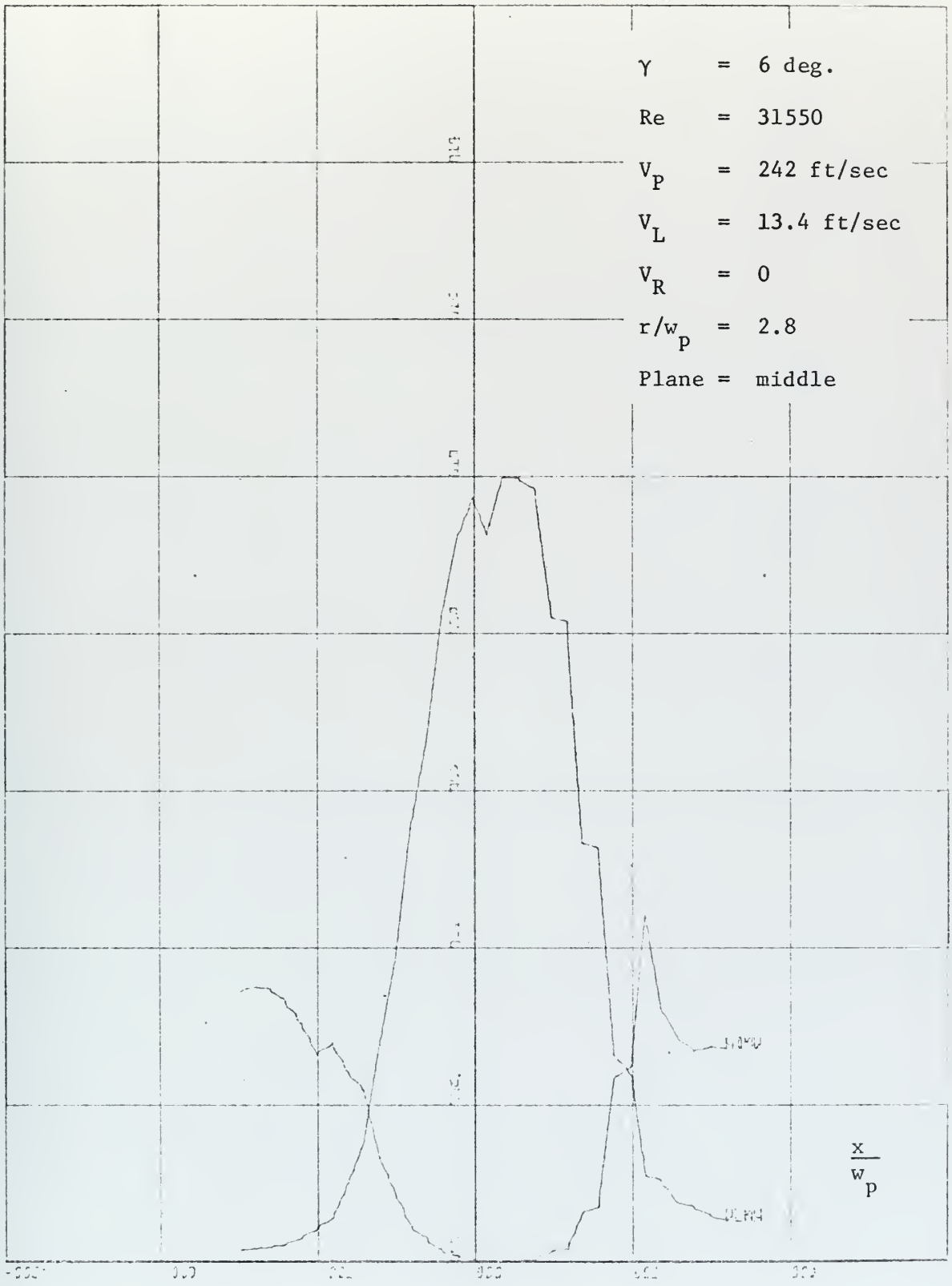

Figure 80. Mean Velocity and Noise

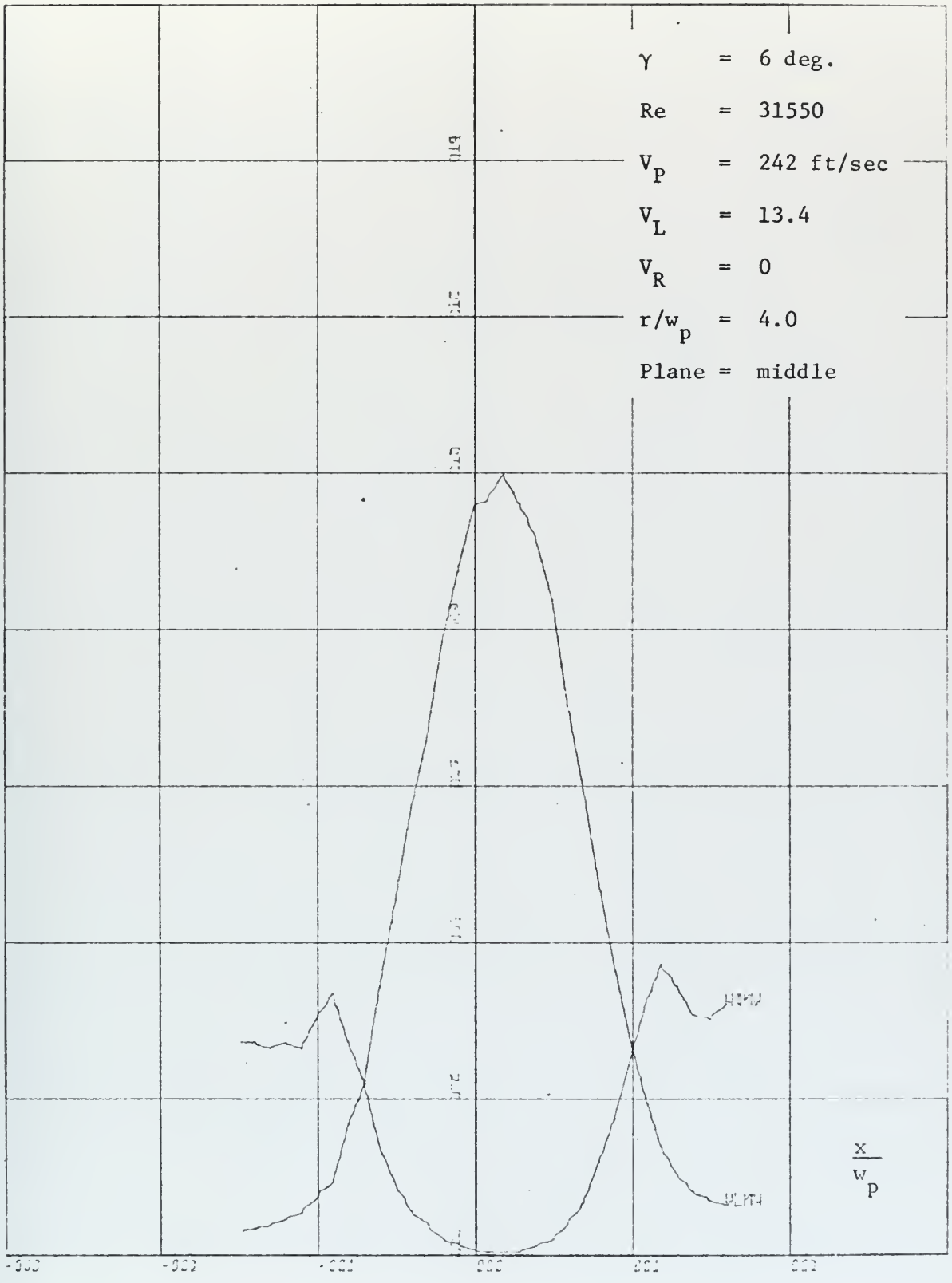

Figure 81. Mean Velocity and Noise

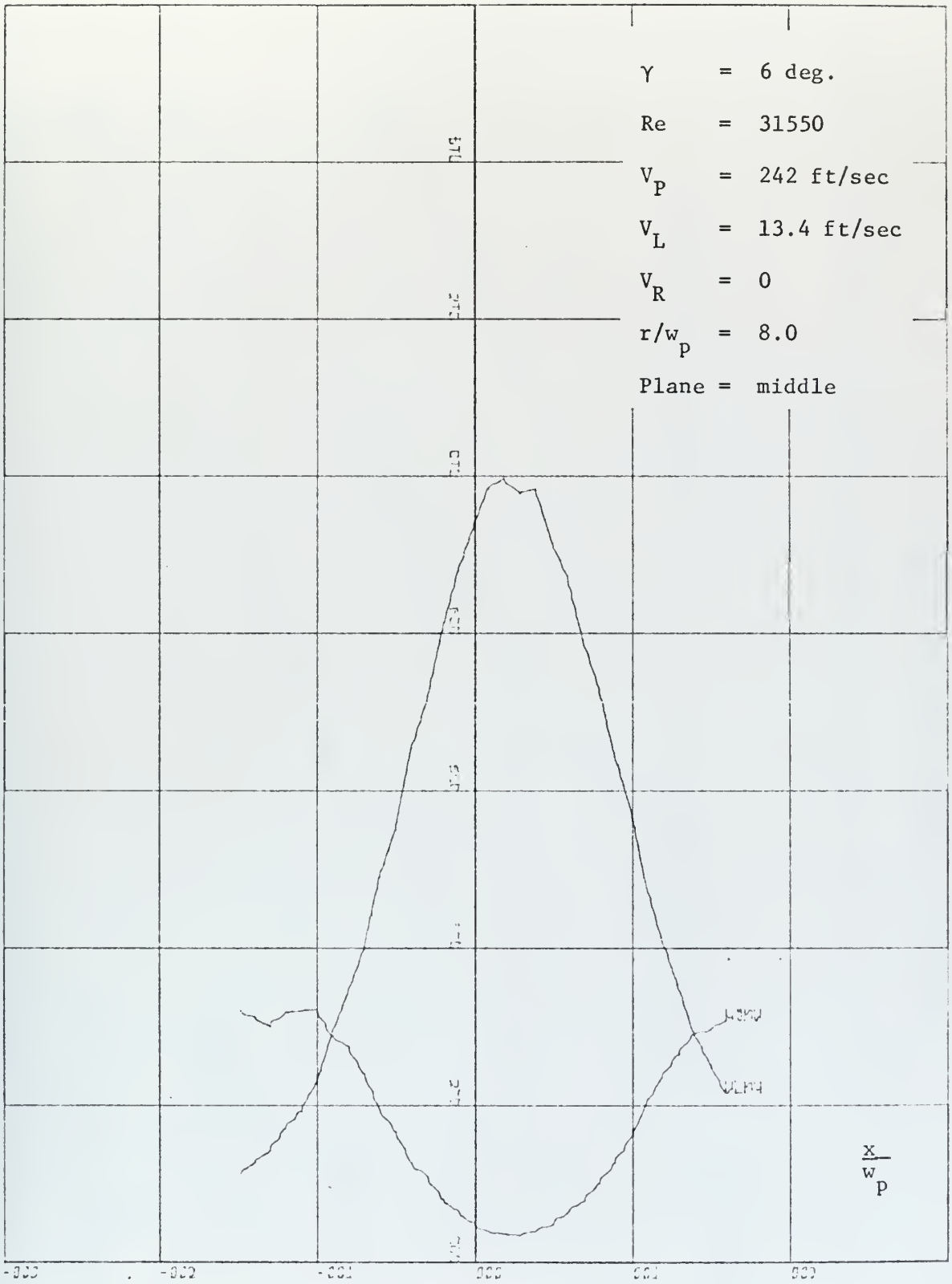

Figure 82. Mean Velocity and Noise

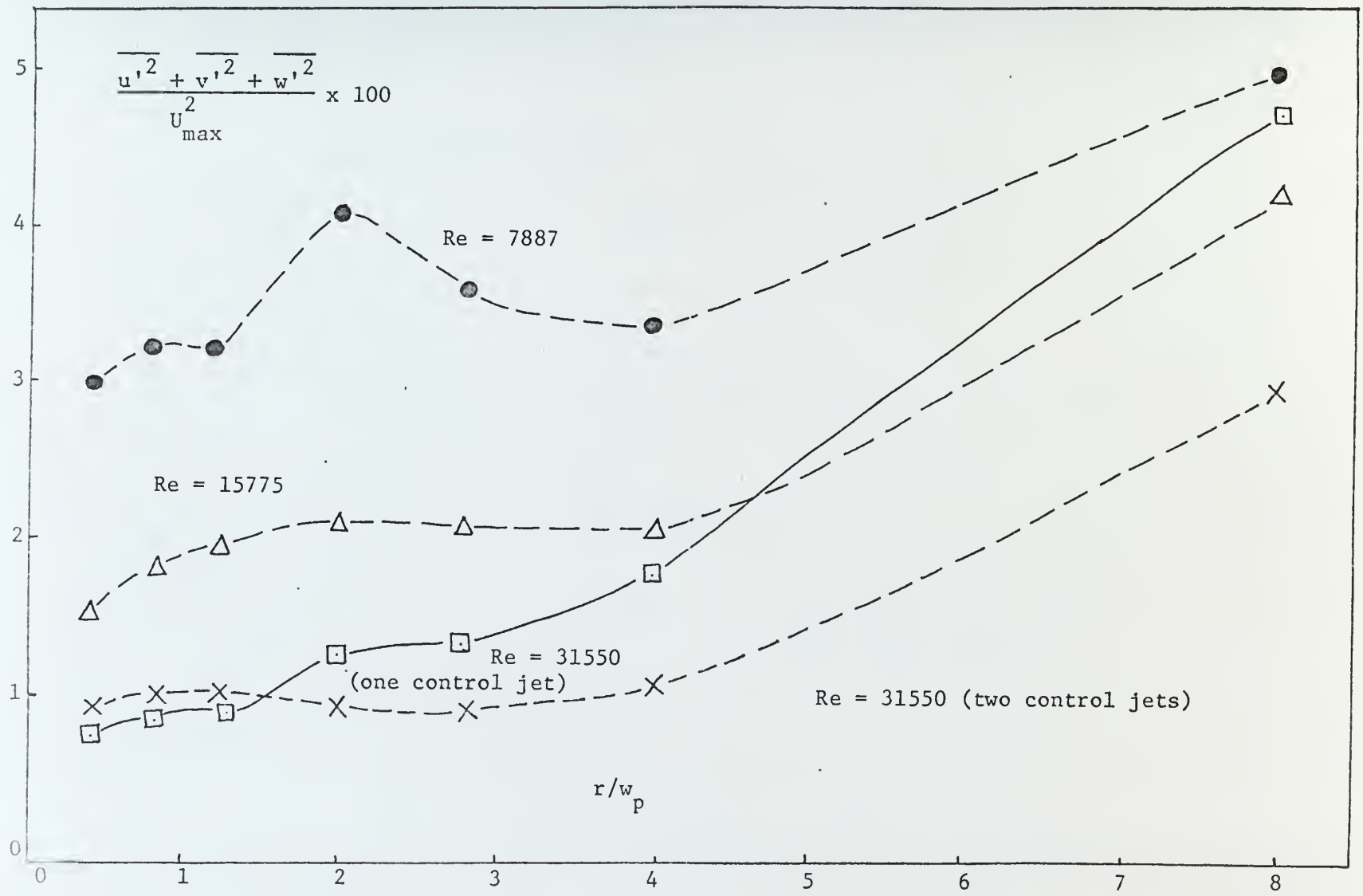

Figure 83. Left Peak Values of Noise.

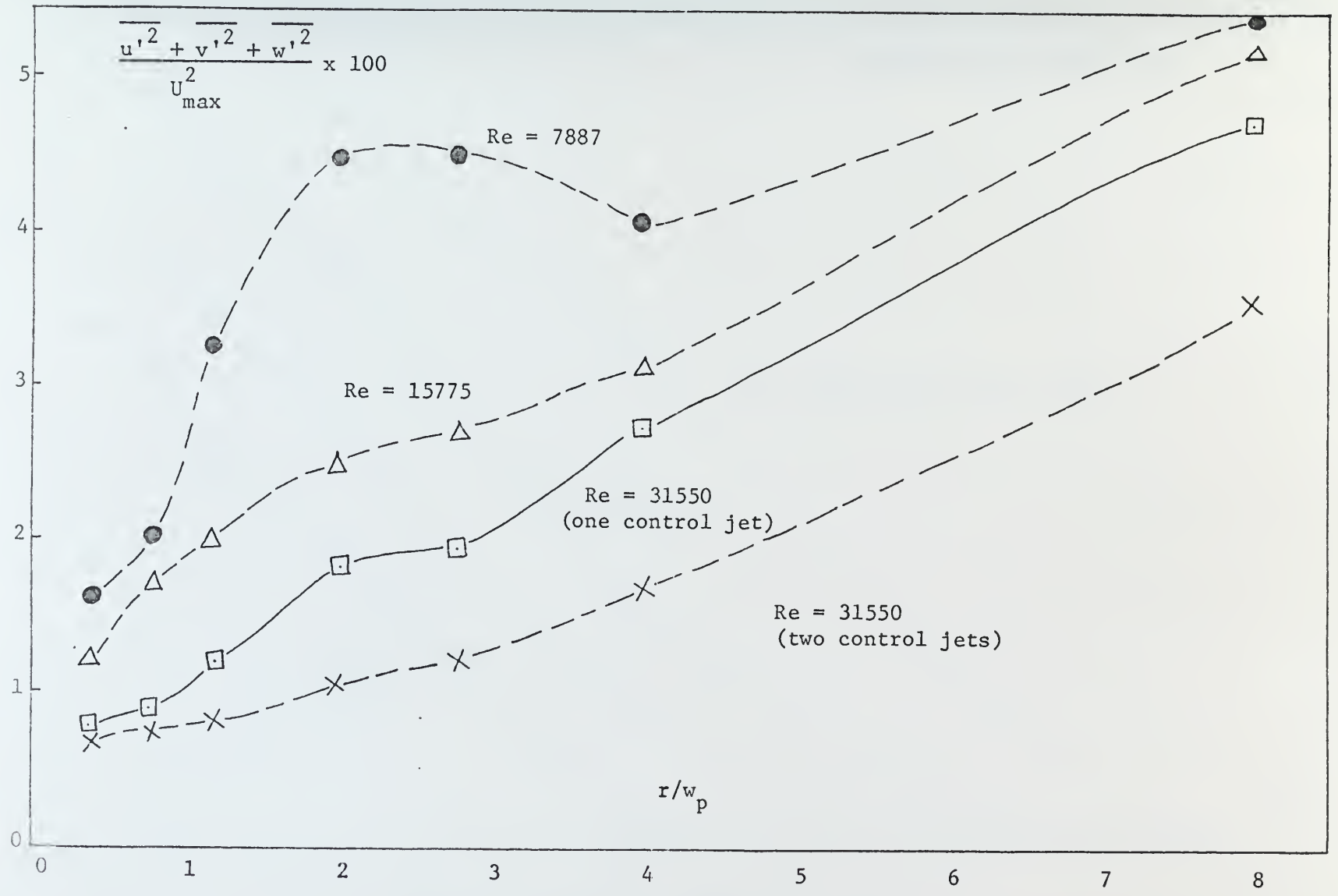

Figure 84. Right Peak Values of Noise.

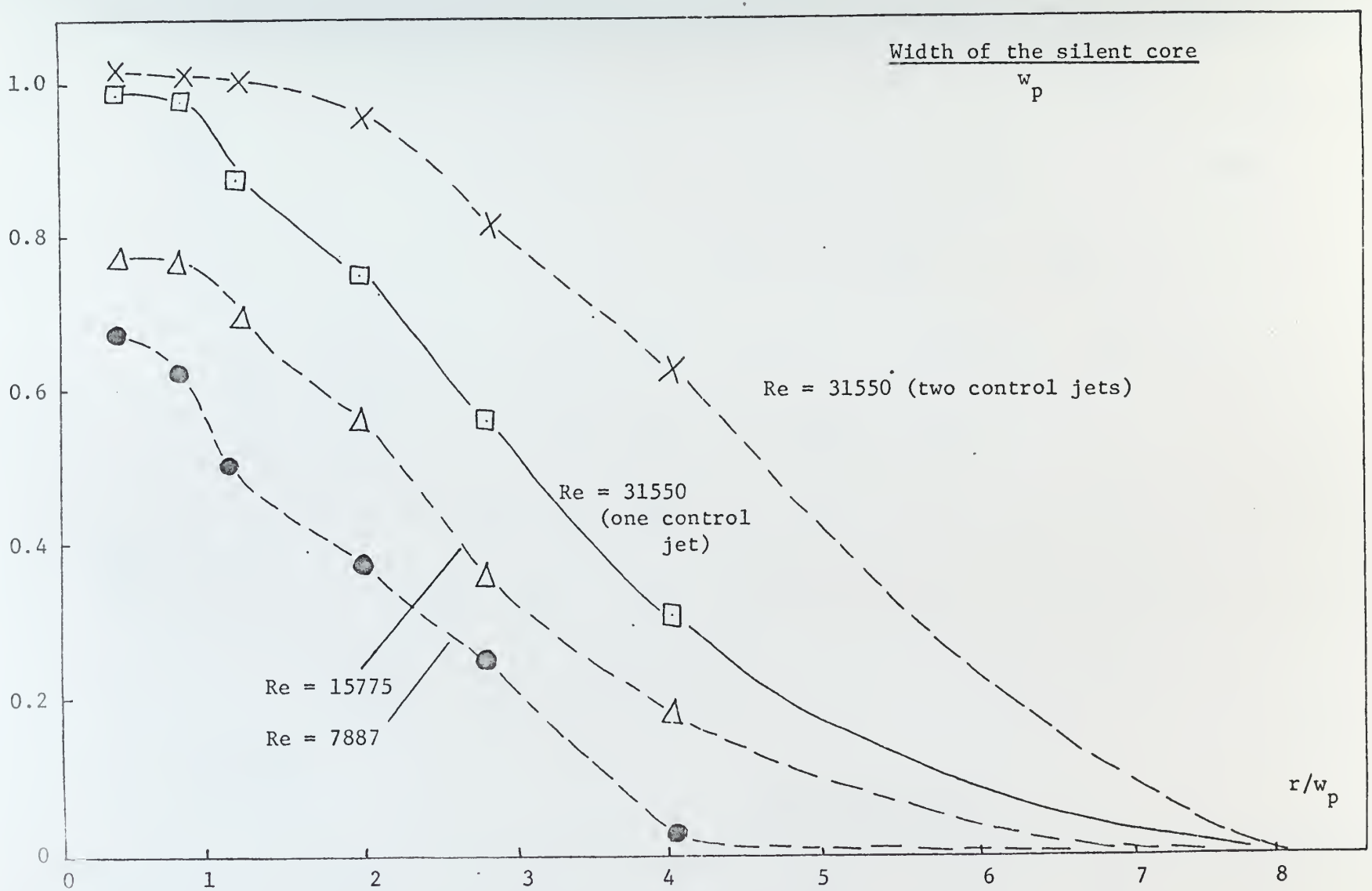

Figure 85. Silent Core Widths.

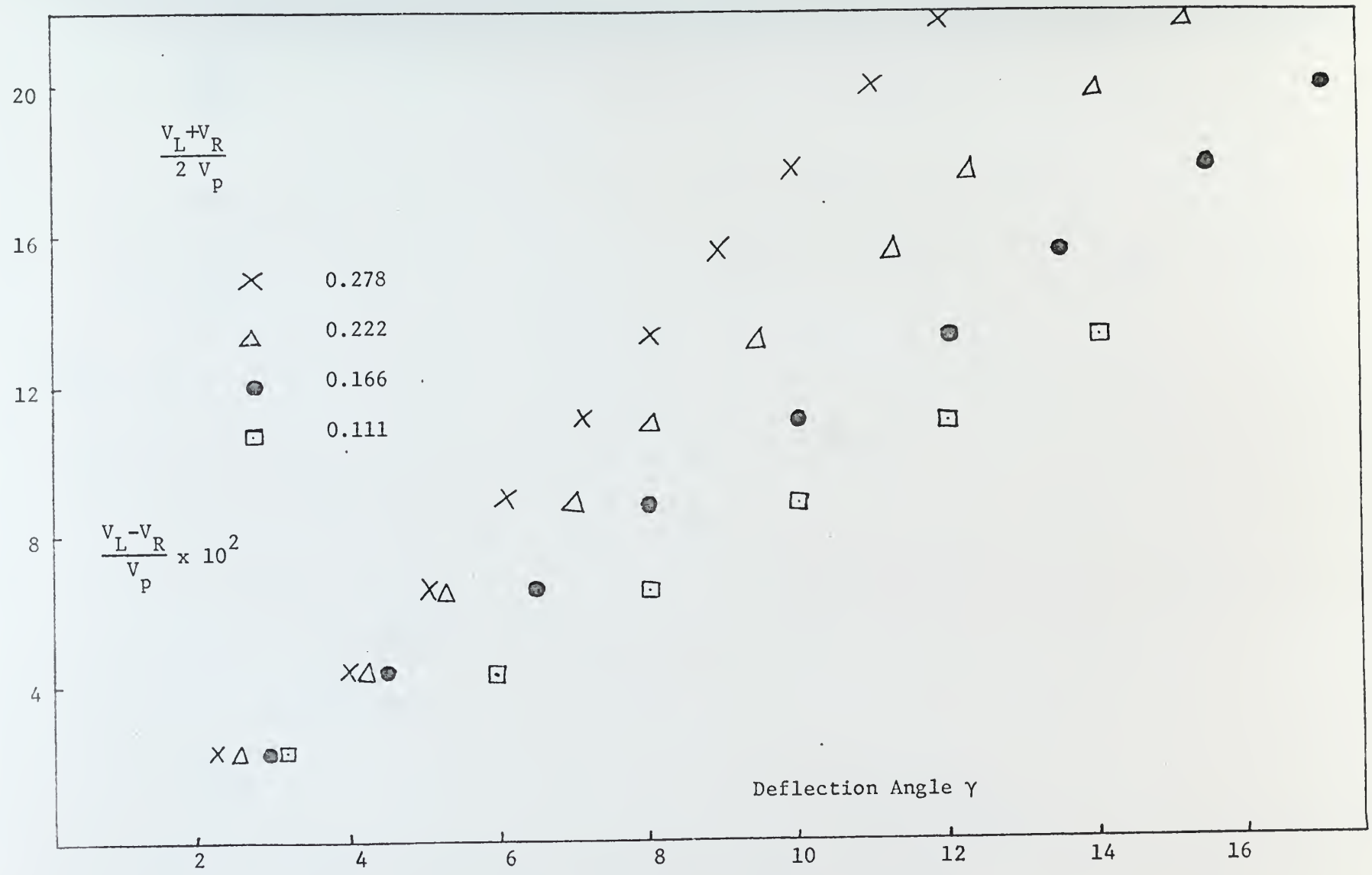

Figure 86. Deflection Angles, Re = 31550 .

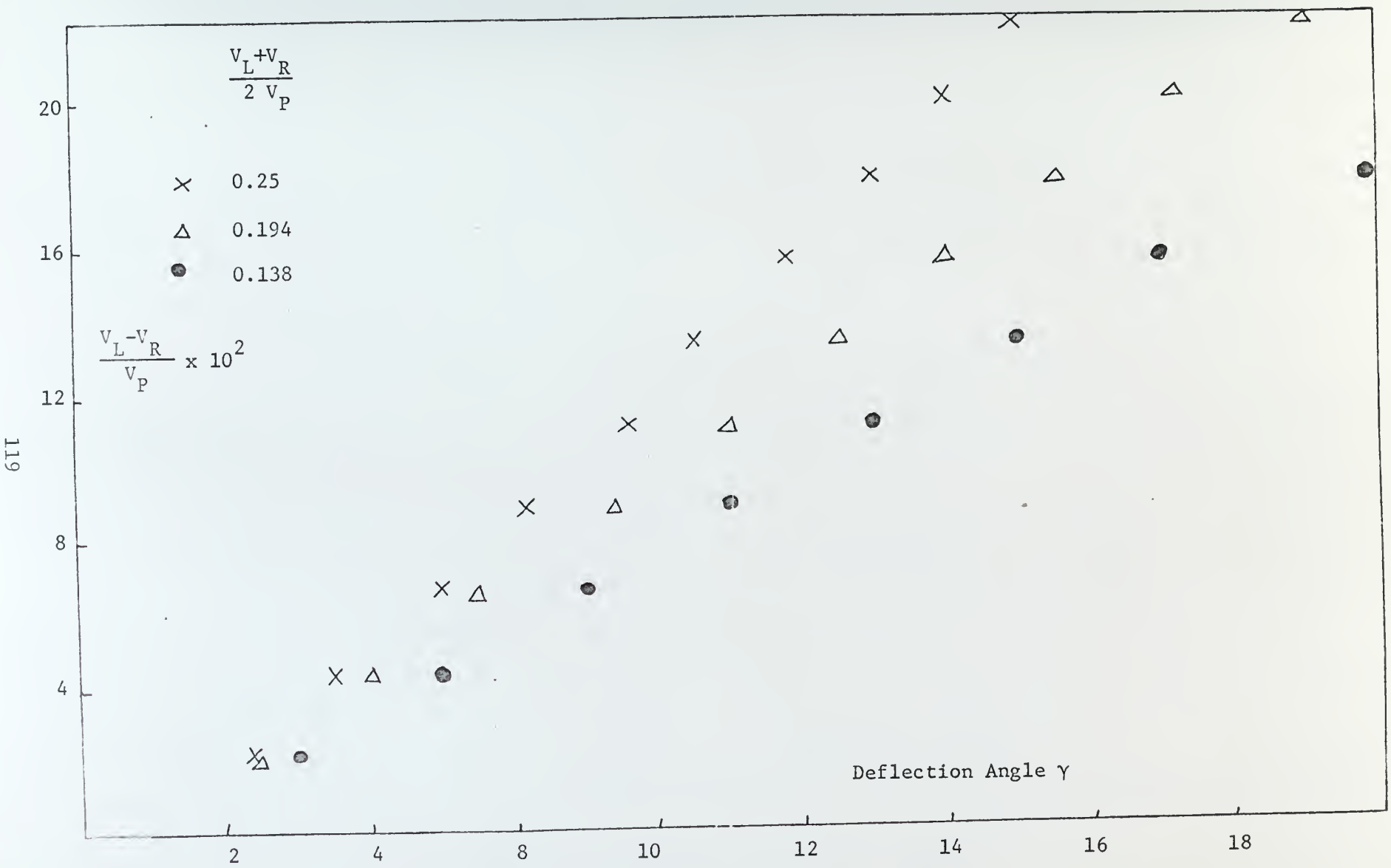

Figure 87. Deflection Angles, Re = 31550

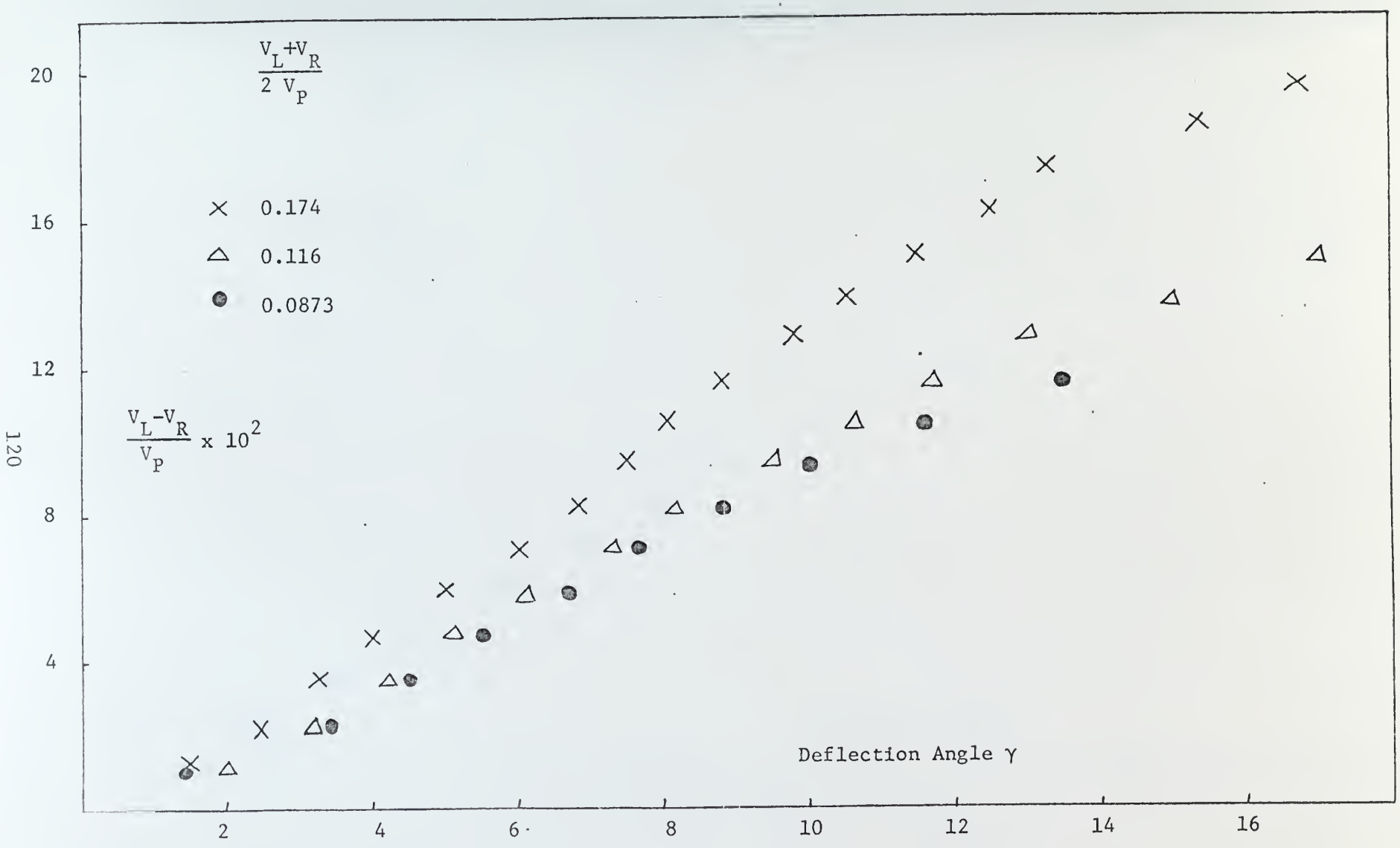

Figure 88. Deflection Angles, Re = 15775

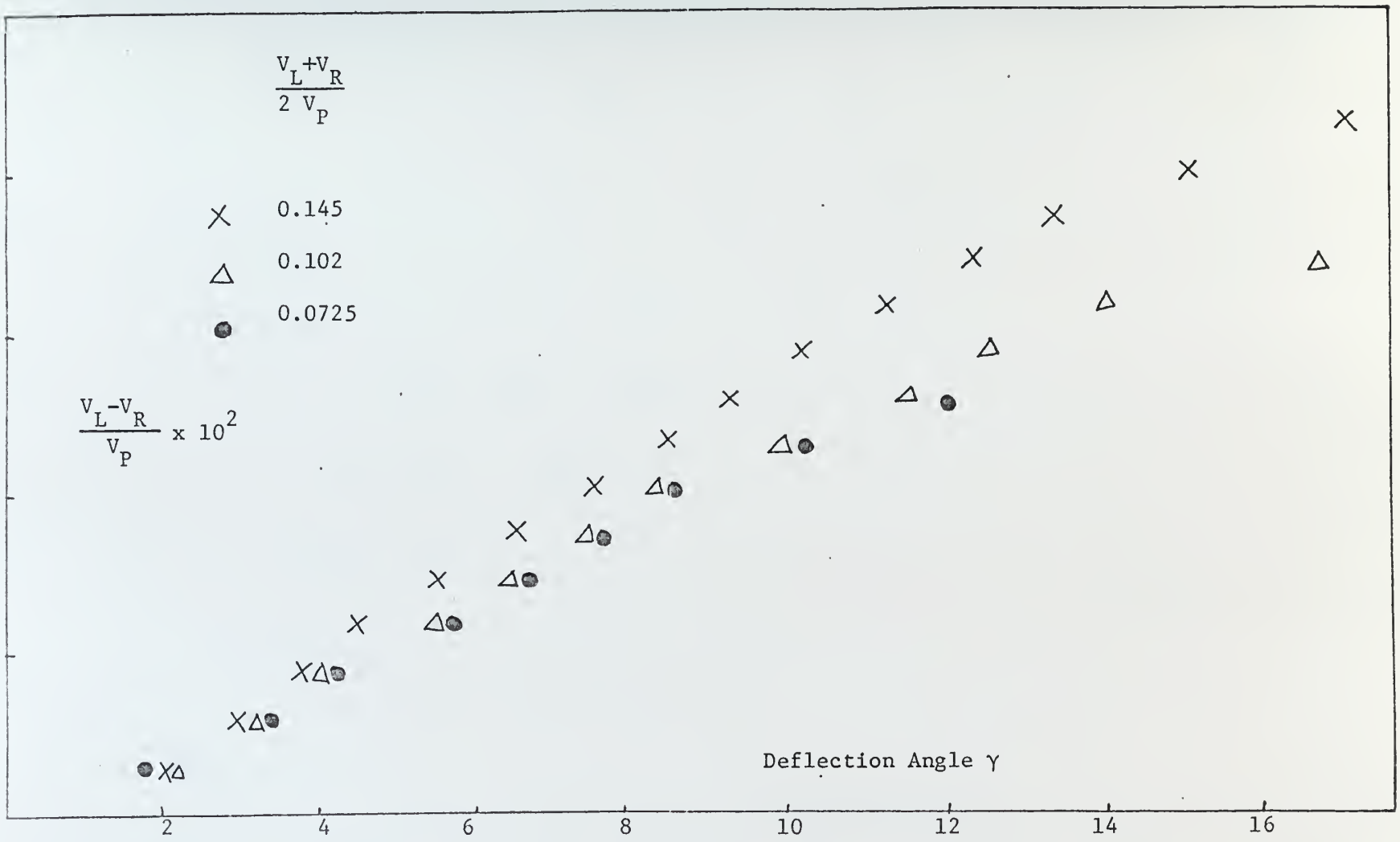

Figure 89. Deflection Angles, Re = 15775

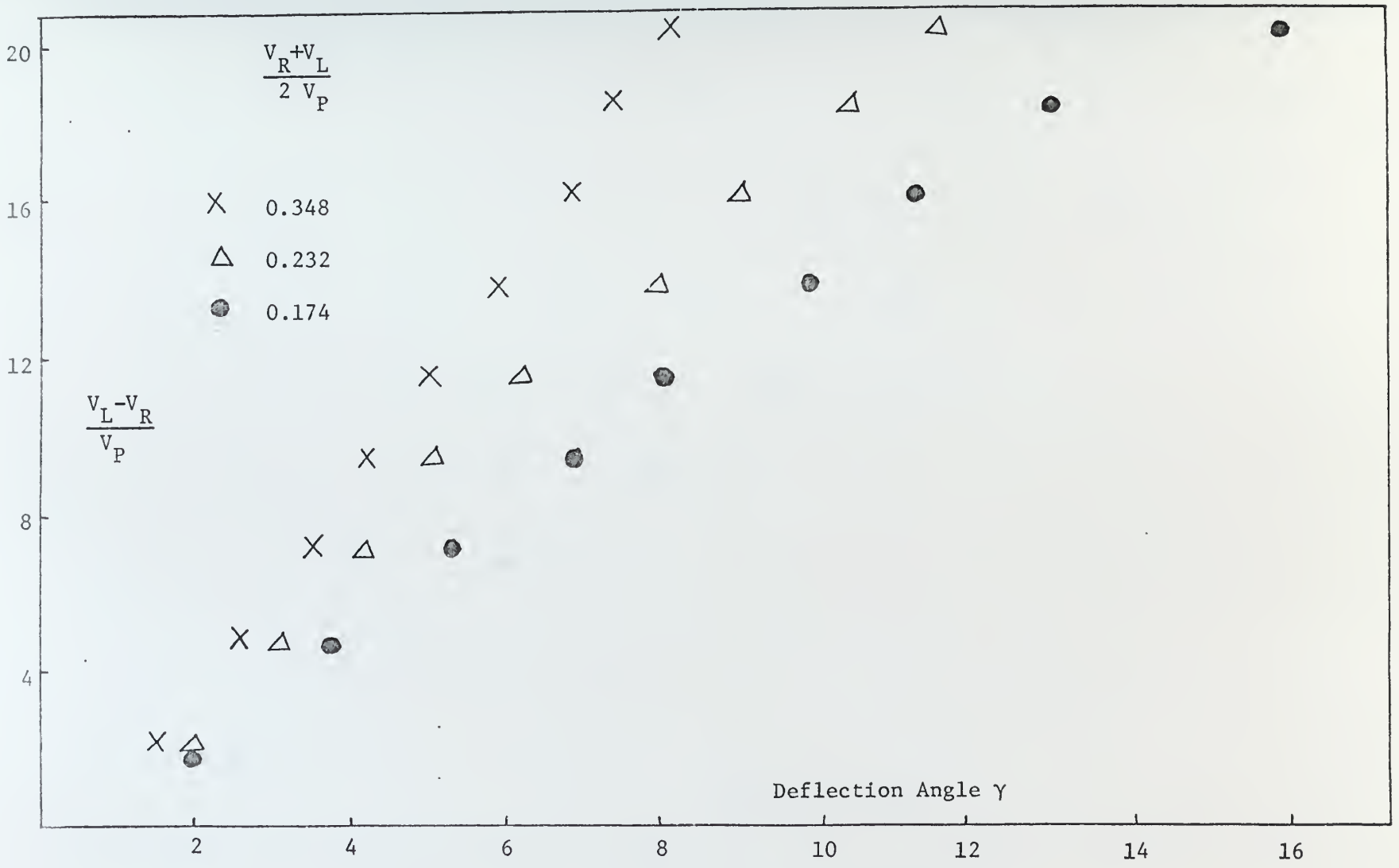

Figure 90. Deflection Angles, Re = 7887

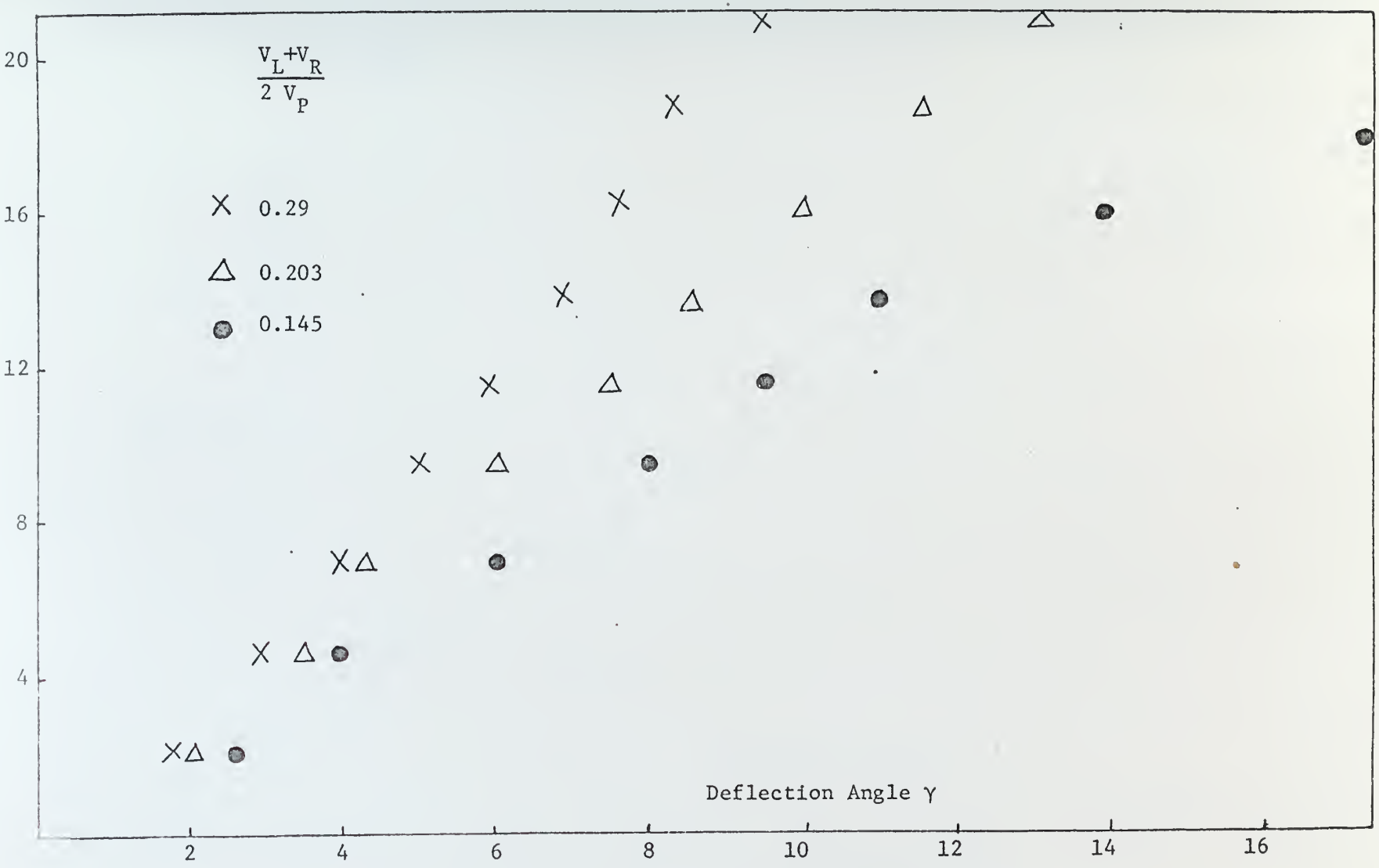

Figure 91. Deflection Angles, Re = 7887

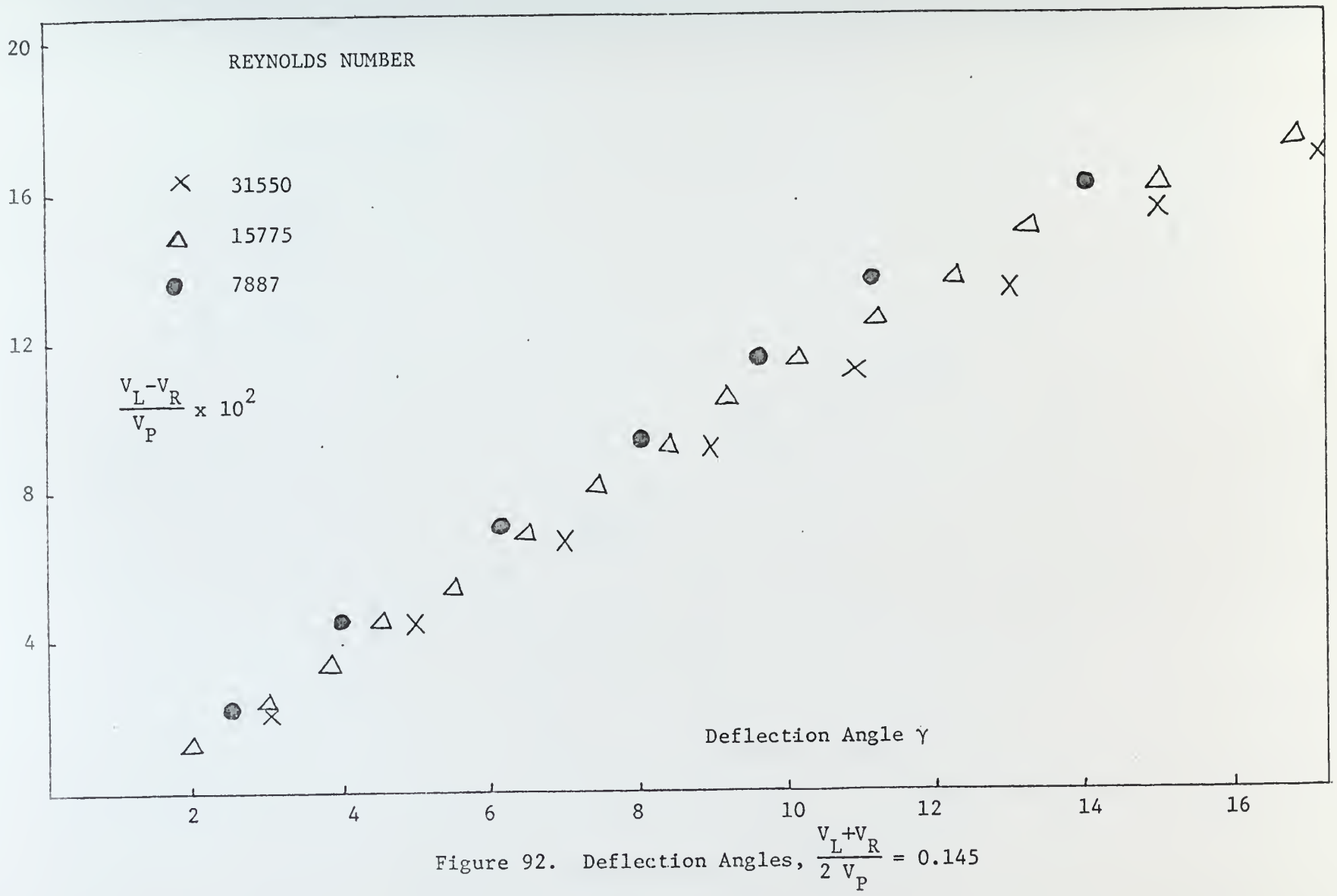

Figure 92. Deflection Angles, $\frac{V_L + V_R}{2\ V_P} = 0.145$

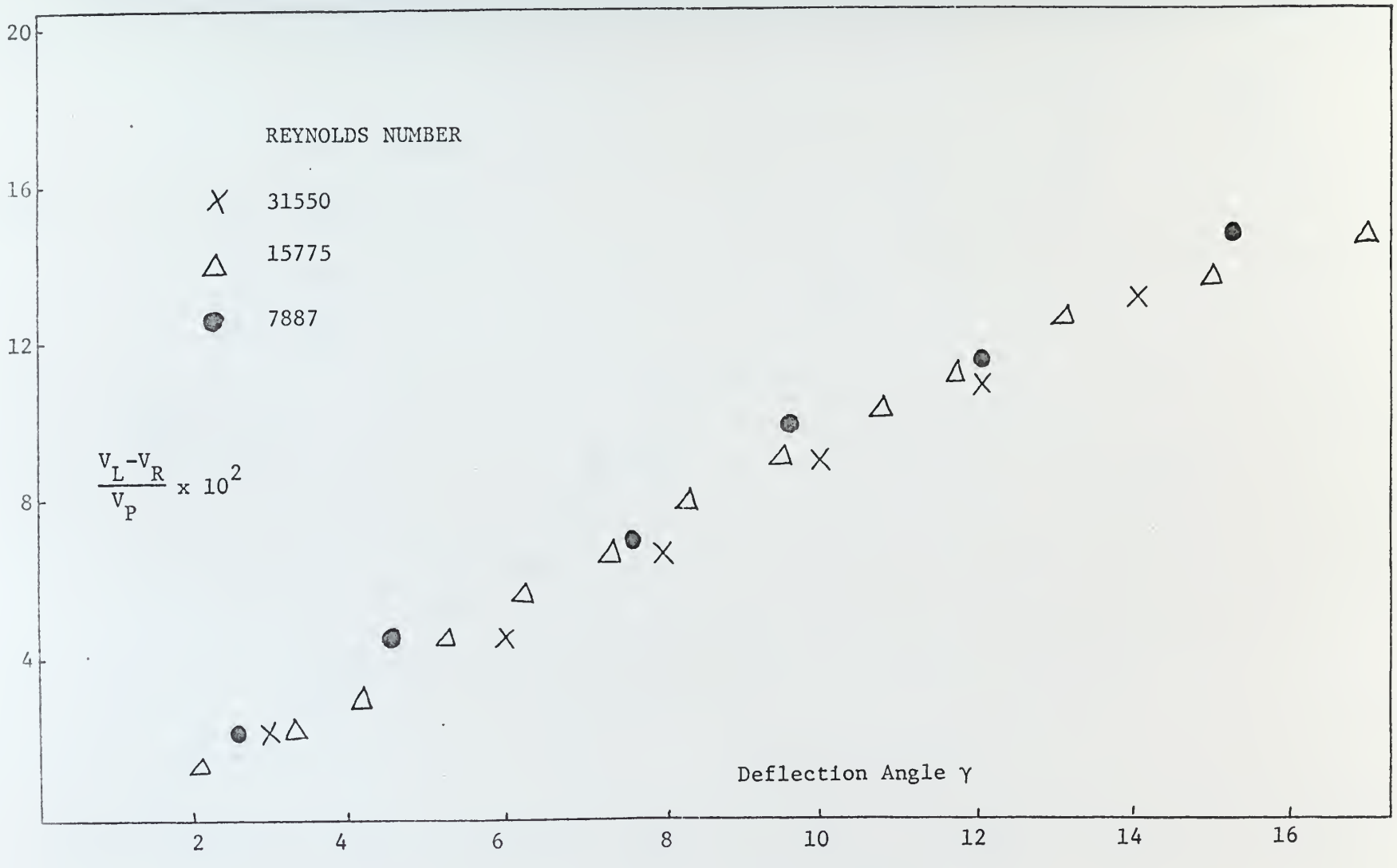

Figure 93. Deflection Angles, $\frac{V_L + V_R}{2\ V_P} = 0.116$

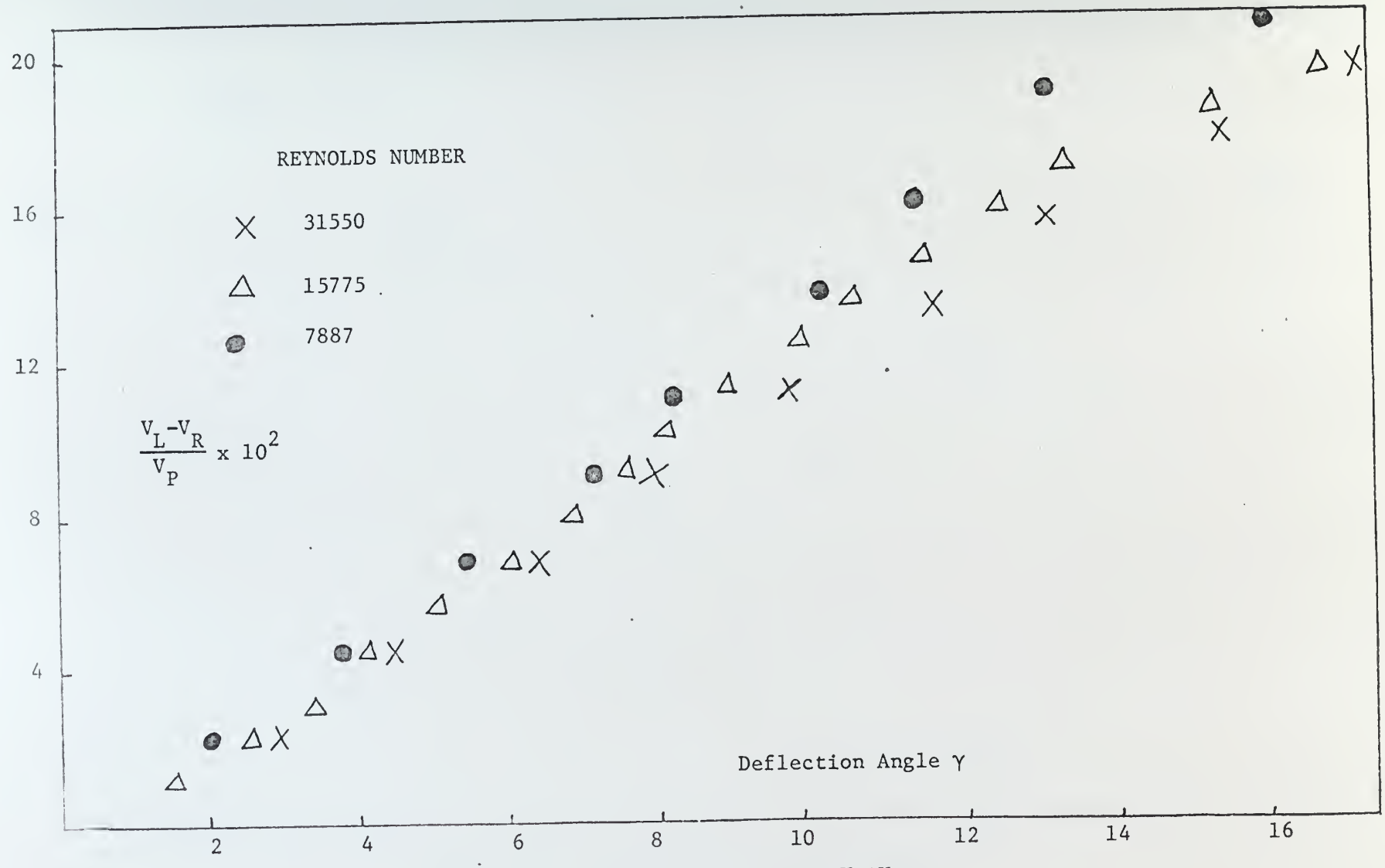

Figure 94. Deflection Angles, $\frac{V_L + V_R}{2\ V_P} = 0.174$

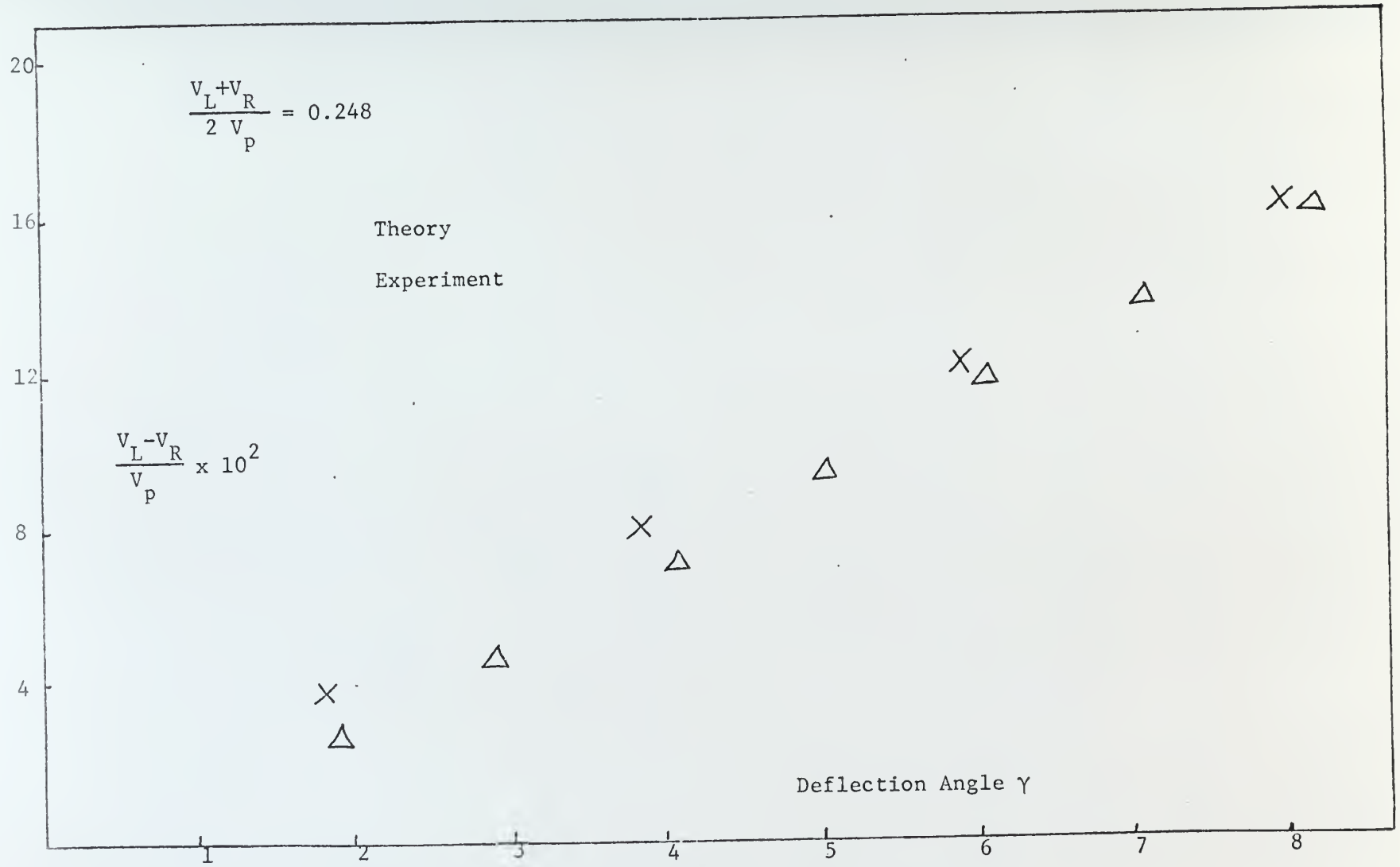

Figure 95. Experimental and Theoretical Deflection Angles

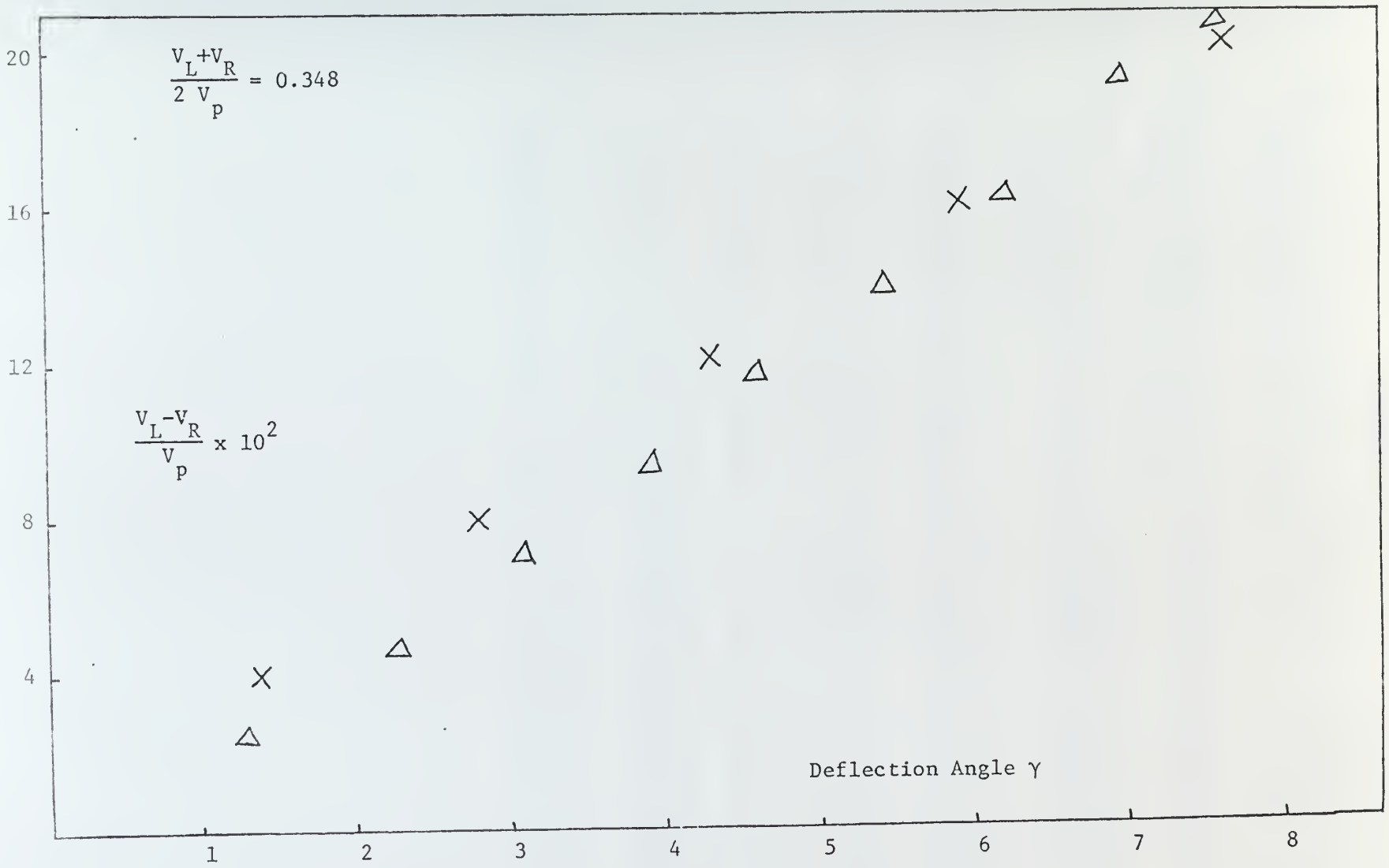

Figure 96. Experimental and Theoretical Deflection Angles

REFERENCES

1. Owczarek, J. A., Rockwell, D. O., and Cha, Y-S., "A Study of Flow from Two Planar Nozzles," Project Themis: "Fluid Amplifiers" Technical Report No. 1, (1970).

2. Wuerer, J., "Experiments on the Control of Plane Jets by Auxiliary Flows," Aeroscnics Laboratory, University of California, Report No. 63-31 (July 1963).

3. Douglas, J. F., and Neve, R. S., "Investigation into the Behaviour of a Jet Interaction Proportional Amplifier," Proceedings of the Second Crandfield Fluidics Conference, Paper C3, pp: 29-38, (January 1967).

4. McCabe, A., and Hughes, D. L., "Characteristics of Proportional Fluidic Amplifiers," Proceedings of the Second Fluid Amplification Symposium, Paper C5, pp: 72-92.

5. Moynihan, F. A., and Reilly, R. J., "Deflection and Relative Flow of Three Interacting Jets," Proceedings of the Second Fluid Amplification Symposium, pp: 123-146, (October 1964).

6. Moynihan, F. A., "Jet Interaction Noise," Proceedings of the Second Fluid Amplification Symposium, pp: 111-122, (October 1964).

7. Sarpkaya, T., "A Theoretical and Experimental Investigation of the Interaction of Jets in Beam-Deflection Type Fluidic Elements," Proceedings of Fourth Crandfield Fluidics Conference, Paper B3, pp: 33-42, (March 1970).

8. Gerardo Hiriart, L. B., "A Theoretical and Experimental Study of the Three Jet Interaction," Thesis, U. S. Naval Postgraduate School, (April 1970).

INITIAL DISTRIBUTION LIST

		No. Copies
1.	Defense Documentation Center Cameron Station Alexandria, Virginia 22314	2
2.	Library, Code 0212 Naval Postgraduate School Monterey, California 93940	2
3.	Professor T. Sarpkaya Chairman, Department of Mechanical Engineering Naval Postgraduate School Monterey, California 93940	2
4.	Dz, Kv. Komt Teknik Daire Baskanligi Ankara, Turkey	2
5.	Istanbul Tehnik University Makina Fakultesi Dekanligi Gumussuyu, Istanbul, Turkey	1
6.	Orta Dogu Teknik Universitesi Makine Fakultesi, Dekanligi Ankara, Turkey	1
7.	LT(jg) Ercan Turken Harem, Iskele Sok. No. 50/8 Uskudar, Istanbul, Turkey	1

Security Classification

DOCUMENT CONTROL DATA - R & D

(Security classification of title, body of abstract and indexing annotation must be entered when the overall report is classified)

1. ORIGINATING ACTIVITY (Corporate author)

Naval Postgraduate School
Monterey, California 93940

2a. REPORT SECURITY CLASSIFICATION

Unclassified

2b. GROUP

3. REPORT TITLE

Jet Deflection, Noise and Pressure Distribution in Proportional Amplifiers

4. DESCRIPTIVE NOTES (Type of report and inclusive dates)

Mechanical Engineer Degree Thesis; September 1971

5. AUTHOR(S) (First name, middle initial, last name)

Ercan Türken

6. REPORT DATE	7a. TOTAL NO. OF PAGES	7b. NO. OF REFS
September 1971	132	8

8a. CONTRACT OR GRANT NO.	9a. ORIGINATOR'S REPORT NUMBER(S)
b. PROJECT NO.	
c.	9b. OTHER REPORT NO(S) (Any other numbers that may be assigned this report)
d.	

10. DISTRIBUTION STATEMENT

Approved for public release; distribution unlimited.

11. SUPPLEMENTARY NOTES	12. SPONSORING MILITARY ACTIVITY
	Naval Postgraduate School Monterey, California 93940

13. ABSTRACT

The present study presents the experimental work done on the determination of angle, noise, and pressure distribution for proportional amplifiers. The deflection angles were measured by means of a small, lightstring attached to a needle. The turbulence components in the three directions were obtained through the use of the hot-wire anemometer. The "momentum balance" principal was employed to predict the deflection angles, by taking into account the effects of the momentum, static pressure, and centrifugal forces. The results so obtained were found to be in agreement with those obtained experimentally. The static wall pressures were obtained with a pressure transducer. The "two dimensional-inviscid" flow model was used throughout the work.

DD FORM 1 NOV 65 1473 (PAGE 1)

S/N 0101-807-6811

Security Classification

KEY WORDS	LINK A		LINK B		LINK C	
	ROLE	WT	ROLE	WT	ROLE	WT
Proportional Amplifiers						
Jet Deflection						
Noise & Pressure Distribution						

128540

Thesis
T937
c.1

Türken
Jet deflection, noise and pressure distribution in proportional amplifiers.